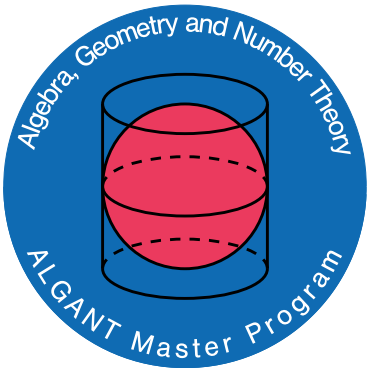

ALGANT Master Program

Dipartimento di Matematica | Fakultät für Mathematik

Implementing the Sarkar-Wang Nicefication Algorithm for Heegaard Diagrams

Ludovico Morellato

Advisors:

Lukas Lewark | Claudius Zibrowius

Università degli Studi di Padova

Universität Regensburg

Academic year 2021/2022

"And now, Harry, let us step into the night
and pursue that flighty temptress, adventure."

Albus P. W. B. Dumbledore
"Harry Potter and the Half-Blood Prince"

Acknowledgements

Since I am writing the acknowledgements for this thesis, it seems that I have indeed reached the finish line. It feels like the end of a very long journey, with a future ahead of me that is not yet clear, but nevertheless filled with hopes and dreams. Like all great experiences in life, the taste left is bittersweet.

I cannot help but wonder if it would have been the same without the amazing people who that I was so lucky to have around me during these last years. They supported and helped me in so many different ways that were fundamental for reaching my goals and for my well-being.

I am incredibly grateful to my supervisors, Lukas Lewark and Claudius Zibrowius, who followed me and my work in the last months. They proposed this master thesis topic that suited my mathematical and programming interests at a time when my ideas about the future were very confused, and guided me throughout the work, even when my motivation was not at its peak. I feel very lucky to have been able to work with them.

A huge thanks goes to my parents Stefania and Valerio, who unconditionally supported me emotionally, financially, and with the day-to-day issues that I encountered. I also want to thank my siblings Vittoria, Bartolomeo, and Ottavia, who especially during the last year were able to make me feel close to them even with more than six-hundred kilometers separating us. With them, I feel like no time has passed while I am away from home, picking up where we left off every time I come back. In particular, the crash course in vector graphics that Bartolomeo gave me truly made the realisation of this thesis within the deadline possible.

To my grandparents and all my extended family (including my "adoptive" uncles), I am grateful for their enormous affection, expressed even when distance could have been an understandable issue. I always felt them very close and involved in my life.

Throughout this journey, I have been fortunate to have stumbled upon friendships that feel long-lasting and have made the road less tough to deal with. I am grateful to each and every one of them.

I owe a special thanks to Dario Sterzi for all the time we spent together studying mathematics. He was always willing to take on new challenges with me, whether they were *cyber* or mathematical. Without his help, I would not be the mathematician that I am today.

I also want to thank Beatrice Ongarato, Eva Shi, and Gloria Luison for being a part of my "family of Torre Archimede" over the years, even when we were all scattered around Europe.

To Francesco Cenzato and Francesco Paolo Gallinaro goes my gratitude for being my older "mathematical brothers", always listening to my complaints and offering me their guidance.

I am also grateful to Giacomo Santato, whose tips and help were crucial in orienting myself, especially during the beginning of my first year of the master's program.

Jacopo Puccini deserves my thanks for always being ready to help me with any technological issue I encountered and for proving that friendships from first grade can be long-lasting.

To my friends from high school, Elena Palmarin, Francesco Lorè, Gregorio Don, Isacco Sturaro, Ruggero Rigodanzo, and Sara Girotto, thank you. You always remind me that becoming adults does not mean we have to stop having fun. We will go camping together again, I promise.

I thank also my "colleague in Consulta" Alberto Levorin, for proving that indeed, the Consulta is an aged cheese, but with the unexpected twist to bind two people for a very long time.

To all my friends in Regensburg that made me feel not alone during the time spent here, I say thank you. I want in particular to thank Chiara Sabadin for all the support given to me and for being always there and Elena Bogliolo, Giacomo Bertizzolo, Giovanni Sartori, Pier Federico Pacchiarotti and Ritheesh Krishna Thiruppathi for all the good time spent together.

To Francesca De Benetti and Tommaso Benciolini, my "parents from München" as everyone in Regensburg knows them, I am incredibly indebted: you made my logistical german life way easier that it could have been and you were always ready to listen to my concerns when the future felt too obscure to deal with.

Huge thanks are due to my "mathematical friends with whom I go mountaineering with": Andrea Ulliana, Cecilia Secchi, Leonardo Schiavo and Nicolò Filippas. It has never been clearer to me how lucky I was to find such friends with whom to share all my passions, dreams and doubts. To Cecilia, for all the "strolling calls" exchanged in the last years. To Andrea, for all the enthusiasm shared abut climbing, running and training. To Leonardo, for being the glue to the group with always one reckless hiking path to put on the table. To Nicolò, for being faithful companion in adventures, a physiotherapist and a psychologist all in one person. In particular, I owe to Leonardo and Nicolò a large part of my growth in recent years.

Lastly, I am endlessly grateful to Lucia Tessarolo. If I was able to keep up with all the challenges that life threw at me in the last year, it is almost exclusively due to you. Your help to endure the difficult times was extraordinary; you made bearable the feeling of not knowing what the next step was. You were always able to make me feel understood, capable and loved. I will be forever grateful.

Contents

Introduction

The main goal of this work is to give an introduction to (Tangle) Heegaard Floer Homology computed via *nice Heegaard diagrams* and to provide a software able to compute such invariant.

Heegaard Floer Homology was first developed by Peter Ozsváth and Zoltán Szabó as a variant of Floer Homology. They were able to compute this new invariant, later proved to be isomorphic to Seiberg–Witten Floer Homology and Embedded Contact Homology, with the use of *Heegaard diagrams*. Heegaard diagrams are a powerful tool of 3-dimensional topology: they are a way to represent a 3-manifold with a genus g surface along with the data of some curves embedded on the surface. The main technical issue is the computation of the proper boundary maps of $\widehat{\mathrm{CF}}$, the chain complex built from a Heegaard diagram on which the hat version of Heegaard Floer Homology $\widehat{\mathrm{HF}}$ is computed. In 2006, Sarkar and Wang were able to find a way around this problem, publishing "An algorithm for computing some Heegaard Floer homologies" ([SW10]). In this article, they proved that there exists a family of diagrams for which the computations of Heegaard Floer Homology can be done in a completely combinatorial way: it is sufficient to count the bigons and rectangles of such special diagrams. These were called *nice Heegaard diagrams*, and it was further proved that any 3-dimensional manifold admits such a diagram. The construction of a nice Heegaard diagram is possible through an algorithm called *Nicefication Algorithm*; this takes any Heegaard diagram and makes it nice using the Heegaard moves, some operations on the embedded curves which do not change the manifold represented by the diagram. This algorithm was implemented in the course of this Master Thesis project, and can be found in [`nicepy`]. Some changes were done in order to optimise the final nice Heegaard diagram obtained with it; these are going to be discussed in Section 4.5.

The focus on the work then shifted on the study of tangles: roughly, a tangle is obtained from a knot by cutting it in n points and pulling apart the endpoints of the n strands created. For tangles, another version of Heegaard Floer Homology was developed: Tangle Floer Homology, denoted by HFT. Tangle Floer Homology is also called *multicurve invariant*, as the topological invariant yielded by it is a collection of loops on the four punctured sphere $\mathcal{S}^2_4$. See Figure 1 for an example.

To be able to nimbly compute nice Heegaard diagrams for general 4-ended tangles, two pieces of software were developed and can be found inside the [`nicepy`] Package: a first one capable of generating a Heegaard diagram for any rational tangle $Q_{p/q}$

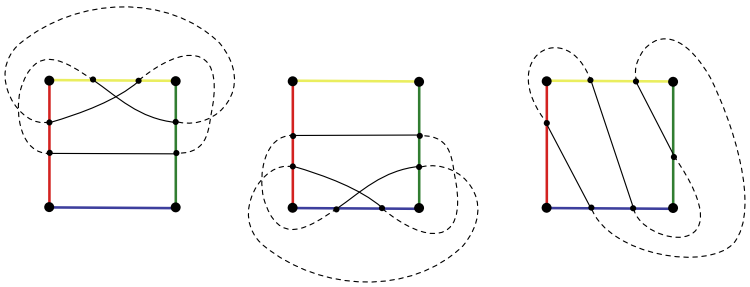

Figure 1: Examples of loops on the four punctured sphere $\mathcal{S}^2_4$: from the left $\mathfrak{s}_2(0;1,4), \mathfrak{s}_2(0;2,3)$ and $\mathfrak{r}(-2)$.

for $p, q \in \mathbb{Z}$ coprime and a second one able to glue together such diagrams. In this setting, it is possible to take any 4-ended tangle, cut it in a sum of n rational tangles and easily generate a Heegaard diagram of genus n for the initial tangle: in fact, it is sufficient to give as input the values of p and q for every tangle, the data of how they are glued together and the Alexander grading of the whole tangle. Of course, as the number of rational tangles needed to obtain the initial tangle grows, the number of generators of the nice Heegaard diagram that we obtain will grow as well; this is something important to keep in mind when trying to compute HFT as a higher number of generators will require more time to do the computations.

With the [`nicepy`] Package and the [`PQM.m`] Mathematica Software developed by Claudius Zibrowius, it was possible to compute several invariants for some families of tangles, obtaining some promising results in the search for some general patterns.

The families of tangles that were mostly investigated are:

- the "natural" gluing of a rational tangle and its mirror image, i.e. $Q_{p/q} + Q_{-p/q}$ for q odd;
- the family of tangles of the form $Q_{p/q} + Q_{1/(2n)}$ for q odd.

See Figure 2 to see two examples of elements of the families described.

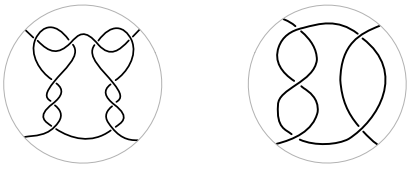

Figure 2: The tangle $Q_{3/7}$ glued with its mirror image $Q_{-3/7}$ (on the left) and the tangle $Q_{1/3}$ glued with $Q_{1/2}$ (on the right).

In Chapter 5, it is possible to see the results obtained and the possible patterns that arise from these initial computations. Among these possible formulas developed, one stands out for its generality and for being in agreement with the known multicurve invariants of Pretzel tangles; we report it here.

Conjecture 0.1 (Conjecture 5.11)**.** *Let $S_{p/q}(2n)$ be the 4-ended tangle obtained as $S_{p/q}(2n) = Q_{p/q} + Q_{1/2n}$, where $p/q \in \mathbb{Q}\mathrm{P}^1$, q an odd integer and $0 < 2n \cdot p < q$.*
Then,

$$\mathrm{HFT}\left(S_{p/q}(2n)\right) = (q - 2n \cdot p) \cdot \mathfrak{r}\left(1/(2n)\right) + p \cdot \left(\sum_{i=0}^{n-1} \mathfrak{s}_4\left(1/(2i+1)\right)\right).$$

Outline of the thesis

We present here the structure of the thesis.

Chapter 1 is devoted to the introductions of all the topological objects that we will need through the developing of this thesis. It begins with a brief discussion about n-manifolds and presents some basic properties that will be needed throughout the rest of the thesis. We then explore handle decompositions and Heegaard splittings, which serve as the fundamental concepts for the subsequent development of Heegaard diagrams and Heegaard Floer Homology. We then shift our interest to knots and tangles, focusing in particular on 4-ended tangles. Following the basic definitions, we establish a covering space for the 4-punctured sphere (the ambient space in which we embed 4-ended tangles), which allows us to define a highly significant and practical family of tangles, known as rational tangles. We moreover give the foundations of an arithmetic for 4-ended tangles. To conclude the first chapter, we provide a brief overview of the theory of sutured, bordered, and sutured bordered manifolds. These are extensions of the concept of manifolds and, like manifolds, have associated a falvor of Heegaard Floer Homology.

Chapter 2 details the construction of Heegaard diagrams for all the objects presented in Chapter 1. We begin by constructing Heegaard diagrams for closed 3-manifolds and introducing Heegaard moves and pointed Heegaard diagrams. We also explore the relationship between Morse theory and closed Heegaard diagrams, understanding how a Morse function on a 3-manifold can define a diagram. We then move on to constructing Heegaard diagrams for sutured, bordered, and sutured bordered manifolds, highlighting both similarities and differences from the closed case. Additionally, we present explicit algorithms for constructing Heegaard diagrams for knots and discuss how they can be regarded as a special case of sutured diagrams. Lastly, we construct Heegaard diagrams for tangles and focus on those for rational tangles; we also show how these diagrams can be interpreted as a special case of bordered sutured diagrams.

Chapter 3 explores the construction of various types of Heegaard Floer Homology, following the framework established in Chapter 2. We begin by developing in detail the hat version $\widehat{\mathrm{HF}}$ for closed 3-manifolds, providing a comprehensive overview of the machinery needed to compute the chain complex $\widehat{\mathrm{CF}}$. Additionally, we include a concrete example: $\widehat{\mathrm{HF}}(L(p,q))$. Next, we turn our attention to Sutured Floer Homology SHF and Knot Floer Homology HFK, seeing how the latter can be viewed as

a special case of the former. Finally, we construct Tangle Heegaard Floer Homology, the primary focus of the chapter, and provide a detailed examination of the invariant produced by this theory.

Chapter 4 introduces the central notion of nice Heegaard diagrams, understanding how it simplifies the computation of Heegaard Floer Homology for closed 3-manifolds. We begin by examining the Nicefication Algorithm for closed Heegaard diagrams in detail, which allows us to construct a nice Heegaard diagram from a generic one without affecting its admissibility. We then generalise the algorithm to other settings, including bordered diagrams, sutured diagrams, bordered sutured diagrams, and peculiar diagrams. Finally, we discuss some modifications made to the original algorithm while implementing [`nicepy`] to optimise the final result.

In Chapter 5, we discuss the results obtained by applying HFT to the families of tangles $Q_{p/q} + Q_{-p/q}$ for q odd and $Q_{p/q} + Q_{1/(2n)}$ for q odd. These results were obtained with the use of the Python software [`nicepy`] and the Mathematica package [`PQM.m`]: the former computed a nice Heegaard diagram for the investigated tangles, which was then passed to the latter software to obtain their peculiar modules CFT^{∂}. These modules were then expressed as multicurves and collected in tables, presented in this chapter. We then discuss possible patterns that HFT seems to follow for some sub-families of tangles and conjecture more general formulas.

Appendix A is a manual for the [`nicepy`] Python package. It contains instructions for setting the input (for closed, bordered, sutured, and tangle Heegaard diagrams) and additional parameters that can be set for a run, along with examples. Examples of outputs and a description of the different stages of a run are also provided.

Chapter 1

Topologist's toolbox

This first chapter is intended to provide a brief overview of all the topological objects that we will need throughout the thesis. Each section also includes one or more references for further reading.

1.1 Basics on 3-manifolds

In the first section, we provide an introduction to the concept of a manifold and its properties.

In rough terms, an n-manifold is a topological space that looks locally like the Euclidean space $\mathbb{R}^n$. To make this idea precise, we introduce the concept of *charts*, which are homeomorphisms from a subset of the manifold to an open subset of $\mathbb{R}^n$ that provide a local coordinate system. Using charts, we can define important concepts such as the tangent space, differentiability and orientation.

The main reference used for this section is [Bar22].

Definition 1.1 (n-dimensional chart)**.** Let Y be a topological space. An *n-dimensional chart* for Y at a point $y \in Y$ is a homeomorphism

$$\begin{array}{ccc} Y & & \mathbb{R}^n \\ \cup & & \cup \\ U & \xrightarrow{\Phi} & V, \end{array}$$

where U is an open neighbourhood of y and one of the following holds:

(i) V is an open subset of R^n, or

(ii) V is an open subset of the upper half-space $\mathbb{H}^n = \{(x_1, \ldots, x_n) \in \mathbb{R}^n \mid x_n \geq 0\}$.

We distinguish between charts of type (i), when case (i) occurs, and charts of type (ii), when case (ii) occurs.

Definition 1.2 (n-dimensional atlas, transition maps)**.** An *n-dimensional atlas* $\mathcal{A}$ for a topological space Y is a family of n-dimensional charts $\mathcal{A} = \{\Phi_i : U_i \to V_i\}_{i\in I}$ such that "they chart all Y", i.e. $\cup_{i\in I} U_i = Y$.

The *transition maps* of $\mathcal{A}$ are the maps that allow us to go from one chart to another, i.e. the maps of the form

$$\begin{array}{ccc} \mathbb{R}^n & & \mathbb{R}^n \\ \cup & & \cup \\ \phi_i\left(U_i \cap U_j\right) & \xrightarrow{\Phi_j \circ \Phi_i^{-1}} & \phi_j\left(U_i \cap U_j\right) \end{array}$$

for $i, j \in I$.

Definition 1.3 (n-manifold)**.** A topological space Y is said to be an *n-dimensional topological manifold* (or *n-manifold*), if

1. it is second-countable (i.e. its topology has a countable basis),
2. it is Hausdorff (i.e. open subsets separate points),
3. for every $y \in Y$ there exists an n-dimensional chart of type (i) at y.

Moreover, we introduce the notion of *closedness* for a manifold, which we will require for the construction of the hat version of Heegaard Floer Homology.

Definition 1.4 (Closed n-manifold)**.** An n-manifold Y is said to be *closed* if it is compact.

We now generalise to the case in which we admit also charts of type (ii), obtaining *n-manifolds with boundary.*

Definition 1.5 (n-manifold with boundary)**.** A topological space Y is said to be an *n-dimensional topological manifold with boundary* (or *n-manifold with boundary*), if

1. it is second-countable (i.e. its topology has a countable basis),
2. it is Hausdorff (i.e. open subsets separate points),
3. for every $y \in Y$ there exists an n-dimensional chart of type (ii) at y.

Remark 1.6. Let Y be an n-manifold with boundary. The *boundary of Y*, denoted by ∂Y, is the set of all boundary points of Y, described in charts as

$$\partial Y = \bigcup_{i\in I} \Phi_i^{-1}(\{x_n = 0\} \cap \mathrm{Im}\Phi_i).$$

Roughly, a point $y \in Y$ is a *boundary point* if it does not admit a chart of type (i).

Another property of manifolds that we will request for Heegaard Floer homologies, is *orientability.* In order to define this new property, we need to restrict ourselves to *smooth manifolds.*

Definition 1.7 (Smooth atlas, smooth n-manifold (with boundary))**.** An atlas is *smooth* if all the transition maps are smooth (i.e., $\mathcal{C}^\infty$).

A *smooth n-manifold (with boundary)* is an n-manifold (with boundary) together with a smooth atlas. This is also sometime called a *differentiable manifold (with boundary) of class $\mathcal{C}^\infty$*.

We also need to define a relation between atlases.

Definition 1.8 (Compatible atlases, maximal atlas)**.** Two smooth atlases $\mathcal{A} = \{\Phi_i\}_{i\in I}$ and $\mathcal{A}' = \{\Phi'_j\}_{j\in J}$ are said *compatible* if every change of chart is smooth, i.e., if the union $\mathcal{A}\cup\mathcal{A}'$ is still a smooth atlas. A smooth atlas is called *maximal* if it is not contained in any strictly larger compatible smooth atlas.

Furthermore it is possible to see that the following proposition holds.

Proposition 1.9 ([Bar22, Proposition 1.9])**.** *Let Y be a smooth manifold. Then every smooth atlas is contained in a unique maximal smooth atlas and two atlases are contained in the same maximal atlas if and only if they are compatible.*

In what follows, we then assume that each atlas describing a smooth manifold is maximal.

Example 1.10. We can see some basic examples of smooth n-manifolds and n-manifolds with boundary.

1. $\mathbb{R}^n$ is a smooth n-manifold. As charts, we can take identity maps on some covering; therefore it is also smooth. Notice that it is not closed: it has no boundary, but it is not compact.

2. Analogously, an open set $U\subset\mathbb{R}^n$ is an n-manifold, not closed for the same argument as above.

3. A closed set $C\subset\mathbb{R}^n$ is a smooth n-manifold with boundary.

4. The sphere $\mathcal{S}^n$ is a smooth, closed n-manifold.

   Consider the sphere as the following subset of $\mathbb{R}^{n+1}$, with the topology induced by $\mathbb{R}^{n+1}$

   $$\mathcal{S}^n = \left\{\underline{x} = (x_1,\dots,x_{n+1})\in\mathbb{R}^{n+1} \mid |\underline{x}|_{\mathbb{R}^n} = 1\right\}\subset\mathbb{R}^{n+1}.$$

   Then consider the two open subsets $U_N = \mathcal{S}^n\setminus\{N\}$ and $U_S = \mathcal{S}^n\setminus\{S\}$, where $N = (0,\dots,0,1)$ is the north pole and $S = (0,\dots,0,-1)$ is the south pole. We want to construct an atlas with only two charts, defined on these open subsets that cover the sphere. Notice that this is the minimum number of charts that we can use for an atlas of $\mathcal{S}^n$: if we could construct an atlas with only one chart, then it would mean that $\mathcal{S}^n$ is homeomorphic to an open subset of $\mathbb{R}^n$, which is false since $\mathcal{S}^n$ is compact.

   We define the charts $\Phi_N : U_N\to\mathbb{R}^n$ and $\Phi_S : U_S\to\mathbb{R}^n$ to be the stereographic projections (from N and S respectively); in coordinates this is expressed as

$$\begin{array}{ccc} U_N & \xrightarrow{\Phi_N} & \mathbb{R}^n \\ \underline{x} & \longmapsto & \frac{1}{1-x_{n+1}}(x_1,\dots,x_n) \end{array} \qquad \begin{array}{ccc} U_S & \xrightarrow{\Phi_S} & \mathbb{R}^n \\ \underline{x} & \longmapsto & \frac{1}{1+x_{n+1}}(x_1,\dots,x_n). \end{array}$$

The transition map $\Phi_S \circ \Phi_N^{-1}$ is described as

$$\begin{array}{ccc} \mathbb{R}^n \smallsetminus \{0\} & \xrightarrow{\Phi_S\circ\Phi_N^{-1}} & \mathbb{R}^n \smallsetminus \{0\} \\ \underline{x} & \longmapsto & \frac{\underline{x}}{|\underline{x}|^2_{\mathbb{R}^n}}. \end{array}$$

Therefore, $\mathcal{S}^n$ is a smooth, closed n-manifold.

We now want to define an orientation on Y using the charts. This is done using a smooth atlas and the Jacobian matrices[1] of the transition maps.

Definition 1.11 (Equioriented charts, oriented atlas)**.** Two smooth charts $\Phi_1 : U_1 \to V_1$ and $\Phi_2 : U_2 \to V_2$ of some manifold Y are said to be *equioriented* if $\det J_f(x_0)(\Phi_2 \circ \Phi_1^{-1}) > 0$ for any $x_0 \in \Phi_1(U_1 \cap U_2)$, where $J(f)$ is the Jacobian matrix of f.

An atlas is *oriented* if every pair of charts are equioriented.

We can now define oriented manifolds.

Definition 1.12 (Oriented n-manifold (with boundary))**.** A smooth n-manifold Y is said to be *orientable* if it admits an oriented atlas. An *orientation* of Y is a choice of an oriented atlas of Y.

Example 1.13 ($\mathcal{S}^n$ is orientable for any $n \geq 1$)**.** We can easily prove that $\mathcal{S}^n$ is orientable for any $n \geq 1$.

The case $n = 1$ is done by hand. To prove the case $n \geq 2$, one uses the fact that local diffeomorphisms do not change sign on connected sets and have sign different than zero. Therefore, the signs of the Jacobians (which are local diffeomorphisms) of the only transition map are different than zero and they all agree because the intersection $U_N \cap U_S$ is connected. If the sign is positive, then we are done. If it is negative, we just to post-compose the second chart to a map that swaps the last two coordinates, obtaining the following new chart

$$\begin{array}{ccc} U_S & \xrightarrow{\Phi'_S} & \mathbb{R}^n \\ \underline{x} & \longmapsto & \frac{1}{1+x_{n+1}}(x_1,\dots,x_{n-2},x_n,x_{n-1}). \end{array}$$

[1] Let f be a map $f : U \subset \mathbb{R}^n \to \mathbb{R}^m$, defined by $\underline{x} = (x_1,\dots,x_n) \mapsto (f_1(\underline{x}),\dots,f_m(\underline{x}))$. Recall that the Jacobian of f in $x_0 \in U$ is defined to be

$$J_f(x_0) = \begin{pmatrix} \frac{\partial f_1}{\partial x_1}(x_0) & \cdots & \frac{\partial f_1}{\partial x_n}(x_0) \\ \vdots & \ddots & \vdots \\ \frac{\partial f_m}{\partial x_1}(x_0) & \cdots & \frac{\partial f_m}{\partial x_n}(x_0) \end{pmatrix}.$$

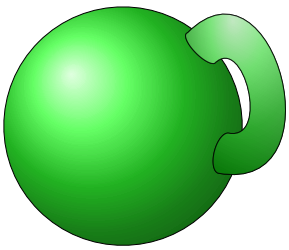

Figure 1.1: Handlebody of genus 1.

1.2 Handle decomposition and Heegaard splittings

The underlying idea of Heegaard splittings (also called Heegaard decompositions) is to decompose a 3-manifold into simpler pieces, called *handlebodies*. Intuitively, we carve out some holes in the 3-manifold, for example g holes, obtaining a handlebody of genus g. Then, we consider the complement of this handlebody in our 3-manifold, obtaining another handlebody of genus g that shares a boundary with the previous handlebody. This forms a Heegaard splitting.

The main references for this section are [OS06a] and [Hom19].

We are going to always assume that 3-manifolds are closed and oriented and that homeomorphisms are orientation-preserving (unless otherwise stated).

Definition 1.14 (n-dimensional k-handle)**.** Consider $0 \leq k \leq n$. We call a *n-dimensional k-handle* a copy of $B^k \times B^{n-k}$, attached to the boundary of a smooth n-manifold Y along $\left(\partial B^k\right) \times B^{n-k}$ by an embedding $\phi : \left(\partial B^k\right) \times B^{n-k} \hookrightarrow \partial Y$. As there is a canonical way to smooth corners, we think of Y with the attached handle as a smooth n-manifold.

Often, we think about an n-dimensional k-handle as a k-cell that we thicken-up until it become n-dimensional.

Definition 1.15 (Handlebody of genus g)**.** We define an *handlebody of genus g* to be a 3-dimensional ball to which we attach g 3-dimensional 1-handles to it.

We can clearly see that the boundary of a handlebody of genus g is a surface of genus g.

Definition 1.16 (Heegaard splitting of genus g)**.** Let Y be a closed and oriented 3-manifold. An *Heegaard splitting of Y of genus g* (also called *Heegaard decomposition*) is a decomposition

$$Y = H_1 \cup_\Sigma H_2$$

in which H_1 and H_2 are handlebodies of genus g such that $\partial H_1 \simeq \partial H_2$ (they are homeomorphic via an orientation-reversing homeomorphism).

Example 1.17 (First examples)**.** We see now some examples that can help to visualise the above definition.

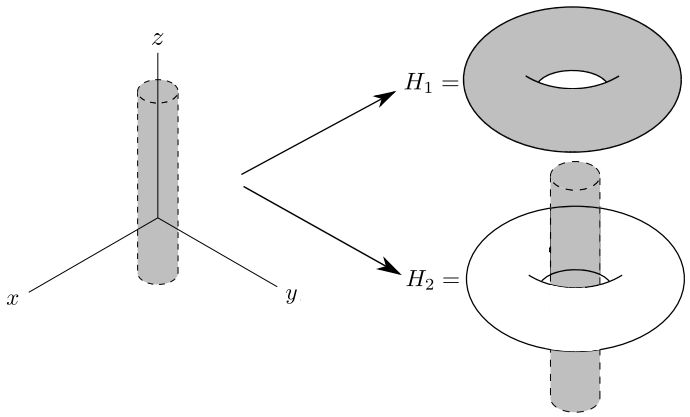

Figure 1.2: Heegaard splitting for $\mathcal{S}^3 \simeq \mathbb{R}^3 \cup \{\infty\}$.

1. **Heegaard splitting of genus 0 of $\mathcal{S}^3$**

   Consider the sphere $\mathcal{S}^3$, and cut it in half into two hemispheres H_1 and H_2, namely $H_1 = \{(x, y, z, w) \in \mathcal{S}^3 \subset \mathbb{R}^4 \mid w \geq 0\}$ and $H_2 = \{(x, y, z, w) \in \mathcal{S}^3 \subset \mathbb{R}^4 \mid w \leq 0\}$. We have that $H_i \simeq B^3$, i.e., they are diffeomorphic to the 3-dimensional ball, and that $\partial H_1 = \partial H_2 \simeq \mathcal{S}^2$. Therefore, this is a genus 0 Heegaard decomposition of $\mathcal{S}^3$.

2. **Heegaard splitting of genus 1 of $\mathcal{S}^3$**

   Regard $\mathcal{S}^3$ as the compactification of $\mathbb{R}^3$ with a point to the infinite. Consider a closed tubular neighbourhood of the circle given by the z-axis and the point to the infinite, this is the first genus-1 handlebody H_1. Let H_2 be the closure of the complement of H_1; this is another handlebody of genus 1. Therefore we have constructed a genus 1 Heegaard splitting of $\mathcal{S}^3$.

3. **Heegaard splitting of genus g of $\mathcal{S}^3$**

   Starting from the 0-genus splitting, we can obtain a g-genus splitting for any g in the following way. Take the two 3-balls H_1, H_2, in H_1 "drill" g unknotted holes (they have to be disjoint) and in H_2 attach g disjoint handles on the outside; call H_1', H_2' the two new handlebodies obtained. Now we need to identify each handle of H_2' with a hole in H_1'. Therefore, the boundary Σ' of the handlebodies has genus g and we have that $\mathcal{S}^3 = H_1' \cup_{\Sigma'} H_2'$.

4. **Heegaard splitting of genus 1 of lens spaces $L(p, q)$**

   We begin by giving the definition of such space. Let p, q be coprime integers and consider the 4-dimensional sphere embedded in $\mathbb{C}^2$

   $$\mathcal{S}^3 = \left\{(z, w) \in \mathbb{C}^2 \,\middle|\, |z|^2 + |w|^2 = 1\right\} \subset \mathbb{C}^2.$$

   Consider now the following $\mathbb{Z}/p\mathbb{Z}$ action on $\mathcal{S}^3$

$$\begin{aligned} \tfrac{\mathbb{Z}}{p\mathbb{Z}} \times \mathcal{S}^3 &\longrightarrow \mathcal{S}^3 \\ (k + p\mathbb{Z}, (z, w)) &\longmapsto \left(e^{\frac{2\pi i k}{p}} z, e^{\frac{2\pi i k q}{p}} w \right). \end{aligned}$$

We define $L(p, q)$ as the quotient of this action.

We can also see that $L(p, q)$ is a closed, 3-dimensional, oriented, smooth manifold, whose orientation is given by the initial orientation of $\mathcal{S}^3$. In fact, since the $\mathbb{Z}/p\mathbb{Z}$ action acts freely, properly and continuously, we have that $L(p, q)$ is a closed 3-manifold and that the projection $p : \mathcal{S}^3 \to L(p, q)$ is a local homeomorphism; moreover, since the action is smooth (i.e., for every $\bar{a} \in \mathbb{Z}/p\mathbb{Z}$ the map $\mathcal{S}^3 \to \mathcal{S}^3$ defined by $x \mapsto \bar{a} \cdot x$ is smooth), we also have that $L(p, q)$ has a unique smooth structure that makes the projection p a local diffeomorphism.

We want to construct now a genus 1 Heegaard splitting. Consider the following two subsets of $\mathcal{S}^3$

$$\begin{aligned} X &= \left\{ (z, w) \in \mathbb{C}^2 \,\middle|\, |z|^2 + |w|^2 = 1 \text{ and } |z|^2 \geq \frac{1}{2} \right\}, \\ Y &= \left\{ (z, w) \in \mathbb{C}^2 \,\middle|\, |z|^2 + |w|^2 = 1 \text{ and } |w|^2 \geq \frac{1}{2} \right\}. \end{aligned}$$

These are both diffeomorphic to the solid 1-torus, $\mathcal{S}^1 \times B^2$ and their intersection is exactly the boundary of a torus $\mathcal{S}^1 \times \mathcal{S}^2$. We can now notice that the action of $\mathbb{Z}/p\mathbb{Z}$ on $\mathcal{S}^3 = X \cup Y$ preserves these two tori set-wise. More precisely, the quotients $X/\mathbb{Z}_p$ and $Y/\mathbb{Z}_p$ are again diffeomorphic to the solid torus. To see this, we pick $r \in \mathbb{N}$ with $r \cdot q \equiv -1 \bmod p$; it is straightforward to see that the maps

$$\begin{aligned} \tfrac{X}{\mathbb{Z}/p\mathbb{Z}} &\xrightarrow{\Phi} S^1 \times B^2 & \qquad \tfrac{Y}{\mathbb{Z}/p\mathbb{Z}} &\xrightarrow{\Psi} S^1 \times B^2 \\ [(z, w)] &\longmapsto \left(\tfrac{z^p}{|z^p|}, \tfrac{z^{-q} w}{|z^{1-q}|} \right) & \qquad [(z, w)] &\longmapsto \left(\tfrac{w^p}{|w^p|}, \tfrac{z w^r}{|w^{1+r}|} \right) \end{aligned}$$

are well-defined diffeomorphisms and that Φ is orientation-preserving: to see the latter, it suffices to show that Φ is orientation-preserving at a single point; using that $p > 0$, one can calculate explicitly that Φ is orientation-preserving at the point $[(1, 0)] \in {}^{X}/_{\mathbb{Z}/p\mathbb{Z}}$ and hence the statement follows.

This shows that

$$L(p, q) = X/\mathbb{Z}_p \cup Y/\mathbb{Z}_p$$

is a genus 1 Heegaard decomposition of the lens space $L(p, q)$.

At first glance, it may seem that admitting a Heegaard splitting is a quite special property. This is in reality not true, as any closed 3-manifold admits a Heegaard splitting; a proof of this fact was given by Singer in [Sin33].

Theorem 1.18 (Existence of Heegaard splitting)**.** *Let Y be a closed, orientable 3-manifold. Then it admits a Heegaard splitting.*

Proof ([Hom19]). Cairns and Whitehead proved that to every smooth manifold can be given a simplicial structure, i.e. a triangulation.

Consider now the 1-skeleton of a triangulation of Y (vertices and edges); this is a graph embedded in Y. Let H_1 be a small regular closed neighbourhood of the 1-skeleton: to visualise this think of replacing each vertex with a closed ball and each edge with a solid cylinder between the two balls at the extremities. It is clear that H_1 is a handlebody of some genus g. If we now call H_2 the closure of $Y \setminus H_1$, we see that this is another handlebody of genus g given by a regular neighbourhood of a graph which vertices stay in the centre of the triangles and tetrahedrons of the 1-skeleton above.

As $\partial H_1 = \partial H_2$, we have a Heegaard splitting of Y. □

Another way to construct a Heegaard splitting for a generic 3-manifold is to exploit a self-indexing Morse function on it. We will explore this particular construction briefly in Section 2.3.

As we have seen in the examples above, there could be different choices of Heegaard splittings for the same 3-manifold. We are now going to see some definitions which will give us a clearer idea of how these choices are related one to another.

Definition 1.19 (Homeomorphic Heegaard splittings)**.** Given two Heegaard splittings of Y, namely

$$Y = H_1 \cup_\Sigma H_2 = H_1' \cup_{\Sigma'} H_2',$$

we say that they are *homeomorphic* if there exists a homeomorphism $Y \xrightarrow{\phi} Y$ such that $\phi(H_i) = H_i'$ for $i = 1, 2$.

There is also a stricter relation between Heegaard splittings that we can consider.

Definition 1.20 (Isotopic Heegaard splittings)**.** Given two Heegaard splittings of Y, namely

$$Y = H_1 \cup_\Sigma H_2 = H_1' \cup_{\Sigma'} H_2',$$

we say that they are *isotopic* if there exists a map $Y \times [0,1] \xrightarrow{\psi} Y$ such that

1. $\psi_{|Y\times\{0\}} = id_Y$;
2. $\psi_{|Y\times\{t\}}$ is a homeomorphism for any t;
3. $\psi_{|Y\times\{1\}}$ sends H_i to H_i' for $i = 1, 2$.

Remark that if two splittings are isotopic, then are also homeomorphic: we can use $\psi_{|Y\times\{1\}}$ as homeomorphism.

Definition 1.21 (Stabilisation)**.** Let $Y = H_1 \cup_\Sigma H_2$ be a Heegaard splitting of genus g. A *stabilisation* (or 1*-fold stabilisation*) of $H_1 \cup_\Sigma H_2$ is a genus $g+1$ Heegaard splitting of Y obtained by adding one more handle to the existing splitting. More precisely, it is constructed in the following way. Choose two point on Σ and connect them with two arcs γ_1 and γ_2 with the following properties:

- γ_1 is embedded in Σ;
- γ_2 is embedded in H_1;
- the closed curve obtained by $\gamma_1 \cup \gamma_2$ bounds an embedded disc $D_\star$ completely in H_1.

Let N be a small tubular neighbourhood of γ_2; define then $H_1' = H_1 \setminus N$, and H_2' as the union $H_2 \cup N$. We call an *n-fold stabilisation* a sequence of n stabilisations.

Remark 1.22. Notice that the isotopy type of a stabilisation of a Heegaard splitting does not depend by the choice of γ_1 and γ_2. In fact, performing a stabilisation means to choose a disc $D_\star \subset H_1$ as above described. Since $D_\star$ is contractible in the handlebody H_1, the stabilisation does not depend on its position.

Therefore we can talk of *the* stabilisation of a Heegaard splitting.

Example 1.23. As an example, we can see that in Example 1.17, the genus 1 decomposition of $\mathcal{S}^3$ is the stabilisation of the Heegaard decomposition of genus 0.

We have a theorem of Reidemeister and Singer, which shows us that any two splittings of a 3-manifold can be connected via stabilisations. A proof can be found in [Rei33] and [Sin33].

Proposition 1.24. *Let Y be a 3-manifold with two different Heegaard splittings $Y = H_1 \cup_\Sigma H_2 = H_1' \cup_{\Sigma'} H_2'$ of genus g and g' respectively. Then, for k large enough, the $(k-g')$-fold stabilisation of the first decomposition is diffeomorphic to the $(k-g)$-fold stabilisation of the second decomposition.*

1.3 Knots and tangles

In this section, we will introduce the concepts of knots and tangles and explain how we can work with them. As main reference, one can look at Section I.1 of [Zib17]. Another reference which can be very helpful for visualising this notions, is [Ada94].

We first introduce the notion of *knot*.

Definition 1.25 (Knot)**.** A *knot* K is an embedding of $\mathcal{S}^1$ into the closed 3-ball B^3

$$K : \mathcal{S}^1 \hookrightarrow B^3 \subset \mathbb{R}^3,$$

i.e. a simple, closed curve in the 3-dimensional space.

In a similar fashion, we introduce *tangles*.

Definition 1.26 (Tangle)**.** A *tangle* T is an embedding of a disjoint union of intervals and circles into the closed 3-ball B^3

$$T : \left((\bigsqcup_{i=1}^{n} I) \sqcup \left(\bigsqcup_{j=1}^{m} \mathcal{S}^1 \right), \partial \right) \hookrightarrow \left(B^3, S \subset \partial B^3 \right)$$

such that the endpoints of the interval lie on a fixed, oriented circle $S \cong \mathcal{S}^1$ contained in the boundary of B^3, together with a labelling of the arcs of $S \setminus \mathrm{im}(T)$. We call a tangle $2n$*-ended* if the number of intervals is n. Moreover, the images of the intervals are called *open components*, the images of the circles are called *closed components*; these components are usually labelled by variables $t_1, t_2, \ldots$, which we call *colours of* T.

Remark 1.27. We will mainly focus on 4-ended tangles without any closed components, that is, tangles of the form

$$T : (I_1 \sqcup I_2, \partial) \hookrightarrow \left(B^3, S \subset \partial B^3 \right).$$

However, we will discuss tangles in general, including 4-ended tangles that admit closed components. We will make it clear when we are restricting ourselves to the family of 4-ended tangles without closed components.

We will consider knots and tangles up to *ambient isotopy*, defined as follows.

Definition 1.28 (Ambient isotopy)**.** Let K and L be two knots $B^3 \subset \mathbb{R}^3$. An *ambient isotopy* from K to L is a continuous map $\phi : B^3 \times [0,1] \to B^3$ such that:

1. for each $t \in [0,1]$, $\phi_t : B^3 \to B^3$ is a homeomorphism;
2. $\phi_0 = \mathrm{id}$, the identity map on B^3;
3. $\phi_1 \circ K = L$.

Note that the orientation must be preserved by any ambient isotopy.

The definition for the tangle case is analogous, with the only difference being that we require ϕ_t to keep the boundary of B^3 fixed, for any $t \in [0,1]$.

When we want to say that two tangles (or knots) A_1 and A_2 are isotopic, we write $A_1 \simeq A_2$.

Remark 1.29 (On the definition of ambient isotopy)**.** We can visualise a knot as a string in the 3-dimensional ball, and a $2n$-ended tangle as a collection of n strings and m circles in the 3-dimensional ball, with the endpoints of the strings laying on the fixed circle $\mathcal{S}$. An *ambient isotopy* is the act of rearranging these strings in 3-dimensional space (hence the word *ambient*) without allowing any string to pass through any other string (including itself) and allowing any deformation of the strings (hence the word *isotopy*). Moreover, for a tangle, we do not allow moving the endpoints of the strings or modifying the orientation of the fixed circle $\mathcal{S}$.

Notice that in an ambient isotopy, we are not allowed to erase some part of the knot or tangle by shrinking any part of it down to a point.

Remark 1.30 (On the definition of ambient isotopy for tangles)**.** The definition of ambient isotopy given above is something in the middle between allowing all the isotopies and allowing only isotopies that fix the whole boundary sphere. In this way, we construct equivalence classes in a reasonable way, differentiating between the right tangles. For instance, if the classes were obtained by quotienting for all the isotopies, all the rational tangles (for the reader that do not knows what a rational tangle is, we will define them in Section 1.5) would fall in the same class. In the same way, fixing all the boundary would be a too rigid requirement.

To represent knots and tangles on paper, we define their *diagrams*.

Definition 1.31 (Knot diagram)**.** A *knot diagram* E is immersion of $\mathcal{S}^1$ into the closed 2-disc

$$E : \mathcal{S}^1 \looparrowright \mathbb{D}^2 \subset \mathbb{R}^2,$$

where all the self-intersections are transverse.

Moreover, we require that the image is a graph with the following properties:

1. vertices can only have valence 4;
2. every vertex carries the under/over information.

We call *regions* the connected components of $\mathbb{D}^2 \setminus \mathrm{im}(E)$.

Definition 1.32 (Tangle diagram)**.** A *tangle diagram* D is an immersion of intervals and circles into the closed 2-disc,

$$D : \left((\bigsqcup_{i=1}^{n} I) \sqcup \left(\bigsqcup_{j=1}^{m} \mathcal{S}^1 \right), \partial \right) \looparrowright \left(\mathbb{D}^2, \partial \mathbb{D}^2 \right),$$

where all the self-intersections are transverse.

Moreover, we require that the image is a graph with the following properties:

1. vertices can only have valence 1 or 4;
2. every 4-valent vertex carries the under/over information;
3. we have a labelling with some index set $\{a, b, c, \dots\}$ of the arcs on the border of $\mathbb{D}^2$ minus the image of D, i.e $\partial \mathbb{D}^2 \setminus D(\partial (\sqcup_{i=1}^{n} I))$.

We call *regions* the connected components of $\mathbb{D}^2 \setminus \mathrm{im}(D)$; the ones that intersect $\partial \mathbb{D}^2$ are called *open regions*, the others *closed regions*. We say that a diagram is *connected* if for any open regions we have that its intersection with $\partial \mathbb{D}^2$ is connected.

From here, unless specified otherwise, diagrams are assumed to be connected and have at least one crossing.

Remark 1.33 (Knots, tangles and their diagrams)**.** We want to understand how loose we can be with the notation when speaking of a knot or a tangle and one of its diagrams. We claim that it is always possible to pass from one to the other without troubles. We prove that it is possible to so for tangles and tangles diagrams, the knot case is done analogously.

We start with a tangle diagram D for some tangle T, we want to reconstruct the tangle starting from D. Let us consider the image of D to stay in the plane $\{z = 0\}$, i.e. $\mathrm{Im}(D) \subset \mathbb{D}^2 = B^3 \cap \{z = 0\}$. We can construct T by pushing the components of the singularities of the immersion D into $\{z < 0\}$ and $\{z > 0\}$, deciding which one goes where using the under/over data of the crossing.

We now see how to construct a diagram starting from a tangle. Let T be a tangle, consider an embedded disc $\mathbb{D}^2 \subset B^3$ bounding the fixed circle $S \cong \mathcal{S}^1$. Then we can generate a well-defined tangle diagram D for the tangle by simply projecting B^3 onto this disc $\mathbb{D}^2$.

Therefore, when we will talk about a tangle (respectively, knot) diagram, it will be clear which unique tangle (respectively, knot) is represented by it.

Clearly there are multiple ways to represent the same knot or the same tangle with a diagram, and by moving the perspective to the 3-dimensional context and operating some ambient isotopy it is clear when two diagrams represent the same object. To express ambient isotopies in a diagram, we use *Reidemeister moves*, which help us to to move between diagrams representing the same knot or tangle without having to work in the 3-dimensional space. We now define these moves, more details can be found in [Ada94], Section 1.3.

Definition 1.34 (Reidemeister moves)**.** We call *Reidemeister moves* the following three operations that we can do on a knot or a tangle diagram. In each of these move, we are assuming to change the diagram only locally in the section stated, leaving all the rest unchanged.

- The first Reidemeister move is called *twist move*; it allows us to put in or take out a twist in the diagram.

Figure 1.3: The first Reidemeister move.

- The second Reidemeister move is called *poke move*; it allows us to either add two crossings or remove two crossings.

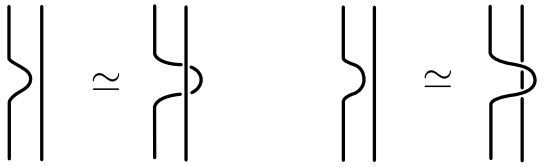

Figure 1.4: The second Reidemeister move.

- the third Reidemeister move is called *slide move*; it allows us to slide a strand of the diagram from one side of a crossing to the other side of the crossing.

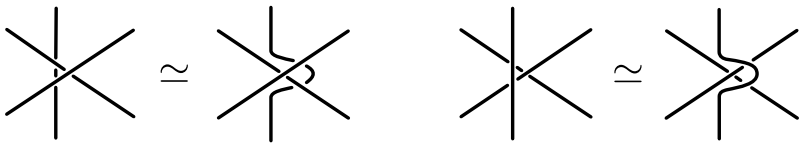

Figure 1.5: The third Reidemeister move.

In 1926, Reidemeister proved the following result.

Theorem 1.35 (Reidemeister, 1926)**.** *If we have two distinct projections of the same knot, we can get from the one to the other via a series of Reidemeister moves and planar isotopies.*

It is possible to generalise such result in the case of tangles, as follows.

Proposition 1.36 ([Zib17])**.** *Let T_1 and T_2 be two oriented connected tangle diagrams that represent the same tangle. Then it is possible to obtain T_2 operating a sequence of Reidemeister moves T_1, obtaining connected diagrams as intermediate steps.*

Proof ([Zib17]). By Reidemeister's theorem (Theorem 1.35), it follows that we can always find a sequence of Reidemeister moves connecting the two diagrams.

We want now to ensure that all intermediate diagrams are connected. Let t_1 be one open strand of the tangle that is near the boundary; before starting the sequence of Reidemeister moves, we deform t_1 following the boundary of the disk, so that it goes once around the whole diagram, using the second Reidemeister move when we find another strand in our way, "isolating" the border regions of the diagram. We now apply the sequence of Reidemeister moves and we undo the move done on t_1 once we have arrived at T_2. □

1.4 A covering space for $\mathcal{S}_4^2$

To proceed with our discussion on tangles and to define *rational tangles*, we need to define a covering space for the 4-punctured sphere $\mathcal{S}_4^2$. This will be necessary on multiple occasions, such as when we talk about the invariants yielded by HFT.

As main reference for this section, one can see Section 2.2 of [Aub22].

Recall that we defined a 4-ended tangle as an embedding

$$T : \left((I \sqcup I) \sqcup \left(\bigsqcup_{j=1}^{m} \mathcal{S}^1\right), \{v_1, v_2, u_1, u_2\}\right) \hookrightarrow \left(B^3, \mathcal{S} \subset \partial B^3\right),$$

where we denoted by v_1, v_2, u_1, u_2 the endpoints of the two open strings, which are mapped to $T(v_1), T(v_2), T(u_1), T(u_2) \subset \mathcal{S}$, where $\mathcal{S} \cong \mathcal{S}^1$ is the fixed circle on ∂B^3.

Definition 1.37 ($\mathcal{S}_4^2$)**.** We define the 4-punctured sphere to be $\mathcal{S}_4^2 = \partial\left(B^3\right) \setminus (\partial(\mathrm{Im}T))$. We are going to refer to the 4 punctures as north-west, south-west, south-east and north-east.

Hence, the images of the strings' ends $T(v_1), T(v_2), T(u_1), T(u_2)$ divide $\mathcal{S}$ into four components, which we call $\boldsymbol{\alpha}$*-arc sites* (or simply *sites*), denoted by the letters a, b, c, d starting from the component between the north-west and south-west punctures and going counter-clockwise. We will use colours to identify the different sites: red for a, blue for b, green for c and yellow for d (see Figure 1.6). Notice that these arcs divide $\mathcal{S}_4^2$ in two components, that we can distinguish thanks to the orientation of $\mathcal{S}$: the *back component* and the *front component*. The back component is the one whose boundary orientation agrees with the orientation of $\mathcal{S}$ (using the right-hand rule and a normal vector field pointing into B^3), the other one is the front component.

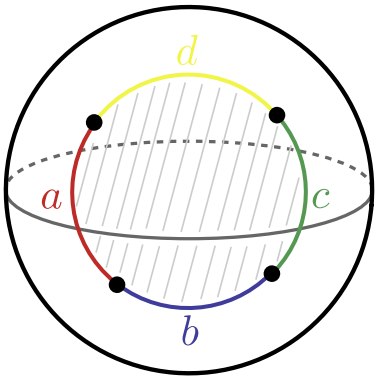

Figure 1.6: The 4-punctured sphere S_4^2 with colours on the sites.

We can now construct a covering space for $\mathcal{S}_4^2$, namely

$$\mathbb{R}^2 \setminus \mathbb{Z}^2 \xrightarrow{\eta} \mathcal{S}_4^2.$$

To prove that this is a covering space, we see how we can regard the 4-punctured sphere as a quotient of $\mathbb{R}^2 \setminus \mathbb{Z}^2$. Let G be the subgroup of the isometries of $\mathbb{R}^2 \setminus \mathbb{Z}^2$ generated by s_v and ρ, where s_v is the translation for a vector $v \in (2\mathbb{Z})^2$ (we take "even vectors" so that that translations of the front is mapped to the front and translations of the back to the back) and ρ is the rotation $(x, y) \mapsto (-x, -y)$; we

then obtain $\mathcal{S}_4^2 \cong \left(\mathbb{R}^2 \smallsetminus \mathbb{Z}^2\right)/G$. Therefore, we obtain the covering space induced by the projection

$$\mathbb{R}^2 \smallsetminus \mathbb{Z}^2 \xrightarrow{\eta} \left(\mathbb{R}^2 \smallsetminus \mathbb{Z}^2\right)/G \cong \mathcal{S}_4^2.$$

See Figure 1.7 for a visualisation of the covering space.

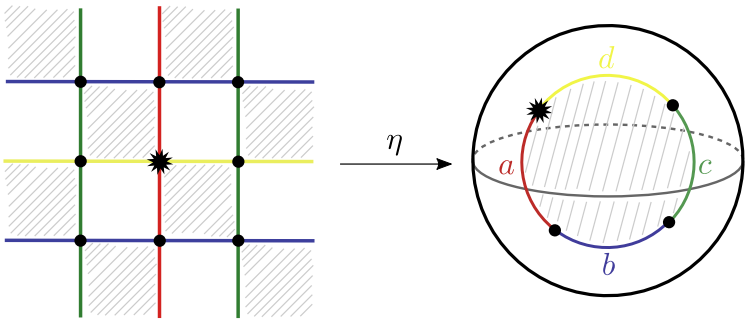

Figure 1.7: Covering space for $\mathcal{S}_4^2$.

Lemma 1.38. *Let $G = \langle s_v, \rho \mid v \in (2\mathbb{Z})^2 \rangle$, with ρ, s_v as above defined. Then, $G \cong (\mathbb{Z}/2) \ltimes (2\mathbb{Z})^2$.*

Sketch of proof. Notice that

- $\rho^2 = id$;
- $\rho \circ s_v = s_{-v} \circ \rho$ for any $v \in (2\mathbb{Z})^2$;
- $s_v \circ s_w = s_{v+w}$ for any $v, w \in (2\mathbb{Z})^2$.

We then have the following bijection of sets

$$\begin{aligned} (\mathbb{Z}/2) \ltimes (2\mathbb{Z})^2 &\xrightarrow{\cong} G \\ (r, v) &\longmapsto \rho^r \circ s_v. \end{aligned}$$

At the level of groups, we obtain $G \cong (\mathbb{Z}/2) \ltimes (2\mathbb{Z})^2$ as we wanted, where the multiplication in the semi-direct product has to be read from right to left (since it is a composition of functions) and it is given by

$$(r_2, v_2) \circ (r_1, v_1) = (r_1 + r_2, v_1 + (-1)^{r_1} v_2)\,.$$

□

We now see how the action of $SL_2(\mathbb{Z})$ in $\mathbb{R}^2 \smallsetminus \mathbb{Z}^2$ induces an action on the 4-punctured sphere, namely the generation of *half-twists*. The group of 2×2 matrices with entries in $\mathbb{Z}$ is generate by τ_1 and τ_2, where

$$\tau_1 = \begin{pmatrix} 1 & 1 \\ 0 & 1 \end{pmatrix} \qquad\qquad \tau_2 = \begin{pmatrix} 1 & 0 \\ 1 & 1 \end{pmatrix}.$$

Observe now that for any $\tau \in SL_2(\mathbb{Z})$ we have that

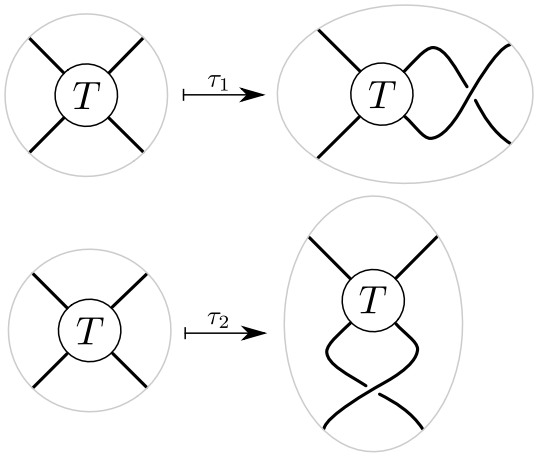

Figure 1.8: Action of $SL_2(\mathbb{Z})$ on $\mathcal{S}^2_4$.

- $\tau \circ s_v = s_{\tau(v)} \circ \tau$ for any $v \in (2\mathbb{Z})^2$;
- $\tau \circ \rho = \rho \circ \tau$.

Therefore, the action of $SL_2(\mathbb{Z})$ on $\mathbb{R}^2 \setminus \mathbb{Z}^2$ induces an action on the quotient $\mathcal{S}^2_4 \cong \left(\mathbb{R}^2 \setminus \mathbb{Z}^2\right)/G$; we still denote the generators of this action by τ_i for $i = 1, 2$. We can visualise this action on $\mathcal{S}^2_4$ as done in Figure 1.8. It is then clear that τ_1 is a *horizontal half-twist*, i.e. the addition of a crossing on the right and that τ_2 is a *vertical half-twist*, i.e. the addition of a crossing on the bottom.

Remark 1.39 (Action of $SL_2(\mathbb{Z})$ on some lines in $\mathbb{R}^2$)**.** It is worth to spend a couple of words about the action of $SL_2(\mathbb{Z})$ on some lines in the plane passing through the origin, as we will need this notion to discuss HFT. Consider the line of slope p/q, for $p, q \in \mathbb{Z}$ coprime, namely $X = \left\{ t \cdot \begin{pmatrix} q \\ p \end{pmatrix} \,\middle|\, t \in \mathbb{R} \right\}$. Then, for any $n \in \mathbb{Z} \setminus \{0\}$ we have that

$$\tau_1^n(X) = \left\{ t \cdot \begin{pmatrix} q \\ p + n \cdot q \end{pmatrix} \,\middle|\, t \in \mathbb{R} \right\}$$

which is the line of slope $(p + nq)/q = n + p/q$ and

$$\tau_2^n(X) = \left\{ t \cdot \begin{pmatrix} n \cdot p + q \\ p \end{pmatrix} \,\middle|\, t \in \mathbb{R} \right\}$$

which is the line of slope $p/(np + q) = 1/(n + q/p)$.

1.5 Rational tangles

We will now focus on the family of *rational tangles*. This type of tangle will prove useful later on when constructing Heegaard diagrams for general tangles. Specifically,

we will often cut a tangle into rational pieces, construct diagrams for each piece, and then glue them back together to obtain a Heegaard diagram for the initial tangle.

For this section, we mainly follow [Aub22], Sections 2.2 and 2.3.

Rational tangles are a special type of 4-ended tangles with a unique property: they can be fully described using a fraction of the form p/q, where p and q are coprime integers and q is positive. We will usually write that $p/q \in \mathbb{Q}\mathrm{P}^1$, where $\mathbb{Q}\mathrm{P}^1$ is the rational projective line, represented as $\mathbb{Q}\mathrm{P}^1 \cong \mathbb{Q} \cup \{\infty\}$. One can think of elements of $\mathbb{Q}\mathrm{P}^1$ as the reduced slopes of lines in $\mathbb{Q}^2$, where $\infty = 1/0$ corresponds to the vertical line.

We start by defining the 0 rational tangle and the ∞ rational tangle.

Definition 1.40 (0 rational tangle and ∞ rational tangle)**.** We call *0 rational tangle* (or *0 tangle*) the unknot tangle with two horizontal strings; it is denote by Q_0.

We call ∞ *rational tangle* (or ∞ *tangle*) the unknot tangle with two vertical strings; it is denote by Q_∞.

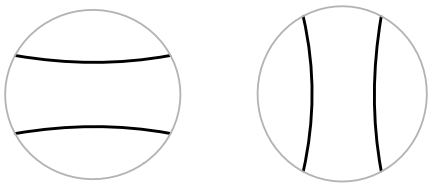

Figure 1.9: 0 rational tangle (on the left) and ∞ rational tangle (on the right).

To define all rational tangles, we need the notion of continued fraction.

Definition 1.41 (Continued fraction)**.** Let $n \in \mathbb{Z}_{>0}$, $a_1, \dots, a_n \in \mathbb{Z}$ and $a_i \neq 0$ for $i = 2, \dots, n$. We define the *continued fraction* $[a_1, a_2, \dots, a_n]$ as

$$[a_1, a_2, \dots, a_n] := a_1 + [a_2, \dots, a_n]^{-1},$$

with the convention that $[\ ] = \infty$.

Remark 1.42 (On the name "continued fraction")**.** The name "continued fraction" is justified by the behaviour of these objects. In fact, given a continued fraction $A = [a_1, a_2, \dots, a_n]$, it behaves as the fraction

$$[a_1, a_2, \dots, a_n] \approx a_1 + \cfrac{1}{a_2 + \cfrac{1}{a_3 + \cfrac{1}{\ddots + \cfrac{1}{a_n}}}}.$$

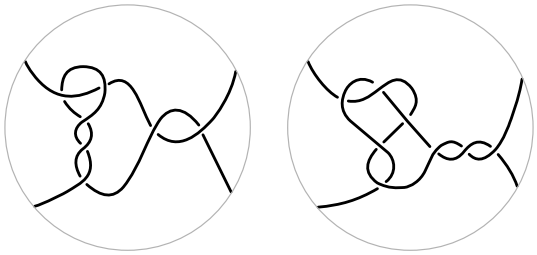

Figure 1.10: Two rational tangles that come from different continued fractions but are equivalent.

We have therefore a map that sends a continued fraction to an element of $\mathbb{Q}\mathrm{P}^1$. This map is evidently not injective; for instance, $A_1 = [2, 3, -2]$ and $A_2 = [3, -2, 3]$ have the same image:

$$A_1 \mapsto 2 + \frac{1}{+3 - \frac{1}{2}} = -2 + \frac{2}{5} = \frac{12}{5}$$
$$A_2 \mapsto 3 + \frac{1}{-2 + \frac{1}{3}} = 3 - \frac{3}{5} = \frac{12}{5}.$$

We therefore write $A_1 \equiv A_2 \in \mathbb{Q}\mathrm{P}^1$ if two continued fractions A_1, A_2 are sent to the same element of $\mathbb{Q}\mathrm{P}^1$ by this map.

We can now link this notion of continued fraction with the construction of some particular tangles. Recall the operators τ_1 and τ_2, defined in Section 1.4, which add half-twists to a tangle. When we talk about (half-) twists, we distinguish between *positive twists* and *negative twists*: these are defined by the slope of the over-strand: it that is positive, then the twist is positive, otherwise it is a negative twist. Hence, we will write τ_i^n for $n \in \mathbb{Z}$ to indicate the operation of adding n half-twists, positive if $n > 0$ and negative otherwise.

We can now define rational tangles.

Definition 1.43 (Rational tangles)**.** *Rational tangles* are 4-ended tangles without any closed components that are obtained from attaching twists to the bottom and to the right of the 0 tangle or the ∞ tangle.

Given a continued fraction $A = [a_1, a_2, \ldots, a_n]$, we define the rational tangle Q_A as

$$Q_A = \begin{cases} \tau_1^{a_1}\tau_2^{a_2}\ldots\tau_2^{a_n}Q_\infty & \text{if } n \text{ is even;} \\ \tau_1^{a_1}\tau_2^{a_2}\ldots\tau_1^{a_n}Q_0 & \text{if } n \text{ is odd.} \end{cases}$$

An intuitive way to describe rational tangles is to give a succession of half-twist to attach to one of the trivial tangles.

This notation is quite intuitive, but unfortunately it is not very effective if we want to have substantially different tangles from different inputs: for instance, the tangles defined by $[2, 3, -2]$ and $[3, -2, 3]$ are actually equivalent (Figure 1.10).

In 1970, John H. Conway proved the following theorem, for which a combinatorial proof was given in [KL04]. Thanks to this result, it is fairly easy to check whether or not two rational tangles are equivalent.

Theorem 1.44 (Conway, [Con70])**.** *Let A_1 and A_2 be two continued fractions. The rational tangles Q_{A_1} and Q_{A_2} are isotopic if and only if $A_1 \equiv A_2 \in \mathbb{Q}\mathrm{P}^1$.*

Hence, using continued fractions it is possible to see when two rational tangles are actually equivalent. We can try to see it in the previous example with $T_1 = Q_{[2,3,-2]}$ and $T_2 = Q_{[3,-2,3]}$: as seen in Remark 1.42, the continued fractions are sent to the same element of $\mathbb{Q}\mathrm{P}^1$. Therefore T_1 and T_2 are indeed the same rational tangle and we are going to denote it by $Q_{12/5}$.

In general, given the cleaned continued fraction p/q for $p, q \in \mathbb{Z}$ coprime, we denote the associated rational tangle by $Q_{p/q}$.

1.6 Arithmetic of 4-ended tangles

One characteristic of 4-ended tangles that we will exploit in Chapter 5 is that we can define arithmetic operations on them. This arithmetic of tangles will help us simplify the notation and gain a deeper understanding of why the class of rational tangles is so special. The operations that we are going to define are:

- addition,
- multiplication,
- rotation,
- mirroring,
- inversion,
- flipping.

All of these are well-defined up to isotopy; therefore we can consider them as operations between classes of tangles.

For this section we mainly follow Section 2 of [KL04] and we assume all the tangles to be 4-ended tangles.

We begin with the two operations that involve a pair of tangles.

Definition 1.45 (Addition, multiplication)**.** Let T and S be two tangles, which we represent as a circle (inside which the tangle has all its twists) with four strings that come out from the angles, the ends of the 2 strings of it.

We define the *sum* $T + S$ and the *multiplication* $T * S$ of the tangles as it is shown in Figure 1.11.

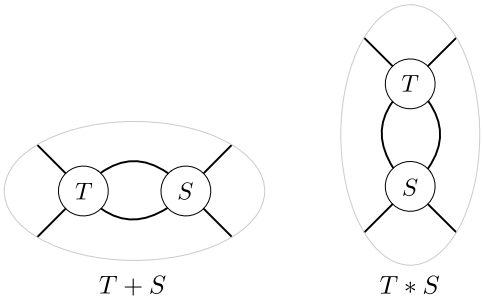

Figure 1.11: Sum and multiplication of two 4-ended tangles.

The remaining operation are defined on a single tangle, as follows.

Definition 1.46 (Rotation)**.** We define the *rotation* of a tangle T_*, denoted by $r(T_*)$, to be a counter-clockwise rotation of the tangle by $\pi/2$.

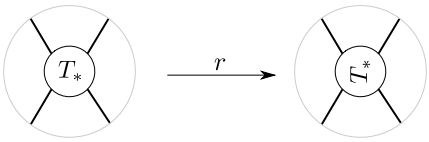

Figure 1.12: Rotation of a tangle T_*.

Definition 1.47 (Mirror image)**.** We define the *mirror image* of a tangle T, denoted by $m(T)$, to be the tangle obtained by swapping all the crossings of T.

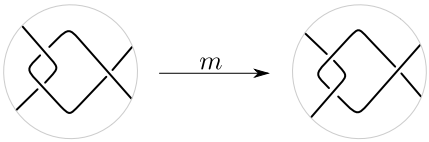

Figure 1.13: Mirror image of a tangle.

Definition 1.48 (Inverse)**.** We define the *inverse* of a tangle T, denoted by $i(T)$, to be the tangle $m(r(T))$.

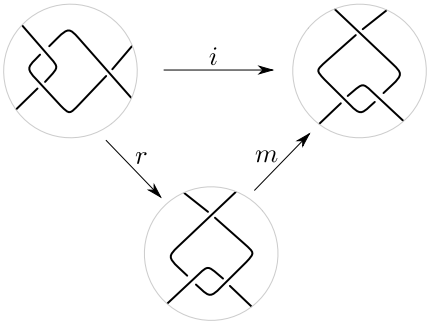

Figure 1.14: Inverse of a tangle.

Remark 1.49. There are several properties that one could prove that explain better of how these operations behave when composed. For instance, one can prove that $m(T + S) = m(T) + m(S)$, $m(T * S) = m(T) * m(S)$ or that for rational tangles holds $m(Q_{p/q}) = Q_{-p/q}$.

Another operation that will be very useful is the *flip* of a tangle.

Definition 1.50 (Flip)**.** Let T_* be a tangle. A *flip* is a rotation in the third dimension by π around some axis. We define the *horizontal flip of* T_*, denoted by T_*^{hflip}, as its rotation around the horizontal axis and the *vertical flip of* T_*, denoted by T_*^{vflip}, as its rotation around the vertical axis.

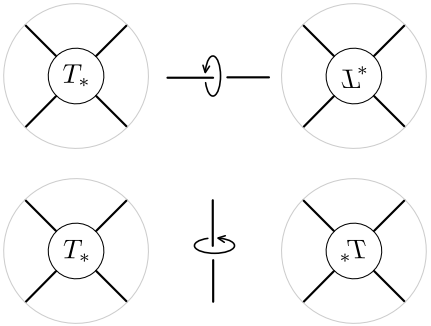

Figure 1.15: Horizontal flip (on top) and vertical flip (on bottom).

Lastly, we define a particular isotopy obtained with a composition of the above operations. This isotopy will be essential to prove an important result of stability result for rational tangles under certain operations. Consider a tangle T_* and apply the following isotopy: fix the four ends of the tangle and flip only the inner box either horizontally or vertically. A graphical representation of this operation can be found in Figure 1.16

The fact that this is an isotopy comes straight from the definition, as we are just re-arranging the inner part of the tangle in the 3-dimensional space without moving the endpoints. using the newly acquired vocabulary, we can say that we proved

$$T_* \simeq Q_1 * T_*^{vflip} * Q_{-1}$$
$$T_* \simeq Q_1 + T_*^{hflip} + Q_{-1}.$$

Hence, using the fact that the operations are well-defined between classes of isotopy, we can add Q_{-1} to both sides of both equations and obtain

$$Q_{-1} * T_* \simeq T_*^{vflip} * Q_{-1}$$
$$Q_{-1} + T_* \simeq T_*^{hflip} + Q_{-1},$$

since for the second Reidemeister move $Q_{-1} + Q_1 \simeq Q_0 \simeq Q_{-1} * Q_1$. Similarly, it also holds

$$Q_1 * T_* \simeq T_*^{vflip} * Q_1$$
$$Q_1 + T_* \simeq T_*^{hflip} + Q_1.$$

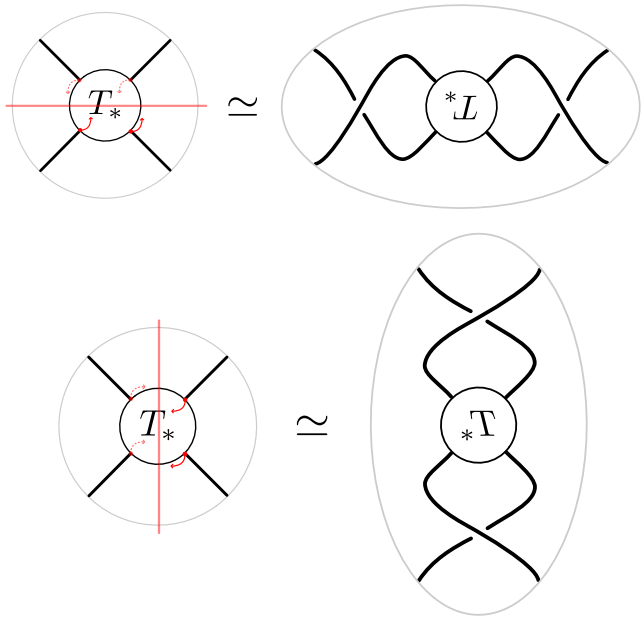

Figure 1.16: Flipping of the inner box with the ends fixed, horizontally (on top) and vertically (on bottom).

Definition 1.51 (Flype)**.** We call *flypes* the isotopies of the above form. We distinguish between *horizontal flypes* and *vertical flypes* according with the above definition of flips.

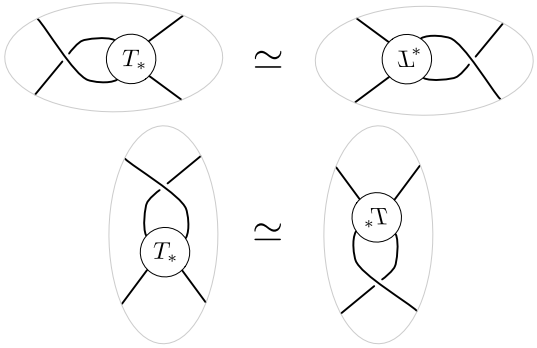

Figure 1.17: Flype isotopies for a tangle T_*: horizontal flype (on top) and vertical flype (on bottom).

We are now able to prove a Lemma which states three distinctive properties of rational tangles, which will be of use in Chapter 5.

Lemma 1.52 (Flipping Lemma, [KL04])**.** *Let R be a rational tangle. Then*

1. $R \simeq R^{vflip}$;
2. $R \simeq R^{hflip}$;

3. $R \simeq i(i(R)) = r(r(R))$.

Proof ([KL04]). The proof of the first two isotopies is done by induction on the number of crossings. It is clear that the statement holds in the base case, i.e. when R is Q_∞, Q_1 or Q_{-1}. Suppose it to be true for all the rational tangles with n crossings. Let R be a rational tangle with $n+1$ crossings; we have then eight possible cases:

(a) $R = L + Q_{\pm 1}$,

(b) $R = Q_{\pm 1} + L$,

(c) $R = L * Q_{\pm 1}$,

(d) $R = Q_{\pm 1} * L$,

where L is a suitable rational tangle with n crossings. We then prove case (a) as in Figure 1.18 and (d) as in Figure 1.19. The other cases are done analogously.

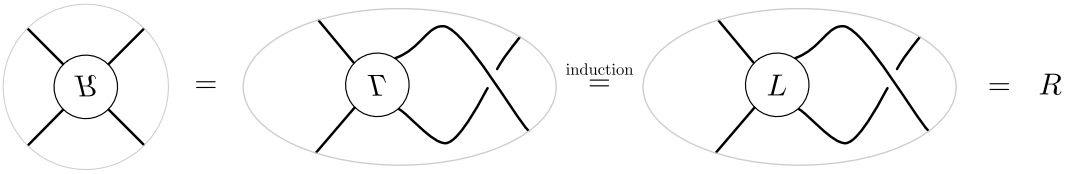

Figure 1.18: Inductive proof of the Flipping Lemma, case (a).

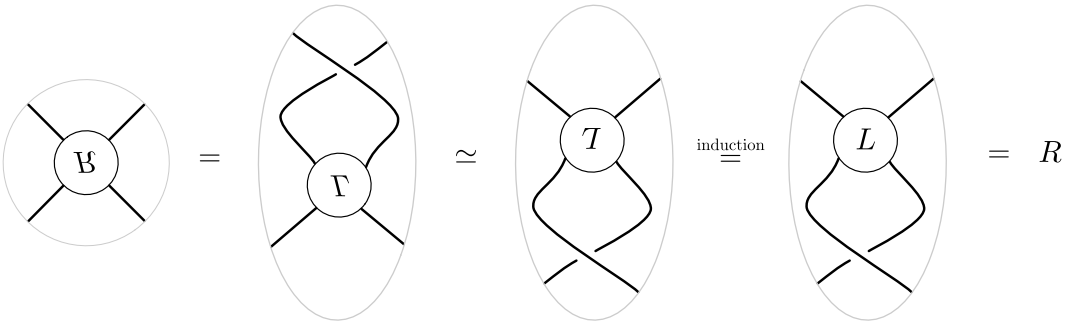

Figure 1.19: Inductive proof of the Flipping Lemma, case (d). The isotopy comes from a vertical flype and the equality comes from applying induction two times.

Lastly, the proof of the third isotopy follows from the first two, as we have $i(i(R)) = \left(R^{hflip}\right)^{vflip} = r(r(R))$. □

Apply the Flipping Lemma to the definition of flype, we obtain the following corollary.

Corollary 1.53. *For R a rational tangle holds*

$$Q_{\pm 1} + R \simeq R + Q_{\pm 1}$$
$$Q_{\pm 1} * R \simeq R * Q_{\pm 1}.$$

Therefore, more generally, we have that the rational tangles of the form $Q_{\pm n}$ commute with any other rational tangle under addition and that $Q_{\pm 1/n}$ commute with any other rational tangle under multiplication.

Remark 1.54. The above corollary justify the definition of rational tangle gave in Section 1.5: in fact, one could define a rational tangle to be a tangle obtained from Q_0 or Q_∞ by a succession of twists operate on any two adjacent ends of the tangle (not only on the right or on the bottom as we did). But then, with Corollary 1.53, we are able to take a rational tangle constructed with this other definition and "push" all the twists on the right and on the bottom of the tangle, obtaining a rational tangle according to the definition that we gave.

1.7 Bordered and sutured manifolds

The focus of this thesis is on 4-ended tangles and Tangle Floer Homology HFT. In [Zib17], the author established a close correlation between HFT, Sutured Floer Homology SHF (developed by Andreas Juhász in [Juh06]) and Bordered Sutured Floer Homology (developed by Rumen Zarev in [Zar11]). Therefore, we briefly review bordered manifolds from the perspective of Bordered Heegaard Floer Homology and discuss sutured manifolds and bordered sutured manifolds to provide a better understanding of the context in which we are working.

The interest in the theory of bordered sutured manifolds stems from the possibility of gluing such manifolds together and the good behavior of this gluing at the level of invariants, which is described by a useful gluing formula for Bordered Sutured Floer Homology ([Zar11]). This gluing property was then adapted to the tangle case by utilizing arguments from Bordered Sutured Floer Homology; further details can be found in Section II.3 of [Zib17].

1.7.1 Bordered manifolds

For this subsection, one can use Sections 3.2 and 4.1 of [LOT18] as reference.

In Section 1.1, we introduced the classical notion of 3-manifolds with a boundary. However, to use this concept in the context of Bordered Heegaard Floer Homology, we need to briefly review it with the help of the notion of *pointed matched circles*.

Definition 1.55 ((Pointed) Matched circle)**.** A *matched circle* is a triple $(Z, \mathbf{a}, M)$, where

1. Z is of an oriented circle,
2. $\mathbf{a} = \{a_1, \dots, a_{4k}\} \subset Z$ is a set of $4k$ distinct points (which we regard as 0-spheres),
3. M is a matching (i.e. a 2-to-1 map $\mathbf{a} \to \{1, \dots, 2k\}$).

Moreover, we require the following property

4. if we perform surgery along the $2k$ pairs of points in Z, we obtain a single circle and not several disjoint circles.

A *pointed matched circle* $\mathcal{Z}$ is a matched circle together with a basepoint $z \in Z \setminus \mathbf{a}$.

Remark 1.56 (Order on $\mathbf{a}$)**.** For a pointed matched circle, there is an order in $\mathbf{a}$ induced by the orientation of Z, with the minimum that is the first point encountered starting from the basepoint.

Remark 1.57. We will represent a pointed matched circle either as a circle or as a segment, whose endpoints are identified and are the basepoint z. See Figure 1.20

Given a pointed matched circle $\mathcal{Z}$, we can construct a unique genus k surface $F(\mathcal{Z})$, called the *surface associated to* $\mathcal{Z}$, in the following way. We take a disc with boundary, whose boundary is Z, and we attach oriented 2-dimensional 1-handles along the pairs specified by M. Then, for condition 4 in the definition, we obtain one boundary component homeomorphic to a circle and we fill it with another disc.

Example 1.58. If we take the pointed circle in Figure 1.20, then the surface represented is the torus.

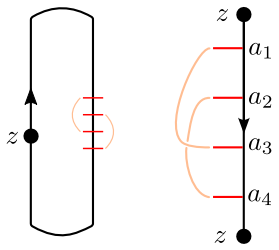

Figure 1.20: Pointed matched circle representing the torus: as a circle (left) and as a segment with identified endpoints (right).

We can now define bordered manifolds in this context, a subclass of 3-manifolds with boundary characterised by having the boundary parametrised by a pointed matched circle.

Definition 1.59 (Bordered 3-manifold)**.** A *bordered 3-manifold* is s triple $(Y, \mathcal{Z}, \phi)$, where

- Y is a compact, oriented 3-manifold with connected boundary ∂Y,
- $\mathcal{Z}$ is a pointed matched circle,
- $\phi : F(\mathcal{Z}) \to \partial Y$ is an orientation-preserving homeomorphism.

We say that two bordered 3-manifolds $(Y, \mathcal{Z}, \phi)$ and $(Y', \mathcal{Z}', \phi')$ are *equivalent*, if there exists an orientation-preserving homeomorphism $\psi : Y \to Y$ such that $\phi' = \psi \circ \phi$.

Remark 1.60. To simplify notation, we will often just refer to $(Y, \mathcal{Z}, \phi)$ as Y. Additionally, we will be considering the equivalence class of bordered 3-manifolds that are equivalent to $(Y, \mathcal{Z}, \phi)$.

1.7.2 Sutured manifolds

For this subsection, we mainly follow Sections 2.1 and 3.1 of [Zar09].

We first build our way to *sutured manifolds*; we do this via *divided surfaces*.

Definition 1.61 (Divided surface)**.** A *divided surface* (S, Γ) is the data of

- a closed and oriented surface S,
- a set of pairwise disjoint, simple, closed, oriented curves $\Gamma = \{\gamma_1, \dots, \gamma_n\}$ on S, which we call *sutures*.

We then define $R(\Gamma) = S \setminus \Gamma$, where every connected component A has the boundary $\partial A \subset \Gamma$, i.e. $\partial A = \cup_{i \in I} \gamma_i$ for some subset $I \subset \{1, \dots, n\}$. Moreover, we impose the following conditions: let A be a connected component of $R(\Gamma)$, then

- A has non-empty boundary,
- the orientation on ∂A induced from the orientation of S either agrees with the orientation of the suture γ_i on each component of ∂A, or disagrees on every component. If they agree, we say that A is a *positive region*; otherwise, we say that it is a *negative region*.

We then divide $R(\Gamma)$ in two pieces: we call $R_+(\Gamma)$ (or R_+) and $R_-(\Gamma)$ (or R_-) the sets

$$R_+(\Gamma) := \overline{\bigcup_{\substack{A \text{ s.t. is} \\ \text{positive region}}} A} \qquad R_-(\Gamma) := \overline{\bigcup_{\substack{A \text{ s.t. is} \\ \text{negative region}}} A},$$

where the line above indicate the topological closure of the set below.

Remark 1.62. We do not require S to be connected, but since each connected component of $R(\Gamma)$ has a non-empty boundary, we are ensuring that each component has at least one suture.

We then define the notion of balancedness for a divided surface.

Definition 1.63 ((Un-)Balanced divided surface)**.** We say that a divided surface (S, Γ) is *balanced* if $\chi(R_+) = \chi(R_-)$. We say that it is k-unbalanced if $\chi(R_+) = \chi(R_-) + 2k$ for some k non-zero integer.

Remark 1.64. The last definition is well posed, since it is possible to prove that $\chi(R_+) - \chi(R_-)$ is always even. This follows from the facts that S is closed and that $\chi(S) = \chi(R_+) + \chi(R_-)$.

We can define *balanced* and *unbalanced sutured manifolds*.

Definition 1.65 ((Un-)Balanced sutured manifold)**.** We say that (Y, Γ) is a *balanced sutured manifold* if Y is a 3-manifold without closed components such that $(\partial Y, \Gamma)$ is a balanced divided surface.

We say that (Y, Γ) is a *k-unbalanced sutured manifold* if Y is a 3-manifold without closed components such that $(\partial Y, \Gamma)$ is a k-unbalanced divided surface.

Remark 1.66 (Sutured manifold associated to a knot)**.** Following what is done in Section 9 of [Juh06], we see how it is possible to regard knots as particular sutured manifolds.

Consider a knot $K \subset \mathcal{S}^3$. Then, we call $(Y_K, \{s_1, s_2\})$ the *sutured manifold associated to* K, where

- Y_K is the manifold with boundary $Y_K = \mathcal{S}^3 \setminus \nu(K)$, with $\nu(K)$ a tubular neighbourhood of K,
- the sutures s_1 and s_2 are two oppositely oriented meridional circles in some part of ∂Y_K.

1.7.3 Bordered sutured manifolds

We want to discuss a more general class of manifolds, called *bordered sutured manifolds*, which contain both bordered manifolds and sutured manifolds. To do this, we introduce the concept of *arc diagram*, which is a generalisation of the pointed matched circle used to parametrise the boundary of a bordered manifold.

As reference, one can look at Section 3.2 of [Zar09].

Definition 1.67 ((Degenerate) Arc diagram)**.** An *arc diagram* $\mathcal{Z} = (Z, \mathbf{a}, M)$ is a triple consisting of

- a collection $Z = \{Z_1, \dots, Z_l\}$ of oriented, open line segments for some $l \geq 0$,
- a collection $\mathbf{a} = \{a_1, \dots, a_{2k}\}$ of distinct points in Z for some $k \geq 0$; we denote by $|Z_i|$ the cardinality of $Z_i \cap \mathbf{a}$,
- a matching M of $\mathbf{a}$, i.e. a 2–to–1 function $\mathbf{a} \xrightarrow{M} \{1, \dots, k\}$,

Additionally, we require that the arc diagram satisfies the *non-degeneracy condition*, which means that after performing surgery on the 1-manifold Z at each $M^{-1}(i)$, which are homeomorphic to $\mathcal{S}^0$, the resulting 1-manifold cannot contain any closed components. An arc diagram that violates this condition is called *degenerate*.

We put on $\mathbf{a}$ the following order: $a_i < a_j$ if $a_i \in Z_{h_i}$, $a_j \in Z_{h_j}$ and $h_i < h_j$; if two points are on the same line segment, we use the order induced by the orientation of the segment.

Given an arc diagram, we can define its graph.

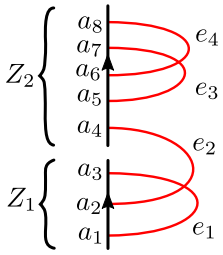

Figure 1.21: Graph of arc diagram.

Definition 1.68 (Graph of an arc diagram)**.** Consider an arc diagram $\mathcal{Z} = (Z, \mathbf{a}, M)$. We define its *graph* $G(\mathcal{Z})$ as the graph obtained by connecting the endpoints of each pair of matched points in $\mathbf{a}$ with a line segment (hence, an edge is added for each pair of matched points). We denote such edges by $e_1, \dots, e_k$, where e_i is the edge associated to the matched points $M^{-1}(i)$. See Figure 1.21 for an example.

We can now define *bordered sutured manifolds*, the class of sutured manifolds on which is defined Bordered Sutured Floer Homology.

Definition 1.69 (Bordered sutured manifold)**.** A *bordered sutured manifold* is a tuple $(Y, \Gamma, \mathcal{Z}, \phi)$, where

- (Y, Γ) is a sutured manifold,
- $\mathcal{Z}$ is an arc diagram,
- $\phi : G(\mathcal{Z}) \hookrightarrow \partial Y$ is an orientation-preserving embedding such that
  - $\phi_{|Z}$ is an orientation preserving embedding into Γ,
  - $\phi(G(\mathcal{Z}) \setminus Z) \cap \Gamma = \emptyset$.

Remark 1.70. From the definition of bordered sutured manifold, it follows that each edge e_i of $G(\mathcal{Z})$ embeds in R_-.

To better prepare us for the construction of Heegaard diagrams for bordered sutured manifolds, we also define *bordered sutured manifolds with $\boldsymbol{\alpha}$- and $\boldsymbol{\beta}$-arcs*, following the approach presented in Section 3.1 of [Zib20]. To achieve this, we first introduce the concept of *arc diagrams of rank k*.

Definition 1.71 (Arc diagram of rank k)**.** We define an *arc diagram of rank k* to be an arc diagram $\mathcal{Z} = (Z, \mathbf{a}, M)$ such that $\mathbf{a}$ contains $2k$ points and requiring also a type between "α" and "β". We usually write $\mathcal{Z}_\alpha$ if it is of type α and $\mathcal{Z}_\beta$ if it is of type β.

Definition 1.72 (Bordered sutured manifold with $\boldsymbol{\alpha}$- and $\boldsymbol{\beta}$-arcs)**.** A *bordered sutured manifold with $\boldsymbol{\alpha}$- and $\boldsymbol{\beta}$-arcs* is a tuple $(Y, \Gamma, \mathcal{Z}_\alpha, \phi_\alpha, \mathcal{Z}_\beta, \phi_\beta)$, where

- (Y, Γ) is a sutured manifold,

- $\mathcal{Z}_\alpha = (Z_\alpha, \mathbf{a}_\alpha, M_\alpha)$ and $\mathcal{Z}_\beta = (Z_\beta, \mathbf{a}_\beta, M_\beta)$ are (possibly degenerate) arc diagrams,
- $\phi_\alpha : G(\mathcal{Z}_\alpha) \hookrightarrow \overline{R_-}$ is an embedding such that $\phi_\alpha(Z_\alpha) \subset \Gamma$,
- $\phi_\beta : G(\mathcal{Z}_\beta) \hookrightarrow \overline{R_+}$ is an embedding such that $\phi_\beta(Z_\beta) \subset \Gamma$,
- $\phi_\alpha(Z_\alpha) \cap \phi_\beta(Z_\beta) = \emptyset$,
- the two arc diagrams are *homologically linear independent*, i.e. the map

$$\pi_0\left(\Gamma \setminus \phi_\alpha(Z_\alpha) \cup \phi_\beta(Z_\beta)\right) \longrightarrow \pi_0\left(\partial Y \setminus (\mathrm{Im}\phi_\alpha \cup \mathrm{Im}\phi_\beta)\right)$$

  is surjective. This condition guarantees that the Bordered Sutured Heegaard Floer Homology is well-defined. It can be shown that this property follows from the others if the arc diagrams are non-degenerate (see Proposition 3.6 of [Zar09]).

Remark 1.73 (Tangles as particular bordered sutured manifolds)**.** We see how we can consider a tangle as a bordered sutured manifold. Recall that we defined the $\boldsymbol{\alpha}$-arc sites of a tangle with n open components to be the connected segments of the fixed circle $\mathcal{S}$ minus the images of the endpoints of the n strings.

Let T be a tangle with n open components and m closed components. We can associate to T a bordered sutured 3-manifold with $\boldsymbol{\alpha}$-arcs $(X_T, \Gamma, \mathcal{Z}_\alpha, \phi_\alpha)$ in the following way:

- the underlying 3-manifold with boundary is $X_T = B^3 \setminus \nu(T)$, where $\nu(T)$ is a tubular neighbourhood of T in B^3;
- we place two oppositely oriented meridional circles around each closed components,
- we place around each tangle end a single suture, where the orientation is chosen such that the boundary of B^3 minus a neighbourhood of the tangle ends lies in R_-,
- on each one of the four sutures around the tangle ends, we place two "ticks", distant from the end points of the $\boldsymbol{\alpha}$-arcs and such that there is one tick in each of the connected component of the suture obtained by removing the $\boldsymbol{\alpha}$-arcs endpoints,
- we define the arc diagram $G(\mathcal{Z}_\alpha)$ via the $\boldsymbol{\alpha}$-arc sites, defining the line segments Z as the suture opened in correspondence of the ticks.

Chapter 2

Heegaard diagrams

In this chapter, we will develop Heegaard diagrams for all the objects defined in Chapter 1. We will start by defining Heegaard diagrams for closed 3-manifolds, which was the first theory historically developed; the construction of these diagrams naturally follows from Heegaard splittings, defined in Section 1.2. However, the construction of the hat version of Heegaard Floer Homology $\widehat{\mathrm{HF}}$ that we will see in Section 3.1 heavily relies on the notion of *pointed Heegaard diagrams*; we define them in Section 2.2 as diagrams to which we add a *basepoint*. This notion of basepoint may seem to appear out of thin air, it is only in the more general context of sutured manifolds that the role of the basepoint becomes better understood. In fact, in Section 2.4, we will see how Heegaard diagrams of closed 3-manifolds can be considered as a special case of Heegaard diagrams of sutured manifolds (Remark 2.35).

2.1 Heegaard diagrams for closed 3-manifolds

We are now ready to discuss Heegaard diagrams for closed 3-manifolds, which allow us to simplify the representation of a Heegaard splitting, "forgetting" about the handlebodies and focus solely on the common surface Σ. This makes Heegaard diagrams a powerful tool for studying 3-manifolds.

The main references for this section are [OS06a] and [Hom19].

We first need to define an object which allows us to retrieve in some way the handlebodies structures from their common boundary Σ.

Definition 2.1 (Set of attaching circles)**.** Let H be a genus g handlebody and let Σ_g be its boundary. A *set of attaching circles* $\Gamma = \{\gamma_1, \dots, \gamma_g\}$ for H is a collection of closed embedded curves in Σ_g with the following properties:

1. the curves γ_i are all disjoint from each other;
2. $\Sigma_g \setminus \Gamma$ is connected;
3. the curves γ_i bound disjoint embedded discs in H.

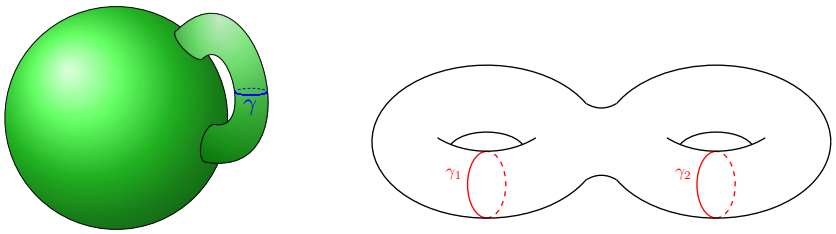

Figure 2.1: Set of attaching circles for a genus 1 (left) and a genus 2 (right) handlebodies.

Remark 2.2. The second property given above is actually equivalent to say that $\{[\gamma_1], \dots, [\gamma_1]\}$ are linearly independent in $H_1(\Sigma, \mathbb{Z})$.

Definition 2.3 (Compatible Heegaard diagram)**.** Consider a genus g Heegaard splitting $Y = H_1 \cup_{\Sigma_g} H_2$ for Y. A *compatible Heegaard diagram* is given by $(\Sigma_g, \boldsymbol{\alpha}, \boldsymbol{\beta})$, where $\boldsymbol{\alpha} = \{\alpha_1, \dots \alpha_g\}$ is a set of attaching circles for H_1, $\boldsymbol{\beta} = \{\beta_1, \dots, \beta_g\}$ is a set of attaching circles for H_2 and the intersections between $\boldsymbol{\alpha}$- and $\boldsymbol{\beta}$-circles are transverse. We are going to draw the $\boldsymbol{\alpha}$-circles in red and the $\boldsymbol{\beta}$-circles in blue.

It is worth noting that a Heegaard splitting of genus > 1 can admit a multitude of compatible Heegaard diagrams. In contrast, given a Heegaard diagram, there exists a unique Heegaard splitting for which it is compatible. Henceforth, we will primarily work with Heegaard diagrams in our discussions.

Example 2.4 (Some examples)**.** We now show some Heegaard diagrams starting from the decompositions given in Example 1.17.

1. **Heegaard diagram of genus 1 of $\mathcal{S}^3$**

   The genus 1 Heegaard splitting of $\mathcal{S}^3$ that we saw in Example 1.17 corresponds to a diagram (Σ, α, β), where the two curves meet transversely at one point x; see Figure 2.2.

2. **Heegaard diagram of genus 1 of $L(p, q)$**

   The genus 1 Heegaard splitting of $L(p, q)$ corresponds to a genus 1 Heegaard diagram (Σ, α, β). Denote by s and t the generators of $H_1(\Sigma) = \mathbb{Z}^2$, as in Figure 2.3; with this notation, the curves of the diagram are given by $[\alpha] = s$ and $[\beta] = qs + pt$, and they intersect at p points.

3. **Heegaard diagram of genus 1 of $L(3, 1)$**

   Let us make a more explicit example with $L(3, 1)$: we have a diagram (Σ, α, β) where $[\alpha] = s$ and $[\beta] = s + 3t$.

Remark 2.5 (Retrieve manifold from its Heegaard diagram)**.** How can we retrieve the original manifold Y from its Heegaard diagram $(\Sigma_g, \boldsymbol{\alpha}, \boldsymbol{\beta})$? We can construct it in the following way: thicken Σ_g to $\Sigma_g \times [0, 1]$ and glue thickened discs along the $\alpha_i \times \{0\}$ and along the $\beta_j \times \{1\}$; the resulting space has two boundary components,

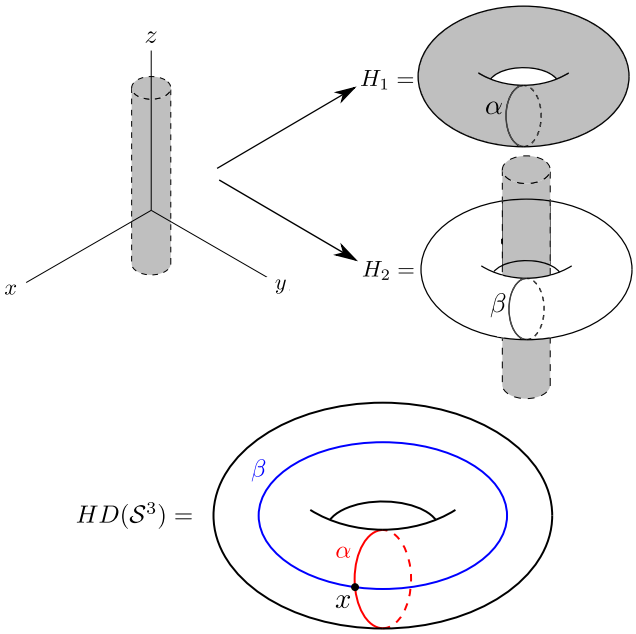

Figure 2.2: Sets of attaching circles for the Heegaard splitting of $\mathcal{S}^3 \simeq \mathbb{R}^3 \cup \{\infty\}$ presented in Example 1.17 (on top) and the respective Heegaard diagram (on bottom).

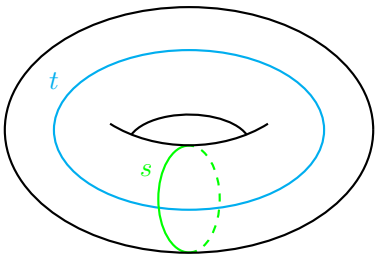

Figure 2.3: Generators of the first homology group of a torus.

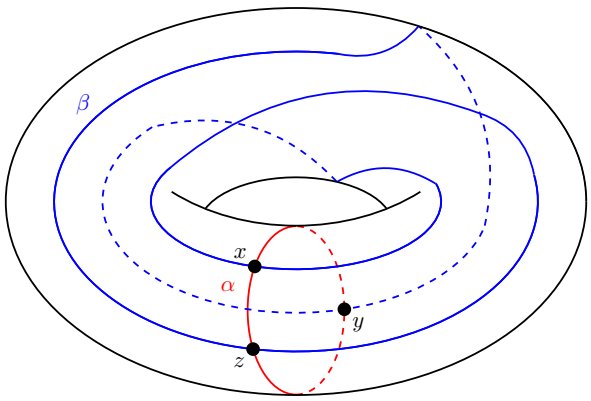

Figure 2.4: Heegaard Diagram of genus 1 for $L(3,1)$.

one "on top" and one "on bottom", each homeomorphic to $\mathcal{S}^2$ and we cap each with a three–ball.

In symbols:

$$\begin{aligned} Y &= H_1 \cup_{\Sigma_g} H_2 \\ &= \Bigg((\Sigma_g \times [0,1]) \underbrace{\sqcup_{\alpha \times I} \left(\mathbb{D}^2 \times I\right)}_{\text{att. circles for } H_1} \underbrace{\sqcup_{\beta \times I} \left(\mathbb{D}^2 \times I\right)}_{\text{att. circles for } H_2} \Bigg) \underbrace{\sqcup_0 \left(B^3\right)}_{\substack{\text{3-ball} \\ \text{attached} \\ \text{"on bottom"}}} \underbrace{\sqcup_1 \left(B^3\right)}_{\substack{\text{3-ball} \\ \text{attached} \\ \text{"on top"}}}. \end{aligned} \tag{$\bowtie$}$$

To conclude this section, we prove the following useful Lemma.

Lemma 2.6. *Let $(\Sigma_g, \boldsymbol{\alpha}, \boldsymbol{\beta})$ be a genus g Heegaard diagram for Y. Then we have the following isomorphism of homology groups*

$$H_1(Y) \cong \frac{H_1(\Sigma_g)}{\langle [\alpha_1], \dots, [\alpha_g], [\beta_1], \dots, [\beta_g] \rangle}. \tag{$\star$}$$

Proof. We consider the genus g Heegaard diagram $(\Sigma_g, \boldsymbol{\alpha}, \boldsymbol{\beta})$ for Y. Recall the construction from the diagram to the manifold given in Remark 2.5 and notice that, if we call $\widetilde{Y}$ the space obtained without attaching the two final balls "on top" and "on bottom", we have that $H_1(Y) \cong H_1(\widetilde{Y})$.

Therefore, we only need to prove $H_1(\widetilde{Y}) \cong H_1(\Sigma_g)/\langle [\alpha_1], \dots, [\alpha_g], [\beta_1], \dots, [\beta_g] \rangle$; in order to do so, we use Mayer-Vietoris on the decomposition

$$\begin{aligned} \widetilde{Y} &= (\Sigma_g \times [0,1]) \ \cup \ \left(\sqcup_{\boldsymbol{\alpha} \times I} \left(\mathbb{D}^2 \times I\right) \ \sqcup_{\boldsymbol{\beta} \times I} \left(\mathbb{D}^2 \times I\right) \right) \\ &= (\Sigma_g \times [0,1]) \ \cup \ A. \end{aligned}$$

If we write down the last terms of the Mayer-Vietoris exact sequence, we obtain

$$\cdots \ H_1(\Sigma_g \times [0,1] \cap A) \xrightarrow{(i_{1*}, i_{2*})} H_1(\Sigma_g \times [0,1]) \oplus H_1(A) \xrightarrow{g_* - j_*} H_1(\widetilde{Y}) \xrightarrow{\ d \ } H_0(\Sigma_g \times [0,1] \cap A) \xrightarrow{(i_{1*}, i_{2*})} H_0(\Sigma_g \times [0,1]) \oplus H_0(A) \xrightarrow{g_* - j_*} H_0(\widetilde{Y}) \longrightarrow 0,$$

where d is the connecting morphism given by Mayer-Vietoris and the other maps are the ones induced by the inclusions

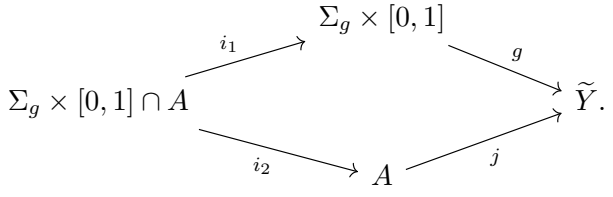

We start by proving that $d \equiv 0$, i.e. that the map (i_{1_*}, i_{2_*}) at level zero $H_0(\Sigma_g \times [0,1] \cap A) \xrightarrow{(i_{1_*}, i_{2_*})} H_0(\Sigma_g \times [0,1]) \oplus H_0(A)$, is injective. This is true: in fact, the connected components of $\Sigma_g \times [0,1] \cap A$ are exactly the connected components of A, hence they are sent injectively by (i_{1_*}, i_{2_*}). Hence, we have proven that $d \equiv 0$ and we obtained the exact sequence

$$\cdots\cdots\ H_1(\Sigma_g \times [0,1] \cap A) \xrightarrow{(i_{1_*}, i_{2_*})} H_1(\Sigma_g \times [0,1]) \oplus H_1(A) \xrightarrow{g_* - j_*} H_1(\widetilde{Y}) \longrightarrow 0.$$

To conclude the proof, we need the following observations:

- $g_* - j_*$ is surjective;
- $H_1(\Sigma_g \times [0,1]) \cong H_1(\Sigma_g)$;
- $H_1(A) = H_1\left(\sqcup_{\boldsymbol{\alpha} \times I}\left(\mathbb{D}^2 \times I\right) \sqcup_{\boldsymbol{\beta} \times I}\left(\mathbb{D}^2 \times I\right)\right) = 0$ (since it is contractible);
- $(\Sigma_g \times [0,1]) \cap \left(\sqcup_{\boldsymbol{\alpha} \times I}\left(\mathbb{D}^2 \times I\right) \sqcup_{\boldsymbol{\beta} \times I}\left(\mathbb{D}^2 \times I\right)\right) = (\boldsymbol{\alpha} \times [0,1]) \sqcup (\boldsymbol{\beta} \times [0,1])$;
- $H_i(\boldsymbol{\alpha} \times [0,1]) \sqcup (\boldsymbol{\beta} \times [0,1]) = H_i(\boldsymbol{\alpha} \sqcup \boldsymbol{\beta})$ for any i;
- the map $H_1(\Sigma_g \times [0,1] \cap A) \xrightarrow{(i_{1_*}, i_{2_*})} H_1(\Sigma_g \times [0,1]) \oplus H_1(A)$ is the map that sends any circle to its equivalence class in $\Sigma_g \times [0,1]$.

Therefore, using the first isomorphism theorem, we get the isomorphism

$$H_1(\widetilde{Y}) \cong \frac{H_1(\Sigma_g)}{\mathrm{Ker}(g_* - j_*)} \cong \frac{H_1(\Sigma_g)}{\mathrm{Im}(i_{1_*}, i_{2_*})} \cong \frac{H_1(\Sigma_g)}{\langle [\alpha_1], \ldots, [\alpha_g], [\beta_1], \ldots, [\beta_g] \rangle},$$

as we wanted.

□

2.2 Heegaard moves

We once again encounter the same problem as with Heegaard splittings: given a Heegaard diagram $(\Sigma, \boldsymbol{\alpha}, \boldsymbol{\beta})$, we can construct a unique manifold Y, but the same manifold admits many Heegaard diagrams. As we did with stabilisation, we will define three "moves" that we can perform on the sets of attaching circles $\boldsymbol{\alpha}$ and $\boldsymbol{\beta}$ that do not change the manifold represented by the diagram.

Again, we mainly follow [OS06a] and [Hom19] for this section.

Let $\{\gamma_1, \ldots \gamma_g\}$ be a set of attaching circles for a genus g handlebody H, let Σ be the border of H.

Definition 2.7 (Isotopy)**.** An *isotopy* moves $\gamma_1, \ldots \gamma_g$ in a one parameter family in such way that the curves remain disjoint.

Definition 2.8 (Finger move)**.** When modifying a Heegaard diagram, we often use a specific type of isotopy called *finger move*. A finger move is constructed as follows: let β_1 be a $\boldsymbol{\beta}$-circle and c an arc with one endpoint on β_1, which does not intersect any other β-circle; we then push "with our finger" β_1 up along c, drawing a small neighbourhood of c that does not touch any $\boldsymbol{\beta}$-circle and leaving all the rest of β_1 unaffected. See Figure 2.5 for an example.

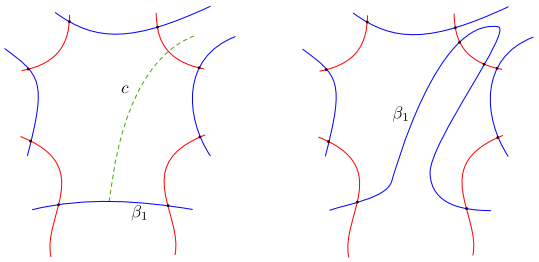

Figure 2.5: Example of a finger move (showed locally).

Definition 2.9 (Handleslide)**.** Without loss of generality, choose two of the curves, say γ_1, γ_2. To perform a *handleslide*, we replace γ_1 with γ_1', where this is a simple closed curve disjoint from any γ_i such that γ_1, γ_2, and γ_1' bound an embedded pair of pants in $\Sigma \setminus \gamma_3 \setminus \cdots \setminus \gamma_g$.

We also have an equivalent definition of handleslide. Suppose that γ_1 and γ_2 can be connected by an arc δ in $\Sigma \setminus \gamma_3 \setminus \cdots \setminus \gamma_g$. Let γ_1' be the connected sum of γ_1 with a parallel copy of γ_2, where the connected sum is taken along a neighbourhood of δ; we then replace γ_1 with γ_1'. See the figure below for the graphic idea.

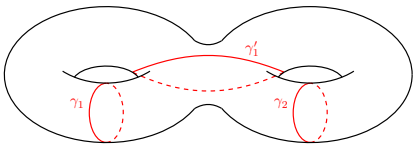

Figure 2.6: Handleslide as embedded pair of pants.

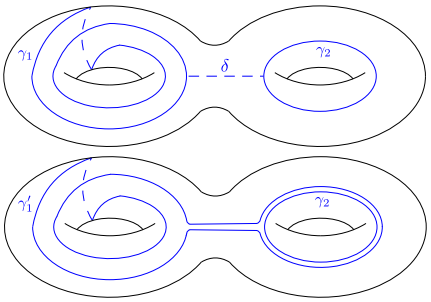

Figure 2.7: Handleslide using the connecting arc.

Lastly we define the stabilisation also for Heegaard diagrams. Consider a genus g Heegaard diagram $(\Sigma, \boldsymbol{\alpha}, \boldsymbol{\beta})$.

Definition 2.10 (Stabilisation)**.** We define the *stabilisation* as follows. Take a genus 1 surface E and consider the connect sum $\Sigma' = \Sigma \# E$, which is a genus $g+1$ surface. As sets of attaching circles, take $\boldsymbol{\alpha}' = \boldsymbol{\alpha} \cup \alpha_{g+1}$ and $\boldsymbol{\beta}' = \boldsymbol{\beta} \cup \beta_{g+1}$, where α_{g+1} and β_{g+1} are embedded on E and meet transversely in one point.

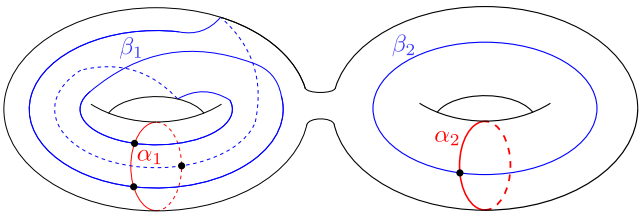

Figure 2.8: Stabilisation of the Heegaard Diagram of $L(3,1)$.

Notice that, if $(\Sigma, \boldsymbol{\alpha}, \boldsymbol{\beta})$ is compatible with the decomposition $Y = H_1 \cup_\Sigma H_2$, then the Heegaard diagram obtained by stabilisation is compatible with the decomposition obtained by stabilisation.

Remark 2.11. In accordance with what we requested in Definition 3.7, we also ask that these moves generate only transverse intersections between $\boldsymbol{\alpha}$- and $\boldsymbol{\beta}$-curves.

As we had Theorem 1.24 for Heegaard splittings, we also have the following Theorem for diagrams (see [Rei33] and [Sin33] for a proof).

Theorem 2.12. *Let Y be a closed and oriented 3-manifold, let $(\Sigma_g, \boldsymbol{\alpha}, \boldsymbol{\beta})$ be a Heegaard diagram of genus g for Y and $(\Sigma_{g'}, \boldsymbol{\alpha}', \boldsymbol{\beta}')$ be a Heegaard diagram of genus g' for Y. Then, by applying a sequence of stabilisations, isotopies and handleslides, we can change the above diagrams in a way that the new diagrams are diffeomorphic to each other.*

To actually compute $\widehat{\mathrm{HF}}$, we will need *pointed Heegaard diagrams*, i.e. Heegaard diagrams with a *basepoint*.

Definition 2.13 (Basepoint, pointed Heegaard diagrams)**.** A *basepoint* on a Heegaard diagram $(\Sigma, \boldsymbol{\alpha}, \boldsymbol{\beta})$ is a point z that stays on the complement of the curves, i.e. $z \in \Sigma \setminus (\boldsymbol{\alpha} \cup \boldsymbol{\beta})$.

We define a *pointed Heegaard diagram* to be a Heegaard diagram with a basepoint z; this is denoted by $(\Sigma, \boldsymbol{\alpha}, \boldsymbol{\beta}, z)$.

Since we are going to work with pointed diagrams, we need to define *pointed Heegaard moves*. These are obtained as a generalisation of the Heegaard moves above presented.

Definition 2.14 (Pointed isotopy)**.** A *pointed isotopy* is a type of isotopy where we require the basepoint to be disjoint from the curves.

Definition 2.15 (Pointed handleslide)**.** A *pointed handleslide*, is a handleslide in which we require that the basepoint is not in the pair of pants region where the handleslide take place.

For the stabilisations there are no differences. As we had Theorem 2.12, we have now the following proposition whose proof can be found in [OS04b].

Proposition 2.16. *Consider two pointed Heegaard diagrams for a closed and oriented 3-manifold Y, $(\Sigma, \boldsymbol{\alpha}, \boldsymbol{\beta}, z_1)$ and $(\Sigma, \boldsymbol{\alpha}, \boldsymbol{\beta}, z_2)$ which differ only for the basepoints. Then, the two diagrams can be connected by a sequence of pointed isotopies and pointed handleslides.*

We then have the following corollary of Propositions 2.12 and 2.16.

Corollary 2.17. *Consider two different pointed Heegaard diagrams of genus g for a closed and oriented 3-manifold Y, namely $(\Sigma, \boldsymbol{\alpha}, \boldsymbol{\beta}, z)$ and $(\Sigma, \boldsymbol{\alpha}', \boldsymbol{\beta}', z')$. Assume moreover that $z \in \Sigma \setminus (\boldsymbol{\alpha}' \cup \boldsymbol{\beta}')$ and $z' \in \Sigma \setminus (\boldsymbol{\alpha} \cup \boldsymbol{\beta})$. Then, the two diagrams can be connected by a sequence of pointed isotopies and pointed handleslides.*

2.3 Heegaard diagrams rise from Morse functions

In Morse theory, one studies a particular class of smooth functions on n-dimensional manifolds. In this section, we see how we can construct Heegaard diagrams starting from Morse functions; as a reference for Morse theory, one can see [Mil63]. Even though this point of view is not exploited for the most part of this thesis, it is widely used in external literature and hence it is worth to briefly look into it.

For this section, we follow Section 3 of [OS06a].

Definition 2.18 (Critical point, non degenerate point)**.** Let f be a smooth function on an n-manifold Y, $f : Y \to \mathbb{R}$. A point $P \in Y$ is a *critical point of f* if $\partial f / \partial x_i = 0$ for $i = 1, \dots, n$. At a critical point, the *Hessian matrix* $H(P)$ is given by the second partial derivatives $H_{ij} = \partial^2 f / \partial x_i \partial x_j$. A critical point P is called *non-degenerate* if $H(P)$ is non-singular.

Definition 2.19 (Morse function)**.** The function $f : Y \to \mathbb{R}$ is called a *Morse function* if all the critical points are non-degenerate.

Definition 2.20 (Index of a critical point)**.** Let f be a Morse function and P a critical point of f. Since $H(P)$ is symmetric, it induces an inner product on the tangent space. We call the *index of P* the dimension of a maximal negative definite subspace.

In other words, if we diagonalise $H(P)$ over the real numbers, and define $\mathrm{index}(P)$ to be the number of negative entries in the diagonal.

Notice that a local minimum of f has index 0 and that a local maximum has index n.

We are only interested in a special class of Morse function, the *self-indexing* Morse functions.

Definition 2.21 (Self-indexing Morse function)**.** A Morse function f is called *self-indexing* if for each critical point P we have $f(P) = \text{index}(P)$.

We have the following result, whose proof can be found in [Mil63].

Proposition 2.22. *Every smooth n-dimensional manifold Y admits a self-indexing Morse function. Furthermore, if Y is connected and has no boundary, then we can choose f so that it has unique index 0 and index n critical points.*

By studying how the level sets $f^{-1}((\infty, t])$ change when t goes through a critical value, it is possible to prove the following two facts:

- If $f : Y \longrightarrow [0,3]$ is a self-indexing Morse function on Y with one minimum and one maximum, then f induces a Heegaard splitting with Heegaard surface $\Sigma = f^{-1}(3/2)$, and handlebodies $U_0 = f^{-1}[0, 3/2], U_1 = f^{-1}[3/2, 3]$.
- If Σ has genus g, then f has g index one and g index two critical points. We denote the index 1 critical points of f by $P_1, \ldots, P_g$ and the ones of index 2 by $Q_1, \ldots, Q_g$.

Moreover, from the Morse function is possible to define a Heegaard diagram on the manifold compatible with the splitting that we found above, as we can see in the next result.

Proposition 2.23. *The Morse function and a Riemannian metric on Y induce a Heegaard diagram for Y.*

Sketch of proof. Consider the gradient vector field ∇f of the Morse function. For each point $x \in \Sigma = f^{-1}(3/2)$ we can look at the gradient trajectory of $\pm\nabla f$ that goes through x. Consider the critical point P_i and call α_i the set of points that flow down to it; symmetrically, for the critical point Q_j we call β_j the set of points that flow up to it.

In [Mil63], is proven the following theorem that studies the local behavior of a Morse function f around a critical point:

> Let P be an index i critical point of f. Then there is a diffeomorphism h between a neighbourhood U of $0 \in \mathbb{R}^n$ and a neighbourhood U' of $P \in Y$ so that
> $$h \circ f = -\sum_{j=1}^{i} x_j^2 + \sum_{j=i+1}^{n} x_j^2.$$

It follows from the above result and the fact that f is self indexing that α_i, β_i are simple closed curves in Σ. Furthermore, it is also possible to see that $\alpha_1, \ldots, \alpha_g$ and $\beta_1, \ldots, \beta_g$ are set of attaching circles for U_0 and U_1 respectively; therefore this is a Heegaard diagram of Y compatible with the given Heegaard splitting. □

2.4 Heegaard diagrams for bordered and sutured manifolds

In this section, we construct Heegaard diagrams for bordered, sutured, and bordered sutured manifolds. Although one could define diagrams for bordered sutured manifolds and see the ones for bordered manifolds and sutured manifolds as a particular case, we will build the pieces step by step. This decision is motivated by the fact that in later chapters we will mainly work with bordered diagrams and sutured diagrams.

2.4.1 Heegaard diagrams for bordered manifolds

For this subsection, one can use Section 4.1 of [LOT18] as reference.

Definition 2.24 (Bordered Heegaard diagram)**.** A *bordered Heegaard diagram* is a quadruple $(\Sigma, \boldsymbol{\alpha} = \boldsymbol{\alpha}^a \cup \boldsymbol{\alpha}^c, \boldsymbol{\beta}, z)$, where

- Σ is a genus g, oriented surface with one boundary component,
- $\boldsymbol{\beta} = \{\beta_1, \dots, \beta_g\}$ are g pairwise disjoint circles in the interior of Σ,
- $\boldsymbol{\alpha}^c = \{\alpha^c_{g-k}, \dots, \alpha^c_{g-k}\}$ are $g-k$ circles in the interior of Σ,
- $\boldsymbol{\alpha}^a = \{\alpha^a_1, \dots, \alpha^a_{2k}\}$ are $2k$ arcs in Σ with boundary on $\partial\Sigma$, transverse to $\partial\Sigma$,
- all the curves of $\boldsymbol{\alpha}$ are pairwise disjoint,
- z is a point in $\partial\Sigma \setminus (\boldsymbol{\alpha} \cap \partial\Sigma)$.

Moreover, we request as in the closed case that the intersections are transverse and that $\Sigma \setminus \boldsymbol{\alpha}$ and $\Sigma \setminus \boldsymbol{\beta}$ are connected (or, equivalently, that $\boldsymbol{\alpha}$ is an independent set in $H_1(\Sigma, \partial\Sigma)$ and that $\boldsymbol{\beta}$ is an independent set in $H_1(\Sigma)$).

We want to see now how we can construct a bordered manifold starting from a bordered Heegaard diagram. For this, we first need to understand how to define a pointed matched circle structure on the boundary of Σ.

Lemma 2.25 ([LOT18, Lemma 4.4])**.** *Consider $(\Sigma, \boldsymbol{\alpha}, \boldsymbol{\beta}, z)$, a bordered Heegaard diagram. Define $Z = \partial\Sigma$ and $\mathbf{a} = \boldsymbol{\alpha}^a \cap \partial\Sigma$. We define a matching M on $\mathbf{a}$ by*

$$M\left(\alpha^a_i \cap \partial\Sigma\right) = i.$$

Then, $\mathcal{Z} = (Z, \mathbf{a}, M, z)$ is a pointed matched circle.

Proof ([LOT18]). We only need to check that if we perform surgery along the $2k$ pairs of points in Z, we obtain a single circle. This follows from the connectivity of $\Sigma \setminus \boldsymbol{\alpha}$.

Call Z' the circle obtained from Z after the surgery and Σ' the manifold obtained from Σ after deleting a tubular neighbourhood of each $\boldsymbol{\alpha}$-circle and gluing two discs

to the result. It is clear by the definitions that Z' is homeomorphic to the boundary of a tubular neighbourhood of $\partial\Sigma \cup (\cup_{i=1}^{2k} \alpha_i^a)$ and this is homeomorphic to the boundary of $\Sigma' \setminus \nu(\boldsymbol{\alpha})$, where $\nu(\boldsymbol{\alpha})$ is a tubular neighbourhood of all the curves of $\boldsymbol{\alpha}$. But then, because of the connectivity of $\Sigma \setminus \boldsymbol{\alpha}$, this a circle. □

Definition 2.26 (Boundary of a bordered Heegaard diagram)**.** We are going to call the *boundary of a bordered Heegaard diagram* $\mathcal{H} = (\Sigma, \boldsymbol{\alpha}, \boldsymbol{\beta}, z)$ the pointed matched circle above defined, and we will denote it by $\partial\mathcal{H}$.

Given a bordered Heegaard diagram $\mathcal{H} = (\Sigma, \boldsymbol{\alpha}, \boldsymbol{\beta}, z)$, we can construct an unique bordered 3-manifold $(Y, \mathcal{Z}, \phi)$ in the following way. We thicken the Heegaard surface to $\Sigma \times [0, 1]$, and we attach 3-dimensional 2-handles to each $\alpha_i^c \times \{0\}$ and to each $\beta_j \times \{1\}$. Then, we take $\mathcal{Z} = \partial\mathcal{H}$ and the boundary of the manifold that we get as result of the above construction is then naturally identified with $F(\mathcal{Z})$.

As in the case of closed 3-manifolds, it is possible to prove that any bordered 3-manifolds is represented by some bordered diagram.

Proposition 2.27 ([LOT18, Lemma 4.9])**.** *Any bordered 3-manifold $(Y, \mathcal{Z}, \phi)$ is represented by some bordered Heegaard diagram.*

A proof of this done via Morse theory can be found in [LOT18].

Furthermore, it is possible to use Heegaard moves to transform one bordered Heegaard diagram representing a bordered 3-manifold into another diagram representing the same manifold. However, the allowable moves are restricted to the types presented in the next result.

Proposition 2.28 ([LOT18, Lemma 4.10])**.** *Any pair of bordered Heegaard diagrams for the same bordered 3-manifolds can be made diffeomorphic after a sequence of*

- *isotopies of the $\boldsymbol{\alpha}$-curves and $\boldsymbol{\beta}$-circles, not crossing $\partial\Sigma$;*
- *handleslides of $\boldsymbol{\beta}$-circles over $\boldsymbol{\beta}$-circles,*
- *handleslides of $\boldsymbol{\alpha}$-curves over $\boldsymbol{\alpha}$-circles,*
- *stabilisations in the interior of Σ.*

2.4.2 Heegaard diagrams for sutured manifolds

Next, we develop Heegaard diagrams for sutured manifolds. For this purpose, we mainly follow Section 4.2 of [Alt13].

Traditionally, the approach used to develop Sutured Heegaard Floer Homology is to define *sutured Heegaard diagrams*, a special class of diagrams with few requirements on the $\boldsymbol{\alpha}$- and $\boldsymbol{\beta}$-circles: we do not ask them to be independent in first homology and we do not ask them to be equal in quantity. Namely, one define this object as follows.

Definition 2.29 (Sutured Heegaard diagram)**.** We define a *sutured Heegaard diagram* to be a tuple $(\Sigma, \boldsymbol{\alpha}, \boldsymbol{\beta})$, where Σ is a compact and oriented 2-manifold with border and $\boldsymbol{\alpha} = \{\alpha_1, \dots, \alpha_m\}, \boldsymbol{\beta} = \{\beta_1, \dots, \beta_n\}$ are two sets of pairwise disjoint simple closed curves in the interior of Σ.

Then, it was discovered that certain constraints were necessary in the construction of Heegaard Floer Homology using Whitney discs, leading to the introduction of *balanced sutured Heegaard diagrams*. For the reader that is familiar to such approach for the construction of Floer Homology, the primary reason for this constraint is that we need $|\boldsymbol{\alpha}| = |\boldsymbol{\beta}|$ and their independence in first homology for the theory to be well-defined on the tori $\mathbb{T}_\alpha$ and $\mathbb{T}_\beta$ of the symmetric product $\mathrm{Sym}^g(\Sigma)$. Since we are using Lipshitz's cylindrical reformulation to construct Heegaard Floer Homology, we can directly define sutured Heegaard diagrams that satisfy these requirements without further justification. For more information on this construction, see Section 4.2 of [Alt13].

Definition 2.30 (Sutured Heegaard diagrams)**.** We define a *sutured Heegaard diagram* (also called *balanced sutured Heegaard diagram*) to be a tuple $(\Sigma, \boldsymbol{\alpha}, \boldsymbol{\beta})$, where Σ is a compact and oriented 2-manifold with border and $\boldsymbol{\alpha} = \{\alpha_1, \dots, \alpha_n\}, \boldsymbol{\beta} = \{\beta_1, \dots, \beta_n\}$ are two sets of pairwise disjoint simple closed curves in the interior of Σ, such that $\{[\alpha_1], \dots, [\alpha_n]\}$ and $\{[\beta_1], \dots, [\beta_n]\}$ are independent sets in $H_1(\Sigma, \mathbb{Q})$.

Given a sutured Heegaard diagram, we can construct an unique sutured manifold (Y, Γ) in a similar fashion of what we saw for 3-manifolds: we thicken up Σ to $\Sigma \times I$ and smoothly attach 3-dimensional 2-handles along the circles $\alpha_i \times \{0\}$ and $\beta_j \times \{1\}$; we then obtain a 3-manifold with boundary and we take $\Gamma = \partial\Sigma \times \{1/2\}$.

The result (Y, Γ) is indeed a sutured manifold, as it holds the following result.

Lemma 2.31 ([Alt13, Lemma 4.16])**.** *Let $(\Sigma, \boldsymbol{\alpha}, \boldsymbol{\beta})$ be a sutured Heegaard diagram and let (Y, Γ) be the object obtained with the above construction. Since the circles in $\boldsymbol{\alpha}$ and the circles in $\boldsymbol{\beta}$ are independent in $H_1(\Sigma)$, every connected component A of $R(\Gamma) = \Sigma \setminus \Gamma$ has non-empty boundary. Hence, (Y, Γ) is a sutured manifold.*

Moreover, it is possible to prove the following result, from which it follows that we are going to work with balanced sutured manifolds.

Lemma 2.32 ([Alt13, Lemma 4.17 and 4.18])**.** *Let $(\Sigma, \boldsymbol{\alpha}, \boldsymbol{\beta})$ be a sutured Heegaard diagram and let (Y, Γ) be the sutured manifold represented by it. Then (Y, Γ) is a balanced sutured manifold.*

Moreover, we can see that that (almost) any balanced sutured manifolds admits a sutured Heegaard diagram.

Proposition 2.33 ([Juh06, Proposition 2.14])**.** *Let (Y, Γ) be a balanced sutured manifold. Then, there exists a sutured Heegaard diagram $(\Sigma, \boldsymbol{\alpha}, \boldsymbol{\beta})$ that represents it.*

As we saw in the case of 3-manifolds, also here all the definitions are well-posed as the next result explains.

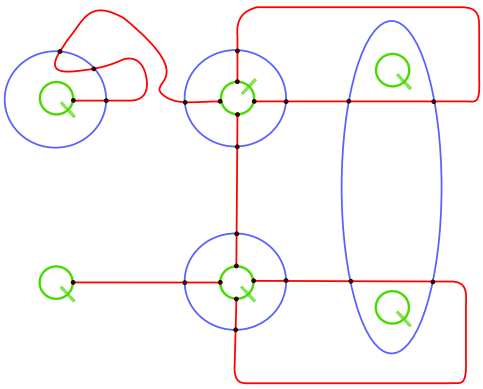

Figure 2.9: An example of a bordered sutured Heegaard diagrams for a bordered sutured manifold with no $\boldsymbol{\beta}$-arcs.

Proposition 2.34 ([Alt13, Proposition 4.20])**.** *Two balanced diagrams represent the same balanced sutured manifold if and only if the diagrams are connected by a sequence of Heegaard moves.*

Remark 2.35 (Re-visitation of Heegaard diagrams for closed manifolds)**.** As anticipated, we can see how we can re-visit Heegaard diagrams for closed 3-manifolds as a special case of sutured Heegaard diagrams.

Let Y be a closed, connected and oriented 3–manifold. We construct a sutured 3-manifold as follows: consider a 3–ball $B_1 \subset Y$ and choose an oriented simple curve $s_1 \subset \partial B_1$; we can then define a sutured manifold $(Y', \{s_1\})$, where $Y' = Y \setminus \mathrm{Int}(B_1)$.

Therefore, enlarging our point of view to the sutured language, we can now think of the basepoint introduced for pointed Heegaard diagrams as the suture s_1 once we shrunk the ball B_1 down to a point.

We will see in Section 3.3 that indeed $\widehat{\mathrm{HF}}$ agrees with SHF in the sense above presented, obtaining

$$\widehat{\mathrm{HF}}(Y) \equiv \mathrm{SFH}(Y', \{s_1\}).$$

2.4.3 Heegaard diagrams for bordered sutured manifolds

We now construct Heegaard diagrams for bordered sutured manifold with $\boldsymbol{\alpha}$- and $\boldsymbol{\beta}$-arcs, following Section 3.1 of [Zib20].

Definition 2.36 (Bordered sutured Heegaard diagram)**.** Let $(Y, \Gamma, \mathcal{Z}_\alpha, \phi_\alpha, \mathcal{Z}_\beta, \phi_\beta)$ be a bordered sutured manifold with $\boldsymbol{\alpha}$- and $\boldsymbol{\beta}$-arcs and considered the sutured Heegaard diagram $(\Sigma, \boldsymbol{\alpha}, \boldsymbol{\beta})$ of the underlying sutured manifold. Then, a *bordered sutured Heegaard diagram* for the bordered sutured manifold is obtained by $(\Sigma, \boldsymbol{\alpha}, \boldsymbol{\beta})$ by adding the graphs of the arc diagrams to it, and we denote it by $(\Sigma, \boldsymbol{\alpha}, \boldsymbol{\beta}, \mathcal{Z}_\alpha, \phi_\alpha, \mathcal{Z}_\beta, \phi_\beta)$.

See Figure 2.9 for an example.

We can explain in more details what the above definition means. Recall that $\phi_\alpha : G(\mathcal{Z}_\alpha) \hookrightarrow \overline{R_-(\Gamma)}$ is an embedding such that $\phi_\alpha(Z_\alpha) \subset \Gamma$; we can consider

the embedding ϕ_α to be such that $\phi_\alpha(G(\mathcal{Z}_\alpha))$ misses the 3-dimensional 2-handles corresponding to the $\boldsymbol{\alpha}$-circles: it suffices to slide them off $\mathcal{S}^0 \times \mathbb{D}^2 \subset R_-(\Gamma)$. We do the same for $G(\mathcal{Z}_\beta)$. Therefore, we have that the line segments are embedded in the border of Y (which corresponds to the sutures), and we have some $\boldsymbol{\alpha}$-segments (namely $\phi_\alpha(G(\mathcal{Z}_\alpha) \setminus Z)$) and $\boldsymbol{\beta}$-segments (namely $\phi_\beta(G(\mathcal{Z}_\beta) \setminus Z)$) between the sutures. We call them respectively *$\boldsymbol{\alpha}$-arcs* and *$\boldsymbol{\beta}$-arcs*. Moreover, we put a *basepoint* (i.e. a marked point), in every open component of the boundary minus the image of Z. We usually draw the sutures in green.

As in the previous cases, we have the following result.

Proposition 2.37 ([Zar09, Proposition 4.5])**.** *Any sutured bordered manifold has a compatible bordered sutured Heegaard diagram.*

Moreover, given any two diagrams which represent the same bordered sutured manifolds, we can connect them with a sequence of

- *isotopies of $\boldsymbol{\alpha}$-circles and $\boldsymbol{\beta}$-circles and isotopies of $\boldsymbol{\alpha}$-arcs that do not move the endpoints,*
- *handleslides of a $\boldsymbol{\beta}$-circle over another $\boldsymbol{\beta}$-circle,*
- *handleslides of any $\boldsymbol{\alpha}$-curve over an $\boldsymbol{\alpha}$-circle*
- *stabilisations in the interior of Σ.*

2.5 Heegaard diagrams for knots

In Section 3.4, we will explore a version of Heegaard Floer Homology, known as Knot Floer Homology, which is used to study knots embedded in $\mathcal{S}^3$. This homology theory is denoted by $\widehat{\mathrm{HFK}}(\mathcal{S}^3, K)$, where K is the knot of interest. To introduce Knot Floer Homology, we first need to understand Heegaard diagrams for knots. In this regard, we follow Section 1.3 of [Hom19].

For HFK, we will need *doubly pointed Heegaard diagrams*, i.e. diagrams with two basepoints that we will denote by z and w. The need for two basepoints may seem arbitrary at first glance, but it will be justified from the sutured perspective in Remark 2.42.

Definition 2.38 (Doubly pointed Heegaard diagram)**.** A *doubly pointed Heegaard diagram* for a knot $K \subset \mathcal{S}^3$ is a tuple $(\Sigma, \boldsymbol{\alpha}, \boldsymbol{\beta}, w, z)$ where w, z are basepoints in $\Sigma \setminus (\boldsymbol{\alpha} \cup \boldsymbol{\beta})$, such that

1. $(\Sigma, \boldsymbol{\alpha}, \boldsymbol{\beta})$ is a Heegaard diagram for $\mathcal{S}^3$;
2. K is the union of arcs a and b, where
   - a is an arc in $\Sigma \setminus \boldsymbol{\alpha}$ connecting w to z, pushed slightly into H_1,

- b is an arc in $\Sigma \setminus \boldsymbol{\beta}$ connecting z to w, pushed slightly into H_2.

Example 2.39 (Trefoil)**.** The following is an example for the lef-handed trefoil.

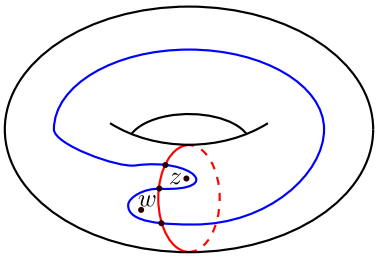

Figure 2.10: Genus 1 doubly pointed Heegaard diagram for the left-handed trefoil

Lemma 2.40. *Every knot $K \subset \mathcal{S}^3$ admits a doubly pointed Heegaard diagram.*

Proof ([Hom19]). There is an explicit way to construct such a diagram for a generic knot K. Let D be a knot diagram for K (i.e., a projection of K on the plane with the information of "over"/"under" on the crossings); let n_c be the number of crossing of D. If we ignore the over/under data of the crossings, we can consider the knot diagram as a closed non-simple curve that divides the plane into n_c+2 regions, n_c+1 of which are bounded and one that is unbounded (the "external region"). Let Σ be the surface obtained by taking a tubular neighborhood of this curve in $\mathbb{R}^3$; then, Σ is a surface of genus n_c+1 that looks like a thickened knot. For each of the bounded regions in the complement of the knot diagram, we put a β-circle on Σ that goes around the corresponding hole of the surface. See Figure 2.11 for an example of this construction done for the left-handed trefoil.

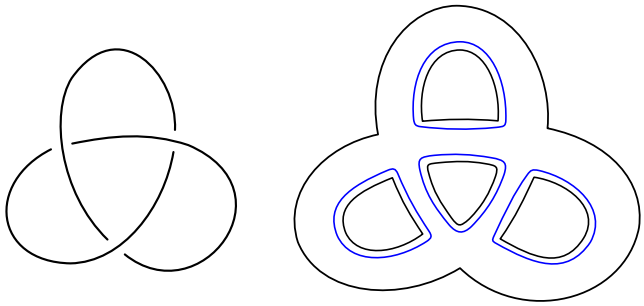

Figure 2.11: Construction of a genus 4 doubly pointed Heegaard diagram for the left-handed trefoil: Σ and $\boldsymbol{\beta}$-circles.

We need now a way to encode the crossings' data on Σ. Recalling how $\boldsymbol{\alpha}$-circles give instruction for the gluing of discs on the Heegaard surface, it is natural to encode such data with the $\boldsymbol{\alpha}$-circles as indicated in Figure 2.12.

We have now a genus $n_c + 1$ surface with $n_c + 1$ circles around the holes, the $\boldsymbol{\beta}$-circles, and n_c circles around the crossings, the $\boldsymbol{\alpha}$-circles. We then add the last $\boldsymbol{\alpha}$-circle, corresponding to a meridian of K and we place the basepoint w on one side

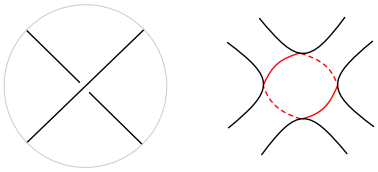

Figure 2.12: How the $\boldsymbol{\alpha}$-circles hold the crossing data.

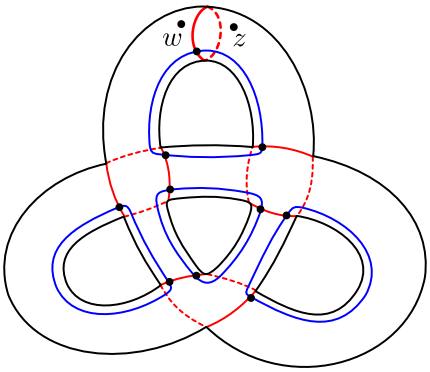

Figure 2.13: Genus 4 doubly pointed Heegaard diagram for the left-handed trefoil.

of it and the basepoint z on the other side. Notice that the choice of the side on which we put w determines the orientation of K.

See Figure 2.13 for the result of this construction for the left-handed trefoil. □

We can now define doubly pointed isotopies and doubly pointed handleslides just as we defined the pointed ones: isotopies are required to miss both w and z and neither w nor z is allowed to be in the pair of pants involved in the handleslide. We then have an analogue of Corollary 2.17, which is proven in [OS04a].

Proposition 2.41 ([OS04a, Proposition 3.5])**.** *Let* $(\Sigma, \boldsymbol{\alpha}, \boldsymbol{\beta}, w, z)$ *and* $(\Sigma', \boldsymbol{\alpha}', \boldsymbol{\beta}', w', z')$ *be two doubly pointed Heegaard diagrams for a knot* $K \subset \mathcal{S}^3$*. Then, it exists a finite sequence of doubly pointed isotopies, doubly pointed handleslides and stabilisations that connects the two diagrams.*

Remark 2.42 (Heegaard diagrams for knots as particular case of sutured Heegaard diagrams)**.** We can provide further motivation for the construction described above by connecting it to the theory of sutured manifolds. For reference, one can consult Section 9 of [Juh06].

Recall the sutured manifold (Y_K, s_1, s_2) associated to a knot K, as defined in Remark 1.66. The two basepoints in the construction of doubly pointed Heegaard diagrams can then be thought of as the two sutures s_1 and s_2, which are shrunk down to a point. In Section 3.4, we will see that this construction of Knot Heegaard Floer Homology agrees with Sutured Floer Homology.

2.6 Heegaard diagrams for tangles

We are now going to see how we can construct a Heegaard diagram for tangles, following Chapter II.2 of [Zib17].

We begin by defining what a Heegaard diagram is in this context. As we did in Section 2.5, we can justify this construction with the bordered sutured point of view, which we will discuss in more detail in Subsection 2.6.2.

Definition 2.43 (Heegaard diagram for a tangle)**.** Consider a tangle T with n open components and m closed components. A *Heegaard diagram for the tangle T* consists of a tuple $(\Sigma, \boldsymbol{\alpha} = \boldsymbol{\alpha}^c \cup \boldsymbol{\alpha}^a, \boldsymbol{\beta})$, where:

- Σ is an oriented surface of genus g with $2(n+m)$ border components. We denote the collection of these border components by $\mathcal{Z}$, which are partitioned into $(n+m)$ pairs;
- $\boldsymbol{\alpha}^c$ is a set of $(g+m)$ pairwise disjoint circles $\alpha_1, \dots, \alpha_{g+m}$ on Σ. These are called $\boldsymbol{\alpha}$-*circles*;
- $\boldsymbol{\alpha}^a$ is a set of $2n$ pairwise disjoint arcs $\alpha_1^a, \dots, \alpha_{2n}^a$ on Σ which are disjoint from $\boldsymbol{\alpha}^c$ and whose endpoints lie on $\mathcal{Z}$. These are called $\boldsymbol{\alpha}$-*arcs*;
- $\boldsymbol{\beta}$ is a set of $(g+m+n-1)$ pairwise disjoint circles $\beta_1, \dots, \beta_{g+m+n-1}$ on Σ. These are called $\boldsymbol{\beta}$-*circles*.

We write $\boldsymbol{\alpha} := \boldsymbol{\alpha}^c \cup \boldsymbol{\alpha}^a$ to indicate all the α-*curves*. Moreover, we impose the following conditions on the data above:

1. contracting all boundary components turns $\boldsymbol{\alpha}^a$ into a single circle. This means that on each component of $\mathcal{Z}$, we could either have no or exactly two endpoints of $\boldsymbol{\alpha}^a$;
2. define the surface $S_{\boldsymbol{\alpha}^c}(\Sigma)$ as the surface obtained by surgery along the curves in $\boldsymbol{\alpha}^c$. We want it to be a disjoint union of m anuli, each of whose boundary is a pair in $\mathcal{Z}$, and a 2-sphere with $2n$ boundary components. We denote by $\mathcal{Z}^\alpha$ the set of circles in $\mathcal{Z}$ which meet the $\boldsymbol{\alpha}$-curves;
3. define the surface $S_{\boldsymbol{\beta}}(\Sigma)$ as the surface obtained by surgery along the curves in $\boldsymbol{\beta}$. We want it to be a disjoint union of $(n+m)$ anuli, each of whose boundary is a pair in $\mathcal{Z}$.

Remark 2.44 (Boundary components in a Heegaard diagram for a tangle)**.** Recall the bordered sutured structure given to a tangle in Remark 1.73. We can then interpret the $2(n+m)$ boundary components of a Heegaard diagram for a tangle in the same way, i.e. two oppositely oriented meridional circles around each closed components and a single suture around each tangle end.

In our work, we are going to focus on 4-ended tangles without any closed component. It could be useful to see the definition of a Heegaard diagram in this particular case.

Definition 2.45 (Heegaard diagram for a 4-ended tangle without closed components)**.** A *Heegaard diagram for a 4-ended tangle without closed components* consists of a tuple $(\Sigma, \boldsymbol{\alpha} = \boldsymbol{\alpha}^c \cup \boldsymbol{\alpha}^a, \boldsymbol{\beta})$, where:

- Σ is an oriented surface of genus g with 4 boundary components. We denote the collection of these border components by $\mathcal{Z}$, which are partitioned into 2 pairs;
- $\boldsymbol{\alpha}^c$ is a set of g pairwise disjoint circles $\alpha_1, \ldots, \alpha_g$ on Σ. These are called $\boldsymbol{\alpha}$-*circles*;
- $\boldsymbol{\alpha}^a$ is a set of 4 pairwise disjoint arcs on Σ, denoted by a, b, c, d, which are disjoint from $\boldsymbol{\alpha}^c$ and whose endpoints lie on $\mathcal{Z}$. These are called $\boldsymbol{\alpha}$-*arcs*;
- $\boldsymbol{\beta}$ is a set of $(g+1)$ pairwise disjoint circles $\beta_1, \ldots, \beta_{g+1}$ on Σ. These are called $\boldsymbol{\beta}$-*circles*.

We write $\boldsymbol{\alpha} := \boldsymbol{\alpha}^c \cup \boldsymbol{\alpha}^a$ to indicate all the $\boldsymbol{\alpha}$-*curves*. Moreover, we impose the following conditions on the data above:

1. contracting all boundary components turns $\boldsymbol{\alpha}^a$ into a single circle. This means that on each component of $\mathcal{Z}$, we could either have no or exactly two endpoints of $\boldsymbol{\alpha}^a$;
2. define the surface $S_{\boldsymbol{\alpha}^c}(\Sigma)$ as the surface obtained by surgery along the curves in $\boldsymbol{\alpha}^c$. We want it to be a 2-sphere with 4 boundary components. We denote by $\mathcal{Z}^\alpha$ the set of circles in $\mathcal{Z}$ which meet the α-curves;
3. define the surface $S_{\boldsymbol{\beta}}(\Sigma)$ as the surface obtained by surgery along the curves in $\boldsymbol{\beta}$. We want it to be a disjoint union of 2 anuli, each of whose boundary is a pair in $\mathcal{Z}$.

Example 2.46 (Heegaard diagram for the 1-crossing tangle)**.** Let T be the 1-crossing tangle Q_1; we can draw a genus 0 Heegaard diagram as it is shown in Figure 2.14.

There is a more intuitive way to think about the construction of this genus 0 Heegaard diagram. We start by considering our tangle embedded in B^3. Our goal is to encode all the information of the tangle on the surface of the ball. To do this, we consider a tubular neighbourhood of our tangle, denoted $\nu(T)$, and drill it out of B^3. This leaves us with $B^3 \setminus \nu(T)$, which can be thought of as a ball with a cave system that clearly encodes the data of the tangle.

Next, we consider $\partial B^3 \setminus \nu(T)$, which is a sphere with 4 punctures on it, known as the four-punctured sphere $\mathcal{S}^2_4$. We can think of the punctures as the entrances to our previous cave system, but we do not know which entrance is linked to which.

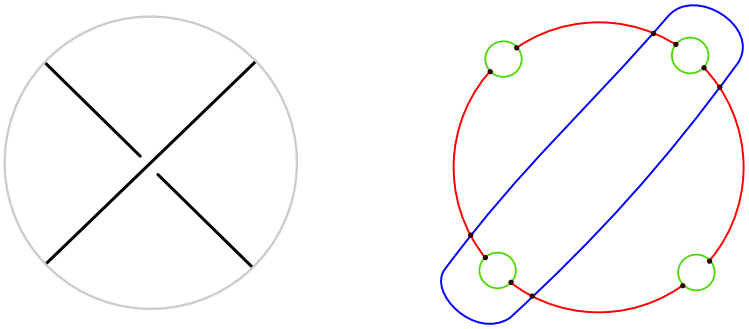

Figure 2.14: Heegaard diagram for the 1-crossing tangle.

This information is given by the $\boldsymbol{\beta}$-circle that we embed on $\mathcal{S}^2_4$. The $\boldsymbol{\beta}$-circle specifies that the north-east suture is linked with the south-west sutures in a "straight way". Specifically, if we embed the disc which has the $\boldsymbol{\beta}$-circle as its boundary, we obtain a separation of the inside of the sphere that agrees with the initial cave system we wanted to encode on $\mathcal{S}^2_4$. We will see in Subsection 2.6.1 how the construction of the $\boldsymbol{\beta}$-circle works for more intricate tangles.

Finally, we add four $\boldsymbol{\alpha}$-arcs to the Heegaard diagram, which represent the fixed circle S on which the tangle ends sit.

As we had Corollary 2.17 for pointed Heegaard diagrams, we have the following result in the tangle case.

Proposition 2.47. *Let T be a tangle. Given any two Heegaard diagrams for the same tangle, one can be obtained from the other by a sequence of the following moves:*

- *isotopies of $\boldsymbol{\alpha}$- or $\boldsymbol{\beta}$-circles and isotopies of $\boldsymbol{\alpha}$-arcs that leave the endpoints fixed;*
- *handleslides of a $\boldsymbol{\beta}$-circle over another $\boldsymbol{\beta}$-circle;*
- *handleslides of an $\boldsymbol{\alpha}$-curve over an $\boldsymbol{\alpha}$-circle;*
- *stabilisations in the interior of Σ.*

Furthermore, exploiting the construction from Example 2.46, we can obtain the following lemma.

Lemma 2.48. *Let T be a tangle without closed components, then it exists a Heegaard diagram that represents it.*

The above lemma has a version for tangles with closed components as well, and in that case, we have to use *ladybugs* to obtain the correct final diagram. For further details, one can refer to Example 2.5 in [Zib17].

Proof ([Zib17]). To prove the statement, we will first show how Heegaard diagrams for different tangles can be glued together. Then, we can cut our original tangle into

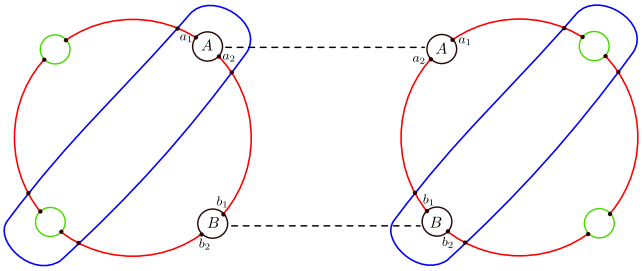

Figure 2.15: How to glue Heegaard diagrams of tangles.

4-ended tangles with a single crossing each and use the bordered sutured structures to glue the corresponding diagrams together, obtaining the complete diagram.

The way to combine Heegaard diagrams is quite straightforward: when we want to reconnect two endpoints of the tangles represented, we glue together the two corresponding sutures of the diagrams. We must be careful of the α-arcs that have endpoints on those sutures, which we must pair and glue as indicated in Figure 2.15 for the case of a tangle with two crossings.

Further details for the gluing can be found in Section 4.6 of [Zar11]. □

Remark 2.49.

- If we apply the above construction to a 4-ended tangle with n crossings, we can notice that by gluing the $\boldsymbol{\alpha}$-arcs we are going to obtain $n-1$ $\boldsymbol{\alpha}$-circles and 4 $\boldsymbol{\alpha}$-arcs. Therefore, the final result is a proper Heegaard diagram of genus $n-1$ for a 4-ended tangle. This makes this construction not very useful in practice, as many tangles actually admit some lower genus diagram (for instance, any rational tangle admits a genus 0 diagram) that are more practical in the actual computations of Tangle Floer Homology.

- In Subsection 2.6.1, we will explore how to cut the tangle into less pieces, by focusing on the largest "rational pieces". This is something that will also help with the input of [`nicepy`], as one can read in Appendix A.

In order to compute combinatorially the invariant HFT, we will need *peculiar Heegaard diagrams*, a slight modification of the diagrams above defined. We define this new notion of diagram for 4-ended tangles with eventually closed components, in agreement with Definition 2.4 of [Zib20].

Definition 2.50 (Peculiar Heegaard diagram)**.** Let T be a 4-ended tangle with m closed components and $(\Sigma, \boldsymbol{\alpha} = \boldsymbol{\alpha}^c \cup \boldsymbol{\alpha}^a, \boldsymbol{\beta})$ be a Heegaard diagram that represents it. A *peculiar Heegaard diagram* for T, denoted by

$$(\Sigma', \boldsymbol{\alpha}^c \cup \{\mathcal{S}\}, \boldsymbol{\beta}, \{p_i\}_{i=1}^4, \{q_j\}_{j=1}^4, \{z_k\}_{k=1}^m, \{w_l\}_{l=1}^m),$$

is the diagram obtained from $(\Sigma, \boldsymbol{\alpha} = \boldsymbol{\alpha}^c \cup \boldsymbol{\alpha}^a, \boldsymbol{\beta})$ after the following local modification around the sutures:

- we collapse the four sutures of $\mathcal{S}_4^2$, obtaining a $\boldsymbol{\alpha}$-circle which is the the union of the four $\boldsymbol{\alpha}$-arcs (isotopic to the fixed circle $\mathcal{S}$), hence obtaining as $\boldsymbol{\alpha}$-circles $\boldsymbol{\alpha}^c \cup \{\mathcal{S}\}$;

Figure 2.16: Collapsing of a suture and placing of the linked p_i and q_j.

- we add two marked points for every collapsed sutured on the two sides of $\mathcal{S}$, denoting by p_i's the ones placed on the front of the sphere and by q_j's the ones placed on the back of the sphere, for $i, j = 1, \ldots, 4$;
- for each of the four collapsed sutures, we connect the respective p_i and q_j with an arc that intersects only the $\boldsymbol{\alpha}$-circle $\mathcal{S}$ in exactly one point (see Figure 2.16);
- we contract all the other boundary components (i.e. the m couples representing the closed components of T) to points, and we call them z_k, w_l for $k, l = 1, \ldots, m$ in a way that z_k and w_k correspond to the two sutures of the same closed components.

The p_i's, the q_j's, the z_k's, and the w_l's are referred to as the *basepoints* of the diagram, and their significance will become clear in Subsection 4.4.4.

Peculiar Heegaard diagrams have a key advantage over general Heegaard diagrams for 4-ended tangles: they allow us to work with closed surfaces instead of bordered ones, which simplifies the theory considerably. Additionally, the number of α-circles and β-circles in a peculiar diagram are always the same.

We need to adapt Heegaard moves for peculiar diagrams.

Definition 2.51 (Peculiar Heegaard moves)**.** The allowed Heegaard moves for peculiar diagrams are:

1. isotopies of the $\boldsymbol{\alpha}$- and $\boldsymbol{\beta}$-circles that do not touch the basepoints and the arcs that connect these,
2. handleslides of $\boldsymbol{\beta}$-circles over $\boldsymbol{\beta}$-circles and handleslides of $\boldsymbol{\alpha}$-circles over $\boldsymbol{\alpha}$-circles different than $\mathcal{S}$,
3. stabilisations.

2.6.1 Heegaard diagrams for rational tangles

Starting from the diagram of the 1-crossing, it is possible to construct the diagram for any rational tangle with the use of *Dehn twists*. In this way, we can draw Heegaard diagrams of genus 0 for rational tangles.

Let us take a look at the tangle Q_2, which is Q_1 with an extra twist on the right. To add this twist to the Heegaard diagram for Q_1 (shown in Figure 2.14), we follow the twist in the tangle that happens between the north-east and the south-east ends,

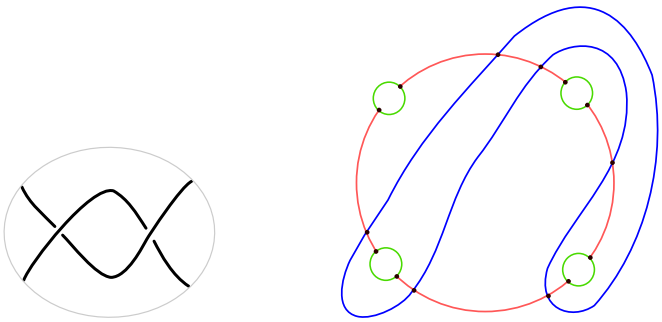

Figure 2.17: Q_2 and a Heegaard diagram for it.

with the south-east end going over the north-east end. We replicate this on the diagram, by linking the south-west suture with the south-east suture, resulting in a β-circle that connects these two sutures. Additionally, since the south-east end goes over the north-east end in the tangle, we need to let the β-circle pass behind the north-east suture (i.e., on the back of $\mathcal{S}^2_4$), giving us the modified diagram as shown in Figure 2.17.

Remark 2.52 (Genus 0 Heegaard diagrams for rational tangles)**.** We can immediately notice that, as a consequence of the above construction, every rational tangle admits a genus 0 Heegaard diagram.

In fact, it actually holds that a 4-ended tangle is rational if and only if it has a genus 0 Heegaard diagram. Indeed, if we consider a genus 0 Heegaard diagram for a 4-ended tangle, it has no $\boldsymbol{\alpha}$-circles and just a single $\boldsymbol{\beta}$-circle. By definition, we know that performing surgery along this $\boldsymbol{\beta}$-circle gives us two cylinders, so it separates two punctures from the other two. Therefore the tangle represented is rational. The other direction is proven by the above construction.

The previous construction can be applied to any added twist on a tangle, but it can become challenging when dealing with a larger number of twists. To overcome this, an alternative construction method (which is also implemented in [`nicepy`]) is more convenient and it is here presented.

Suppose we want to construct a genus 0 diagram for a rational tangle $Q_{p/q}$. We start by placing four sutures and four $\boldsymbol{\alpha}$-arcs between them on the plane; the sites are labeled as a, b, c, d, starting from the site between the north-west and south-west sutures and moving counter-clockwise. Then, we place the intersection points on the $\boldsymbol{\alpha}$-arcs by putting p points on sites b and d and q points on sites a and c.

To lay down the $\boldsymbol{\beta}$-circle, we need to take the sign of p/q into account.

- If $p/q > 0$, we start from the north-west suture and find the first intersection point the d site (i.e. the first point "on the right" of the suture) and the first point on the a site (i.e. the first point "below" the suture). We then link them with a straight blue edge, which stays on the front component of $\mathcal{S}^2_4$.

  We continue this process by linking the second intersection point on the d site with the second point on the a site, and so on. After linking the first p

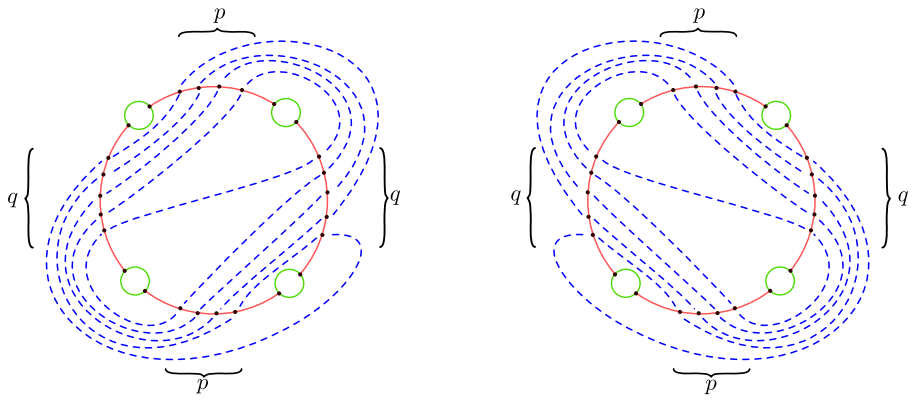

Figure 2.18: The construction for a genus 0 Heegaard diagram for the rational tangle $Q_{p/q}$ with $p/q > 0$ (on the right) and with $p/q > 0$ (on the left).

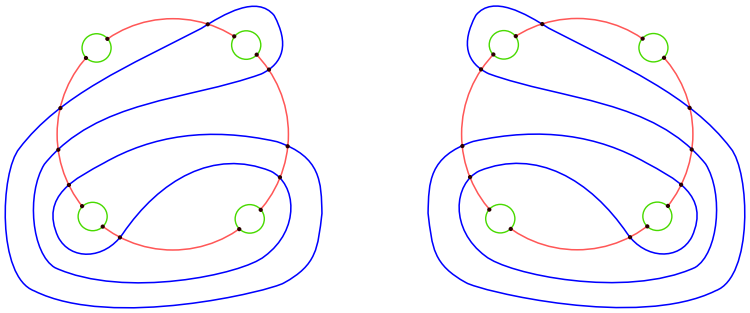

Figure 2.19: Final diagrams for $Q_{1/3}$ (left) and $Q_{-1/3}$ (right).

couples, we have finished the points on site d and move on to the points on site c, scanning them from the top to the bottom. Similarly, after q couples, we move on to the points on site b as the points on site a will be finished and we scan them from the right to the left. The last couple to link will be the one "around" the south-east suture.

Finally, we need to link the points on the back of the sphere, outside of the rectangle, in a similar fashion as before, starting from the north-east suture and moving around to the south-west suture.

- If $p/q < 0$, the procedure is almost the same, but we start from different sutures: for the edges on the front we start from the north-east suture and for the edges on the back we start from the north-west suture.

It is possible to visualise the general construction in Figure 2.18 and in Figure 2.19 it is possible to see the examples for $Q_{\pm 1/3}$.

Remark 2.53.
- In order to remember which one is the right construction, we can notice that if $p/q > 0$ the edges on the front have positive slopes and that if $p/q < 0$ they have negative slope.

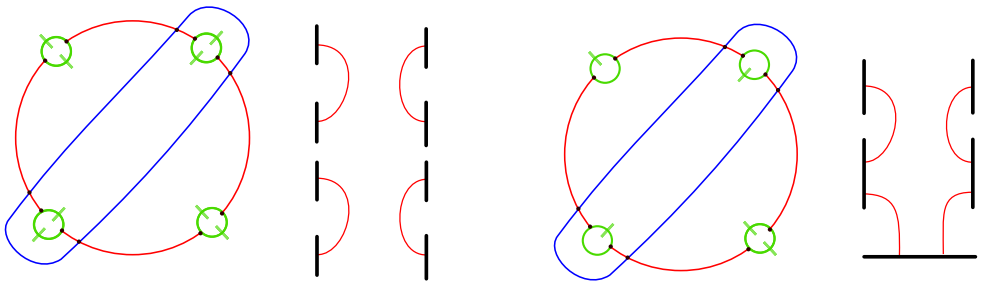

Figure 2.20: Two bordered sutured structures on the tangle Heegaard diagram of Q_1: a trivial one (on the left) and a more interesting one (on the right).

- The coprimality of p and q guarantees that that we will have an unique $\boldsymbol{\beta}$-circle in the final result of the construction.

2.6.2 Heegaard diagrams for tangles as particular case of sutured Heegaard diagrams

As we did in Remark 2.42, we are going to motivate the construction of Heegaard diagrams for tangles with the bordered sutured perspective.

As a reference, one can see Section II.2 of [Zib17].

Starting from a Heegaard diagram for a tangle, we can construct a bordered sutured Heegaard diagram. In fact, the $\boldsymbol{\alpha}$-arcs on the boundary almost define th arc diagram structure, we just need to decide where to "open up" the sutures, i.e. which are the segments of the arc diagram $\mathcal{Z}_\alpha$. We indicate with a green tick the spot on which we cut a suture, we need to put at least one on each suture in order to have a well-defined bordered sutured diagram. In particular, remark that these ticks are going to have the role of basepoints in Bordered Sutured Floer Homology (more details in 4.4.3).

We can see an explicit example of the construction explained above.

Example 2.54. Consider the Heegaard diagram for the 1-crossing tangle presented in Figure 2.14.

One possible choice to make it into a bordered sutured Heegaard diagram is to put two ticks for suture, one on the back and one on the front. This choice would yield the diagram in the left part of Figure 2.20.

By removing some of these ticks, we can obtain a more interesting bordered sutured structure, as shown in the right part of Figure 2.20.

Moreover, we will see in Subsection 3.5.4 how HFT inherits a useful gluing property from Bordered Sutured Floer Homology.

Chapter 3

Heegaard Floer homologies

Now that we have defined Heegaard diagrams for all the topological objects that we are interested in, we can build our way to Heegaard Floer homologies. We see in details the construction of $\widehat{\mathrm{HF}}$, the one for the closed 3-manifold case, which we then adapt to the more general context of sutured 3-manifolds and to the case of 4-ended tangles. After defining the chain complex $\widehat{\mathrm{CF}}$ on which we compute $\widehat{\mathrm{HF}}$, it will be clear that the difficulty of this homology lies in the construction of the boundary map: this is the main motivation for our interest in *nice Heegaard diagrams*, that will be discussed in extension in Chapter 4. In the last section, we construct tangle Heegaard Floer Homology, the main focus of this thesis work. The description of the invariant yielded by it is going to be of use in Chapter 5, where we will see the invariants obtained from the computation of HFT for some families of tangles.

3.1 Hat version of Heegaard Floer Homology $\widehat{\mathrm{HF}}$

We start the construction of the hat version of Heegaard Floer Homology for closed 3-manifolds, denoted by $\widehat{\mathrm{HF}}$. Traditionally, this was done with the use of *symmetric products*, i.e. products in which the order of the elements in a tuple does not matter. However, following closely what is done in [SW10], we are going to use Robert Lipshitz's cylindrical reformulation of $\widehat{\mathrm{HF}}$, which allows us to completely avoid the discussion on symmetric products. This reformulation is presented in [Lip06], where further details can be found. Details on the construction of $\widehat{\mathrm{HF}}$ via symmetric products can be found in [OS06a], Sections from 4 to 8, or in [Hom19], Section 2.2.

For this section, one can use Section 2 of [SW10] as reference.

We start with the construction of the chain complex $\widehat{\mathrm{CF}}\left(\Sigma, \boldsymbol{\alpha}, \boldsymbol{\beta}, z\right)$, the complex with coefficients in $\mathbb{F}_2 = \mathbb{Z}/2\mathbb{Z}$ on which $\widehat{\mathrm{HF}}$ is computed. For the entirety of this section, let $(\Sigma, \boldsymbol{\alpha}, \boldsymbol{\beta}, z)$ be a genus g pointed Heegaard diagram for some closed 3-manifold Y.

Definition 3.1 (Generator)**.** A *generator* $\mathbf{x}$ in $(\Sigma, \boldsymbol{\alpha}, \boldsymbol{\beta}, z)$ is a collection of g points of Σ, denoted by $\mathbf{x} = \{x_1, \ldots, x_g\}$, such that for any $1 \leq i \leq g$ we have that

- $x_i \in \alpha_i$;
- exists an unique j such that $x_i \in \beta_j$.

We are therefore asking that we have one (and only one) point on each α-curve and on each β-curve. Remark that this implies $x_i \neq z$ for any i.

This name comes to the fact that they are going to be the generators of the chain complex $\widehat{\mathrm{CF}}(\Sigma, \boldsymbol{\alpha}, \boldsymbol{\beta}, z)$, as explained in the next definition.

Definition 3.2 ($\widehat{\mathrm{CF}}(\Sigma, \boldsymbol{\alpha}, \boldsymbol{\beta}, z)$)**.** Let $(\Sigma, \boldsymbol{\alpha}, \boldsymbol{\beta}, z)$ be a Heegaard diagram. We define $\widehat{\mathrm{CF}}(\Sigma, \boldsymbol{\alpha}, \boldsymbol{\beta}, z)$ to be the vector space over $\mathbb{F}_2$ generated by all the generators $\mathbf{x}$ of the diagram.

Now that we have defined $\widehat{\mathrm{CF}}$, we are going to focus on the construction of the main ingredient that we are missing: the boundary map

$$\partial : \widehat{\mathrm{CF}} \longrightarrow \widehat{\mathrm{CF}}.$$

The construction of the boundary map turns out to be the difficult part of this construction, as it involves counting the number of points in certain moduli spaces of holomorphic embeddings of domains in our diagram. Once we reduce ourselves to the nice Heegaard diagram case, we will see that this differential can be computed completely in a combinatorial way; however, we first review the general case.

3.1.1 Domains

The first step is to define *domains* in Heegaard diagrams, i.e. linear combinations of regions delimited by the intersections of $\boldsymbol{\alpha}$-curves and $\boldsymbol{\beta}$-curves on Σ.

Definition 3.3 (Region, 2-chain)**.** A *region* is a connected component of $\Sigma \setminus (\boldsymbol{\alpha} \cup \boldsymbol{\beta})$. A formal sum of region with integer coefficients is called a *2-chain*.

In general, for a 2-chain $\phi = \sum_i a_i \cdot \phi_i$ we will denote by $\partial\phi$ its boundary

$$\partial\phi = \sum_i a_i \cdot \partial\phi_i.$$

Moreover, we denote by $\partial(\phi)_{|\boldsymbol{\alpha}} = \partial(\phi) \cap \boldsymbol{\alpha}$ the $\boldsymbol{\alpha}$-edges on the boundary of ϕ and by $\partial(\phi)_{|\boldsymbol{\beta}} = \partial(\phi) \cap \boldsymbol{\beta}$ the $\boldsymbol{\beta}$-edges.

Definition 3.4 (Domains and $\pi_2(\mathbf{x}, \mathbf{y})$)**.** Let now $\mathbf{x}, \mathbf{y}$ be two generators. We are going to denote by $\pi_2(\mathbf{x}, \mathbf{y})$ the collection of all 2-chains ϕ such that $\partial(\partial(\phi)_{|\boldsymbol{\alpha}}) = \mathbf{y} - \mathbf{x}$, all the elements of this set are called *domains*. We also say that $\partial\phi$ *connects* $\mathbf{x}$ *to* $\mathbf{y}$ when $\phi \in \pi_2(\mathbf{x}, \mathbf{y})$.

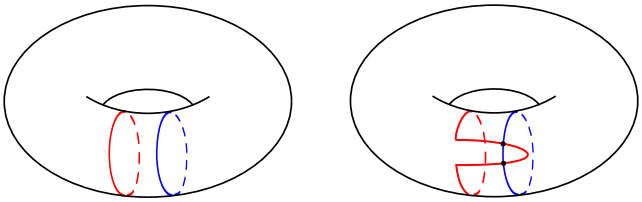

Figure 3.1: An example of a non-admissible diagram and how it is possible to make it admissible.

We can define an additive structure on the set $X = \{\pi_2(\mathbf{x}, \mathbf{y}) \mid \mathbf{x}, \mathbf{y} \text{ generators}\}$ in the following way: let ϕ, ϕ' be two domains such that $\phi = \sum_i a_i \cdot \phi_i$ connects $\mathbf{x}$ to $\mathbf{y}$ and $\phi' = \sum_j a'_j \cdot \phi'_j$ connects $\mathbf{y}$ to $\mathbf{z}$; then we can sum them to get a domain which connects $\mathbf{x}$ to $\mathbf{z}$ as

$$\phi + \phi' := \sum_i a_i \cdot \phi_i + \sum_j a'_j \cdot \phi'_j \in \pi_2(\mathbf{x}, \mathbf{z}).$$

This operation results in an addition

$$\pi_2(\mathbf{x}, \mathbf{y}) \times \pi_2(\mathbf{y}, \mathbf{z}) \xrightarrow{+} \pi_2(\mathbf{x}, \mathbf{z}).$$

Given a point $p \in \Sigma \setminus (\boldsymbol{\alpha} \cup \boldsymbol{\beta})$, we define the *algebraic intersection number of p in ϕ*, denoted $n_p(\phi)$, to be the coefficient of the region containing p in ϕ; we say that a domain ϕ is *positive* if $n_p(\phi) \geq 0$ for all points $p \in \Sigma \setminus (\boldsymbol{\alpha} \cup \boldsymbol{\beta})$.

Moreover, we define $\pi_2^0(\mathbf{x}, \mathbf{y})$ to be the collection of domains such that have algebraic intersection number 0 on the basepoint z (i.e. the collection of domains that do not contain the basepoint). In symbols,

$$\pi_2^0(\mathbf{x}, \mathbf{y}) = \{\phi \in \pi_2(\mathbf{x}, \mathbf{y}) \mid n_z(\phi) = 0\}.$$

Remark 3.5. The addition of domains is also well-defined in this last case, i.e.

$$\pi_2^0(\mathbf{x}, \mathbf{y}) \times \pi_2^0(\mathbf{y}, \mathbf{z}) \xrightarrow{+} \pi_2^0(\mathbf{x}, \mathbf{z}).$$

Definition 3.6 (Periodic domains)**.** Let $\mathbf{x}$ be a generator. We call $\phi \in \pi_2^0(\mathbf{x}, \mathbf{x})$ a periodic domain if, for each i, the segments of α_i appear with the same multiplicity on $\partial\phi$ and the same happens for any β_i.

More informally, we are asking that $\partial\phi$ can be expressed as a sum of the $\boldsymbol{\alpha}$-circles and $\boldsymbol{\beta}$-circles.

Definition 3.7 (Admissible Heegaard diagram)**.** We say that a Heegaard diagram is *admissible* if, for any generator $\mathbf{x}$ and any non-zero periodic domain $\phi \in \pi_2^0(\mathbf{x}, \mathbf{x})$, we have that ϕ has positive and negative coefficients. This property is sometimes also called *weak admissibility*.

It is possible to see an example of a non-admissible diagram in Figure 3.1.

The condition of being admissible for Heegaard diagrams is necessary when the first Betti number $b_1(Y)$ of the 3-manifold Y is greater than zero.

There may not be a domain that connects two given generators $\mathbf{x}$ and $\mathbf{y}$. Determining whether or not $\pi_2(\mathbf{x},\mathbf{y})$ is empty can be challenging from a graphical perspective, but we can use an algebraic method to check this more easily.

Definition 3.8 ($\varepsilon(\mathbf{x},\mathbf{y})$)**.** Let $\mathbf{x},\mathbf{y}$ be two generators, explicitly written as $\mathbf{x} = \{x_1,\dots,x_g\}$ and $\mathbf{y} = \{y_1,\dots,y_g\}$. We are now going to construct two paths from $\mathbf{x}$ to $\mathbf{y}$, such that one is composed only by $\boldsymbol{\alpha}$-arcs and one only by $\boldsymbol{\beta}$-arcs. We define the path a as a union of g arcs in $\alpha_1 \cup \dots \cup \alpha_g$, say $a = \gamma_1 \cup \dots \cup \gamma_g$, such that $\partial a = y_1 + \dots + y_g - x_1 - \dots - x_g$. In the same way, let $b = \delta_1 \cup \dots \cup \delta_g \subset \beta_1 \cup \dots \cup \beta_g$ be a path with $\partial b = y_1 + \dots + y_g - x_1 - \dots - x_g$. Therefore, the difference $a - b$ is a closed 1-cycle in Σ and we define

$$\varepsilon(\mathbf{x},\mathbf{y}) := [a-b] \in H_1(Y,\mathbb{Z}).$$

Notice that $\varepsilon(\mathbf{x},\mathbf{y})$ is independent of the choice of the paths a and b.

As anticipated before, the following criterion explains how we can use $\varepsilon(\mathbf{x},\mathbf{y})$ to determine whether we have or not a domain connecting $\mathbf{x}$ and $\mathbf{y}$; this is going to be quite useful for the study of Heegaard diagrams.

Proposition 3.9 (Criterion for existence of connecting domain ([Lip06, Lemma 2.2]))**.** *Let $\mathbf{x},\mathbf{y}$ be two generators of a genus g Heegaard diagram $(\Sigma,\boldsymbol{\alpha},\boldsymbol{\beta})$ of a 3-manifold Y. Consider two paths a, b as described above; then*

$$\varepsilon(\mathbf{x},\mathbf{y}) = 0 \iff \pi_2(\mathbf{x},\mathbf{y}) \neq \emptyset.$$

We observe that the generators of a Heegaard diagram can be naturally classified into equivalence classes, with each class corresponding to an element in an affine space over $H_1(Y;\mathbb{Z})$.

This shows that the set of generators of a Heegaard diagram naturally falls into equivalence classes labelled by elements in an affine space over $H_1(Y;\mathbb{Z})$.

Sketch of proof ([Lip06]). ($\Rightarrow$) The main idea to prove this direction is to exploit the fact that a 2-chain $\phi \in H_2(Y)$ can be thought as a domain in $\pi_2(\mathbf{x},\mathbf{y})$ as well. When $g \geq 2$, we have to exploit the following isomorphism

$$H_2(Y) \cong \frac{H_2\big((\Sigma\times I) \cup \sqcup_{\boldsymbol{\alpha}\times I}\left(\mathbb{D}^2\times I\right) \sqcup_{\boldsymbol{\beta}\times I}\left(\mathbb{D}^2\times I\right)\big)}{\langle e_1+\dots+e_n\rangle},$$

where $e_1,\dots,e_n$ are the regions of the diagram. To see this, one can use Mayer-Vietoris on the decomposition

$$Y = \Big((\Sigma\times I) \cup \sqcup_{\boldsymbol{\alpha}\times I}\left(\mathbb{D}^2\times I\right) \sqcup_{\boldsymbol{\beta}\times I}\left(\mathbb{D}^2\times I\right)\Big) \sqcup \Big(\sqcup_0 B^3 \sqcup_1 B^3\Big),$$

exploiting similar arguments to the ones used proving Lemma 2.6.

Since $\varepsilon(\mathbf{x},\mathbf{y}) = 0 = [a-b] \in H_1(Y)$, we have $a - b = \partial\phi$ for some ϕ. Such ϕ can be pushed on Σ (via the isomorphism above indicated), obtaining a domain in $\pi_2(\mathbf{x},\mathbf{y})$ as we wanted.

($\Leftarrow$) For the converse, assume that $\pi_2(\mathbf{x},\mathbf{y}) \neq 0$. This means that we have a domain ϕ such that $\partial(\partial(\phi)_{|\boldsymbol{\alpha}}) = \mathbf{y} - \mathbf{x}$ and $\partial(\partial(\phi)_{|\boldsymbol{\beta}}) = \mathbf{y} - \mathbf{x}$; we define

$$\varepsilon(\mathbf{x},\mathbf{y}) = \left[\partial(\partial(\phi)_{|\boldsymbol{\alpha}}) - \partial(\partial(\phi)_{|\boldsymbol{\beta}})\right] \in H_1(Y).$$

Hence, we clearly have $\varepsilon(\mathbf{x},\mathbf{y}) = [\partial\phi] = 0$. □

Remark 3.10. The notion of $\varepsilon(\mathbf{x},\mathbf{y})$ involves additional details, including the notion of *Spin$^{\mathbb{C}}$-structure*. However, since we do not require it for our current purpose, we will not discuss it in detail and simply refer readers to Section 6 of [OS06a] for further information.

3.1.2 The Maslov index

We now define the *Maslov index*, a central notion in the construction of the boundary map of $\widehat{\mathrm{CF}}$.

For this, we follow Lipshitz cylindrical reformulation presented in [Lip06], as it is done in [SW10].

Fix a domain ϕ and two generators $\mathbf{x},\mathbf{y}$ such that $\phi \in \pi_2^0(\mathbf{x},\mathbf{y})$. We want to define what a *holomorphic embedding* of ϕ is. Let S be a surface with boundary, with $2g$ marked points $(X_1,\dots,X_g,Y_1,\dots,Y_g)$ on ∂S, such that the X-points and the Y-points alternate. The $2g$ arcs on ∂S in the complement of the marked points are divided into two groups, call them A and B, each containing g arcs, such that the A-arcs and the B-arcs alternate.

Let p_1 and p_2 be the projection maps from $\Sigma \times \mathbb{D}^2$ onto the two factors of the product; we consider $\mathbb{D}^2 \subset \mathbb{C}^2$ and we call $e_1 \subset \partial\mathbb{D}^2$ the arc that connects $-i$ to i and $e_2 \subset \partial\mathbb{D}^2$ the one from i to $-i$.

Let $u : S \to \Sigma \times \mathbb{D}^2$ be the map in the following diagram

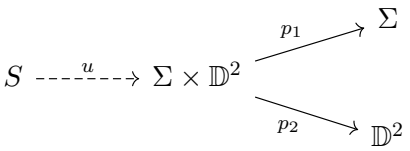

such that the following properties are satisfied:

- $p_1 \circ u$ is equal to ϕ in $H_2(\Sigma)$;
- in the second homology group $H_2(\mathbb{D}^2,\partial\mathbb{D}^2)$, $[p_2 \circ u] \equiv g\mathbb{D}^2$;
- $p_1 \circ u\,(\{X_1,\dots X_g\}) = \{x_1,\dots,x_g\}$ and $p_2 \circ u\,(\{X_1,\dots X_g\}) = \{-i\}$;
- $p_1 \circ u\,(\{Y_1,\dots Y_g\}) = \{y_1,\dots,y_g\}$ and $p_2 \circ u\,(\{Y_1,\dots Y_g\}) = \{i\}$;
- $p_1 \circ u\,(A) \subset \boldsymbol{\alpha}$ (more precisely, every A-arc is sent to some $\boldsymbol{\alpha}$-arc) and $p_2 \circ u\,(A_i) \subset e_1$ for any A-arc A_i;

- $p_1 \circ u(B) \subset \boldsymbol{\beta}$ (more precisely, every B-arc is sent to some $\boldsymbol{\beta}$-arc) and $p_2 \circ u(B_i) \subset e_2$ for any B-arc B_i.

Definition 3.11 (Holomorphic embedding for a domain)**.** For a domain ϕ and two generators $\mathbf{x}, \mathbf{y}$ such that $\phi \in \pi_2^0(\mathbf{x}, \mathbf{y})$, we call a map that satisfies the properties of the map u described above a *holomorphic embedding* of ϕ, sometimes also referred to as a *holomorphic representative*. Remark that the existence of such map for a given domain is not guaranteed.

Remark 3.12 (On the definition of S)**.** In the construction of $\widehat{\mathrm{HF}}$ done via Whitney discs, the surface with boundary S is generated starting from a representation f of some domain ϕ, where $f : \mathbb{D}^2 \to \mathrm{Sym}^g(\Sigma)$, as

$$S = \left\{(c, d) \in \mathbb{D}^2 \times \Sigma \mid d \in f(c)\right\}.$$

Therefore, the projection $p_2 : S \to \mathbb{D}^2$ is a g-fold branched covering map and the projection $p_1 : S \to \Sigma$ defines a 2–chain in Σ. Then, we proceed by taking two points a, b on $\partial\mathbb{D}^2$ which map to $\mathbf{x}$ and $\mathbf{y}$ and the $2g$ marked points $(X_1, \dots, X_g, Y_1, \dots, Y_g)$ on ∂S are obtained as the inverse images of a, b under p_2. The construction then continues as we presented above.

Definition 3.13 (Trivial disc)**.** We call a *trivial disc* a component of S that is mapped to a point by $p_1 \circ u$.

Now fix complex structures on Σ and $\mathbb{D}^2$ and take the product complex structure on $\Sigma \times \mathbb{D}^2$.

Remark 3.14. To do things properly, now we would have to talk about *almost-complex structures* and *perturbations*. However, for the main topic of this thesis, these are not needed and we will gloss over these details. However, as one can see in [Lip06] or in Theorem 3.4 of [SW10], the hypothesis needed for our work are satisfied once a choice of a generic perturbation on the $\boldsymbol{\alpha}$-circles and on the $\boldsymbol{\beta}$-circles is made.

Consider now all the holomorphic embeddings u described above for a fixed domain ϕ. They form a *moduli space*, denoted by $\mathcal{M}(\phi)$, that we claim to be a finitely dimensional, smooth manifold. We will not prove such properties of $\mathcal{M}(\phi)$, however one can find in [OS04b], Proposition 3.9, a proof of the smoothness.

Definition 3.15 (Maslov index)**.** We can now define the *Maslov index* for a domain ϕ. It is denoted by $\mu(\phi)$, and it is defined to be the expected dimension of $\mathcal{M}(\phi)$.

At first glance, this index seems to be quite difficult to compute. However, it turns out that it can be computed combinatorially in terms of the *Euler measure* and the *point measures*, which are defined as follows.

Definition 3.16 (Point measure)**.** For a generator $\mathbf{x} = \sum_i x_i$ and a domain ϕ, the point measure on a single x_i, denoted $\mu_{x_i}(\phi)$, is defined to be the average of the coefficients of the four regions around x_i in ϕ (see Figure 3.2).

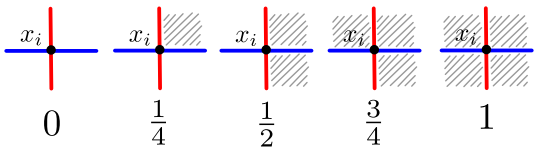

Figure 3.2: Point measure $\mu_{x_i}(\phi)$ (the shadowed part of the drawing represents ϕ).

The *point measure* $\mu_{\mathbf{x}}(\phi)$ is defined as

$$\mu_{\mathbf{x}}(\phi) = \sum_{i=1}^{g} \mu_{x_i}(\phi).$$

Definition 3.17 (Euler measure)**.** If we fix a metric on Σ which makes all the α and β circles geodesic, intersecting each other with right angles, then the *Euler measure* $e(\phi)$ is defined to be $1/2\pi$ of the integral of the curvature on ϕ.

Remark 3.18 (Combinatorial formula for Euler measure)**.** As shown by Lipshitz in [Lip06] (Corollary 4.10), the Euler measure can be computed combinatorially in the following way. Let us consider a region ϕ; then we have that

$$e(\phi) = \chi(\phi) - \frac{1}{4}\#\{\text{acute corners}\} + \frac{1}{4}\#\{\text{obtuse corners}\},$$

where $\chi(\phi)$ is the Euler characteristic of ϕ (this number can be computed as $\chi(\phi) = k_0 - k_1 + k_2 - k_3 + \dots$, where k_i is the number of i-cells in ϕ as a CW-complex). To better explicit what we mean by "acute corners" and "obtuse corners", look at Figure 3.3.

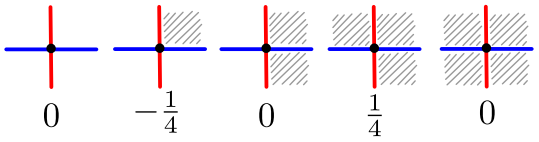

Figure 3.3: Acute and obtuse corners and their contribute for Euler measure, where the shadowed part of the drawing represents ϕ.

Remark now that the Euler measure is additive. Therefore, if we consider a domain $\phi = \sum_i r_i\phi_i$, we can compute its Euler measure as

$$e(\phi) = \sum_i r_i \left(\chi(\phi_i) - \frac{1}{4}\#\{\text{acute corners}\} + \frac{1}{4}\#\{\text{obtuse corners}\}\right).$$

Remark 3.19. If ϕ is a $2n$-gon region, then it is topologically a disk and hence $\chi(\phi) = 1$. Therefore, $e(\phi) = 1 - {}^{(2n)}/_4 = 1 - {}^{n}/_2$.

We have then the following formula, proven by Lipshitz in [Lip06], that explain exactly how to compute the Maslov index in terms of the point measure and the Euler measure.

Proposition 3.20 (Lipshitz Formula ([Lip06]))**.** *For a domain $\phi \in \pi_2(\mathbf{x}, \mathbf{y})$, the Maslov index is given by*

$$\mu(\phi) = e(\phi) + \mu_{\mathbf{x}}(\phi) + \mu_{\mathbf{y}}(\phi).$$

Remark 3.21 (Additivity of Maslov index ([Lip06]))**.** It is possible to prove that the Maslov index is additive, i.e.

$$\mu(\phi_1 + \phi_2) = \mu(\phi_1) + \mu(\phi_2).$$

This can be seen with some analytical arguments, see for instance [Lip06], or with some combinatorial arguments closer to the setting presented here, see Theorem 3.3 of [Sar11].

3.1.3 Hat version of Heegaard Floer Homology

We can almost define the boundary map in the chain complex $\widehat{\mathrm{CF}}$. The last piece that is missing, which is also the only non-combinatorial part of $\widehat{\mathrm{HF}}$, is a *count function* that counts the points of a manifold constructed starting from $\mathcal{M}(\phi)$.

Definition 3.22 ($\mathbb{R}$-action on $\mathcal{M}(\phi)$)**.** If ϕ is non-trivial, then $\mathcal{M}(\phi)$ admits a free $\mathbb{R}$-action coming from the one-parameter family of holomorphic automorphisms of $\mathbb{D}^2$ which preserves $\pm i$ and the boundary arcs e_1, e_2.

One way to see this $\mathbb{R}$-action is to use the Riemann mapping theorem to change the unit disc to the infinite strip $[0,1] \times i\mathbb{R} \subset \mathbb{C}$, where e_1 corresponds to $\{1\} \times i\mathbb{R}$ and e_2 to $\{0\} \times i\mathbb{R}$. Then the $\mathbb{R}$-action corresponds to vertical translations.

We let $\widetilde{\mathcal{M}}(\phi) = \mathcal{M}(\phi)/\mathbb{R}$. If $\mu(\phi) = 1$, then $\widetilde{\mathcal{M}}(\phi)$ is a compact zero dimensional manifold (see [OS04b], Theorem 3.18).

Therefore, when $\mu(\phi) = 1$, we can then define a *count function* that counts the points of $\widetilde{\mathcal{M}}(\phi)$.

Definition 3.23 (Count function $c(\phi)$)**.** Let $\phi \in \pi_2^0(\mathbf{x}, \mathbf{y})$ be a domain such that $\mu(\phi) = 1$. We define the *count function* $c(\phi)$ to be the number of points in $\widetilde{\mathcal{M}}(\phi)$, counted modulo 2.

Remark 3.24 (On the relation of $\mu(\phi)$ and $c(\phi)$)**.** As we stated above, $\mu(\phi)$ is the expected dimension of $\mathcal{M}(\phi)$. In particular, even if $\mu(\phi) = 1$, we cannot say for sure that ϕ has some holomorphic embeddings and that $\widetilde{\mathcal{M}}(\phi)$ has at least one point; $\mathcal{M}(\phi)$ can be empty even if $\mu(\phi) = 1$. On the other hand, if ϕ does not have any holomorphic embedding and $\mu(\phi) = 1$, then $c(\phi) = 0$.

Thanks to this count function, we can define the boundary map of $\widehat{\mathrm{CF}}$.

Definition 3.25 (Boundary map of $\widehat{\mathrm{CF}}$)**.** The *boundary map* ∂ in the chain complex $\widehat{\mathrm{CF}}$ is defined as

$$\mathbf{x} \mapsto \partial\mathbf{x} = \sum_{\mathbf{y}} \left(\sum_{\substack{\phi \in \pi_2^0(\mathbf{x},\mathbf{y}) \\ \text{s.t. } \mu(\phi)=1}} c(\phi) \cdot \mathbf{y} \right).$$

It is shown in [Lip06] (Lemma 8.1) that indeed this is a chain complex. Therefore, we can then define hat Heegaard Floer Homology for a Heegaard diagram.

Definition 3.26 ($\widehat{\mathrm{HF}}(\Sigma,\boldsymbol{\alpha},\boldsymbol{\beta},z)$)**.** Given a Heegaard diagram $(\Sigma,\boldsymbol{\alpha},\boldsymbol{\beta},z)$, we define the *Floer Homology group* of the diagram to be the Homology group of the chain complex $\left(\widehat{\mathrm{CF}}(\Sigma,\boldsymbol{\alpha},\boldsymbol{\beta},z),\partial\right)$, which is denoted by $\widehat{\mathrm{HF}}(\Sigma,\boldsymbol{\alpha},\boldsymbol{\beta},z)$.

As one can read in Section 8 of [OS06a], the following result holds.

Theorem 3.27 ([OS06a, Theorem 1])**.** *Let $(\Sigma,\boldsymbol{\alpha},\boldsymbol{\beta},z)$ and $(\Sigma',\boldsymbol{\alpha}',\boldsymbol{\beta}',z')$ be two Heegaard diagrams representing the same closed 3-manifold Y. Then $\widehat{\mathrm{HF}}\,(\Sigma,\boldsymbol{\alpha},\boldsymbol{\beta},z)$ and $\widehat{\mathrm{HF}}\,(\Sigma',\boldsymbol{\alpha}',\boldsymbol{\beta}',z')$ are isomorphic.*

Therefore, we can define Heegaard Floer Homology for closed 3-manifolds.

Definition 3.28 ($\widehat{\mathrm{HF}}(Y)$)**.** We define $\widehat{\mathrm{HF}}(Y)=\widehat{\mathrm{HF}}(\Sigma,\boldsymbol{\alpha},\boldsymbol{\beta},z)$, for some choice of Heegaard diagram of Y.

In fact, in [Lip06] is proved that the chain complex $\widehat{\mathrm{CF}}(\Sigma,\boldsymbol{\alpha},\boldsymbol{\beta},z)$ that we constructed is indeed an invariant for the closed 3-manifold Y.

Remark 3.29. All the theory developed so far is quite *combinatorial* (in the sense that it could be easily handled by a calculator) except for this count function above defined.

The problem can be solved using *nice Heegaard diagrams*. In fact, if a diagram has the property of being *nice* (a notion that will be defined in Chapter 4), we can make also this final piece of the theory combinatorial, and the invariant can be computed using a calculator.

3.2 A first example: $\widehat{\mathrm{HF}}(L(p,q))$

In this section, we will demonstrate how to compute Heegaard Floer Homology through a simple example. While we will not need to calculate the complex boundary map of the chain complex in this case, this example will still serve to illustrate how these objects can be manipulated and provide insight into working with them.

We compute the Heegaard Floer Homology of the general Lens space $L(p,q)$. Recall the definition of $L(p,q)$, given already in Example 1.17 as the quotient of $\mathcal{S}^3$ by the action of $\mathbb{Z}/p\mathbb{Z}$ previously defined.

Our goal is to prove that

$$\widehat{\mathrm{HF}}(L(p,q))=(\mathbb{F}_2)^p.$$

We begin by constructing a Heegaard diagram for $L(p,q)$. As mentioned earlier, it is known that $L(p,q)$ has a genus 1 Heegaard diagram (Σ,α,β). Let s and t denote the generators of $H_1(\Sigma)=\mathbb{Z}^2$, as shown in Figure 3.4.

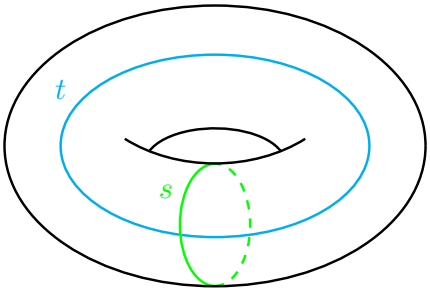

Figure 3.4: Generators of the first homology group of the torus.

With this notation, the curves of the Heegaard diagram are described as $[\alpha] = s$ and $[\beta] = qs + pt$; the curves intersect at p points, hence there are p generators of $\widehat{\mathrm{CF}}$.

3.2.1 Particular case: $\widehat{\mathrm{HF}}(L(3,1))$

Let us start with a more specific example, where $p = 3$ and $q = 1$. This gives us $[\alpha] = s$ and $[\beta] = s + 3t$, with three generators of $\widehat{\mathrm{CF}}$ denoted as x, y, and z.

There are different ways to visualise this Heegaard diagram, but not all of them are useful for computing $\widehat{\mathrm{HF}}$. For instance, the torus embedded in $\mathbb{R}^3$ as shown in Figure 3.5 is not particularly helpful.

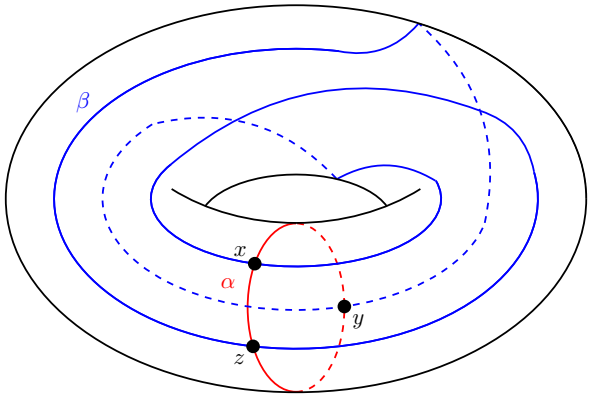

Figure 3.5: Representation of the Heegaard diagram of $L(3,1)$ on an embedded torus.

We could also use the planar representation in Figure 3.6, where we represent the torus as the plane in which we cut out two discs and connect the two boundary components with a handle in the third dimension. However, for the general case of $L(p,q)$, even this representation becomes less helpful.

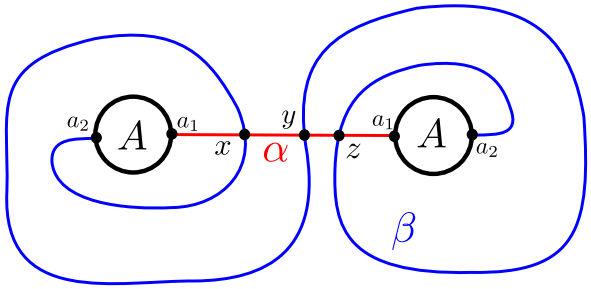

Figure 3.6: Representation of the Heegaard diagram of $L(3,1)$ on a plane with an handle.

A more convenient representation of the Heegaard diagram for $L(p,q)$ is a 2-dimensional rectangle with identified borders, displayed in Figure 3.7. This representation makes it easy to understand the regions obtained and is particularly useful for dealing with the general case of $L(p,q)$.

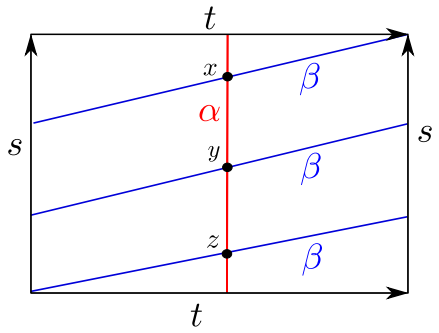

Figure 3.7: Representation of the Heegaard diagram of $L(3,1)$ on a rectangle with identified borders.

There are three regions in this Heegaard diagram, each with all three generators as vertices, with one generator repeated twice. We want to understand the differentials of $\widehat{\mathrm{CF}}$ for this diagram. As a first step, we investigate whether there are any regions that connect two generators. To do so, we use Proposition 3.9 to show that π_2^0 is empty for all pairs of generators. For example, we compute $\varepsilon(x,y)$.

First of all, we need to compute $H_1(L(3,1))$; for $(\star)$ we have that

$$H_1(L(3,1)) \cong \frac{H_1(\Sigma)}{\langle [\alpha],[\beta]\rangle} \cong \frac{\langle s,t\rangle}{\langle s, s+3t\rangle} \cong \frac{\mathbb{Z}}{3\mathbb{Z}}.$$

We need now two paths, $a \subset \mathbb{T}_\alpha$ and $b \subset \mathbb{T}_\beta$ that link x to y; we choose them as in Figure 3.8.

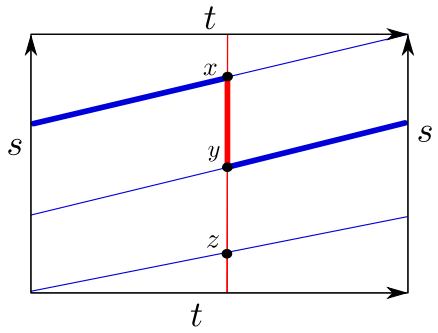

Figure 3.8: The paths a and b that connect x and y: the thickened vertical red edge is a, the thickened blue diagonal edges compose b.

It is clear that $[a-b] = [t] = 1 \in H_1(L(3,1))$, therefore $\varepsilon(x,y) \neq 0$. We can conclude that there are not domains that connect x and y, i.e. $\pi_2(x,y) = \emptyset$. The same reasoning works for all the combinations of generators; henceforth the differential map in $\widehat{\mathrm{CF}}$ is trivial. Since we have three generators for our chain complex, we conclude that $\widehat{\mathrm{HF}}(L(3,1))$ is a 3-dimensional space over $\mathbb{F}_2$, hence

$$\widehat{\mathrm{HF}}(L(3,1)) \cong (\mathbb{F}_2)^3 .$$

3.2.2 General case

Now let us consider the general case of $L(p,q)$. To draw its Heegaard diagram, we start by taking the 2-dimensional torus representation and dividing it into p horizontal stripes and q vertical stripes. Then we draw the α circle on the vertical edges of the rectangles (i.e., on the s edge), and the β circle along the diagonals of the rectangles given by the stripes-subdivision.

It is worth noting that we have exactly p regions. Starting from the left, these regions can only go "strictly" to the right, and they are path-connected since they are connected by hypothesis and the torus is path-connected. To count them, we only need to count how many starting points of paths there are immediately on the right of the curve α drawn on the left, which are exactly p.

Now we want to understand how the differential behaves in this case. As before, we will use Proposition 3.9.

We first compute $H_1(L(p,q))$:

$$H_1(L(p,q)) \cong \frac{H_1(\Sigma)}{\langle [\alpha], [\beta] \rangle} \cong \frac{\langle s,t \rangle}{\langle s, qs+pt \rangle} \cong \frac{\langle s,t \rangle}{\langle s, pt \rangle} \cong \frac{\mathbb{Z}}{p\mathbb{Z}}.$$

Take now two distinct generators x_i, x_j. Clearly any path $b \subset \beta$ that links them goes from left to right completely at least one time and strictly less than p times (as $x_i \neq x_j$); therefore $0 \neq \varepsilon(x_i, x_j) = k \in \mathbb{Z}/p\mathbb{Z}$ and $\pi_2(x_i, x_j) = \emptyset$ for any pair of generators.

As in the particular case, we have found that the differential map is trivial in $\widehat{\mathrm{CF}}$. Since we have p generators, the Heegaard Floer Homology is a p-dimensional

vector space over $\mathbb{F}_2$. We have then proved

$$\widehat{\mathrm{HF}}(L(p,q)) \cong (\mathbb{F}_2)^p .$$

3.3 Sutured Floer Homology SHF

In this section we introduce sutured Floer Homology, a generalisation of $\widehat{\mathrm{HF}}$ constructed for sutured manifolds.

As reference, one can look at Section 9 of [Juh06] and Section 6 of [Juh13].

The construction of the chain complex for sutured Floer Homology is similar to that of $\widehat{\mathrm{HF}}$ for closed manifolds, with the same definitions for generators, domains, $\pi_2(\mathbf{x},\mathbf{y})$, admissible diagrams, and the Maslov index. However, we require sutured diagrams to be admissible. Nonetheless, this is not a limitation since the following lemma holds.

Lemma 3.30 ([Juh06, Proposition 3.15])**.** *Every sutured Heegaard diagram is isotopic to an admissible one.*

Let $(\Sigma,\boldsymbol{\alpha},\boldsymbol{\beta})$ be an admissible sutured Heegaard diagram for some balanced sutured manifold (Y,Γ).

We then define $\mathrm{CF}(\Sigma,\boldsymbol{\alpha},\boldsymbol{\beta})$ to be the vector space over $\mathbb{F}_2$ generated by all the generators $\mathbf{x}$ of $(\Sigma,\boldsymbol{\alpha},\boldsymbol{\beta})$.

To construct the boundary map, we first notice that each border component of Σ has only one region in $\Sigma \setminus (\boldsymbol{\alpha}\cup\boldsymbol{\beta})$ that contains it (recall that we do not allow $\boldsymbol{\alpha}$-arcs in the sutured context). This allows us to regard the sutured diagram as a multi-pointed Heegaard diagram, where we place a basepoint z_i in any region containing a border component.

We define the boundary map in a similar fashion to the closed case, posing

$$\mathbf{x} \mapsto \partial\mathbf{x} = \sum_{\mathbf{y}} \left(\sum_{\substack{\phi\in\pi_2(\mathbf{x},\mathbf{y}) \\ \text{s.t. } n_{z_i}(\phi)=0\,\forall i \\ \text{and } \mu(\phi)=1}} c(\phi)\cdot\mathbf{y} \right).$$

Thanks to Theorem 7.2 of [Juh06], we can see that the one defined is indeed a chain complex.

Proposition 3.31 ([Juh06, Theorem 7.2])**.** $(\mathrm{CF}(\Sigma,\boldsymbol{\alpha},\boldsymbol{\beta}),\partial)$ *is a chain complex.*

Definition 3.32 ($\mathrm{SHF}(\Sigma,\boldsymbol{\alpha},\boldsymbol{\beta})$)**.** Let $(\Sigma,\boldsymbol{\alpha},\boldsymbol{\beta})$ be an admissible sutured Heegaard diagram. We define the *Sutured Floer Homology group* for the diagram to be the homology group of the chain complex $(\mathrm{CF}(\Sigma,\boldsymbol{\alpha},\boldsymbol{\beta}),\partial)$ and we denote it by $\mathrm{SHF}(\Sigma,\boldsymbol{\alpha},\boldsymbol{\beta})$.

Moreover, we can see that this definition leads us to an invariant of the balanced sutured manifold (Y, Γ).

Proposition 3.33 ([Juh06, Theorem 7.5])**.** *Let $(\Sigma, \boldsymbol{\alpha}, \boldsymbol{\beta})$ and $(\Sigma', \boldsymbol{\alpha}', \boldsymbol{\beta}')$ be two admissible sutured Heegaard diagrams for the same balanced sutured manifold. Then holds*

$$\mathrm{SHF}(\Sigma, \boldsymbol{\alpha}, \boldsymbol{\beta}) \cong \mathrm{SHF}(\Sigma', \boldsymbol{\alpha}', \boldsymbol{\beta}').$$

Therefore, we can define sutured Floer Homology for a generic balanced sutured manifold.

Definition 3.34 ($\mathrm{SHF}(Y, \Gamma)$)**.** Let (Y, Γ) be a balanced sutured manifold. We define $\mathrm{SHF}(Y, \Gamma) = \mathrm{SHF}(\Sigma, \boldsymbol{\alpha}, \boldsymbol{\beta})$, where $(\Sigma, \boldsymbol{\alpha}, \boldsymbol{\beta})$ is an admissible sutured Heegaard diagram for (Y, Γ).

Remark 3.35 ($\widehat{\mathrm{HF}}$ in terms of SHF)**.** As anticipated, we can re-visit $\widehat{\mathrm{HF}}$ in terms of SHF. Let Y be a closed 3-manifold. Recall the construction for $(Y', \{s_1\})$ done in Remark 2.35. Then, as it is proven in Proposition 9.1 of [Juh06], it holds

$$\widehat{\mathrm{HF}}(Y) \cong \mathrm{SHF}(Y', \{s_1\}).$$

Therefore, we can see $\widehat{\mathrm{HF}}$ as a special case of SHF.

3.4 Knot Floer Homology HFK

We can naturally extend the construction we did for $\widehat{\mathrm{CF}}$ to the case of knots in $\mathcal{S}^3$. This theory can be further generalised to knots in any 3-manifold, and references for this include [OS04a] and [Ras03].

As reference for this section, one can look at Section 10 of [OS06a].

Definition 3.36 (Knot chain complex $(C(K), \partial_K)$)**.** Let $K \subset \mathcal{S}^3$ be a knot and $(\Sigma, \boldsymbol{\alpha}, \boldsymbol{\beta}, w, z)$ be a compatible doubly pointed Heegaard diagram for K.

We define $C(K)$ to be the vector space over $\mathbb{F}_2$ generated by the generators $\mathbf{x}$ of the diagram. We let

$$\partial_K : C(K) \longrightarrow C(K)$$

to be given by

$$\mathbf{x} \mapsto \partial_K(\mathbf{x}) = \sum_{\mathbf{y}} \left(\sum_{\substack{\phi \in \pi_2(\mathbf{x},\mathbf{y}) \text{ s.t. } \mu(\phi)=1 \\ \text{and } n_z(\phi)=n_w(\phi)=0}} c(\phi) \cdot \mathbf{y} \right).$$

We then have the following result, whose proof can be found in [OS04a].

Theorem 3.37 ([OS04a])**.** $(C(K), \partial_K)$ *is a chain complex.*

Moreover, its homology $\widehat{\mathrm{HFK}}(C(K), \partial_K)$ *is the same given any choice of doubly pointed Heegaard diagrams representing the knot* K*.*

Therefore, we can define the Knot Floer Homology of a knot in $\mathcal{S}^3$.

Definition 3.38 ($\widehat{\mathrm{HFK}}(\mathcal{S}^3, K)$)**.** Let $K \subset \mathcal{S}^3$ be a knot. We define its *Knot Floer Homology* as

$$\widehat{\mathrm{HFK}}(\mathcal{S}^3, K) := \widehat{\mathrm{HFK}}(C(K), \partial_K)$$

for some choice of Heegaard diagrams representing K.

Remark 3.39. With the above description, it is clear how $\widehat{\mathrm{HFK}}$ is a special case of Sutured Floer Homology, in the sense of what said in Remark 2.42.

3.5 Tangle Floer Homology HFT

In this section, we build the invariant HFT for 4-ended tangles.

To understand the construction of Tangle Floer Homology presented by Claudius Zibrowius in [Zib17] and [Zib20], it would be necessary to discuss a specific type of $\mathcal{A}_\infty$-category: the wrapped Fukaya category for the 4-punctured sphere, denoted by $\mathrm{Fuk}(\mathcal{S}^2_4)$. For readers already familiar with the algebraic fundamentals, we can provide a rough idea of this object: $\mathrm{Fuk}(\mathcal{S}^2_4)$ is an $\mathcal{A}_\infty$-category where the objects are Lagrangians on a 4-punctured sphere equipped with a certain 1-form, and the morphisms correspond to intersection points between these Lagrangians. The higher composition maps are defined by "counting some polygons" drawn by these Lagrangians on $\mathcal{S}^2_4$. For more information on this topic, readers may refer to [Abo08], [Abo+13], and [Fuk93], in addition to Zibrowius' articles.

The master thesis excludes the discussion of the construction of HFT through the wrapped Fukaya category for the 4-punctured sphere, as it suffices to consider curves on $\mathcal{S}^2_4$ without delving into that theory. Nonetheless, the thesis acknowledges the use of arguments involving $\mathrm{Fuk}(\mathcal{S}^2_4)$ in proving some results.

As general reference, one can use Chapter III of [Zib17].

As first step, we adapt the notion of *generator* to the case of tangle Heegaard diagrams (non peculiar).

Definition 3.40 (Generator in a tangle Heegaard diagram)**.** Let T be a tangle with n open components and m closed components and let $(\Sigma, \boldsymbol{\alpha} = \boldsymbol{\alpha}^c \cup \boldsymbol{\alpha}^a, \boldsymbol{\beta})$ be a genus g Heegaard diagram representing T.

A *generator in* $(\Sigma, \boldsymbol{\alpha} = \boldsymbol{\alpha}^c \cup \boldsymbol{\alpha}^a, \boldsymbol{\beta})$ is a tuple $\mathbf{x} = (x_1, \dots, x_{g+m+n-1})$, of points $x_1, \dots, x_{g+m+n-1} \in \boldsymbol{\alpha} \cap \boldsymbol{\beta}$ with the properties that:

- there is exactly one point on each $\boldsymbol{\alpha}$- and $\boldsymbol{\beta}$-circle,
- there is at most one point on each $\boldsymbol{\alpha}$-arc.

We denote by $\mathbb{T}$ the set of all the generators of the tangle Heegaard diagram.

We now focus on the case of 4-ended tangles without closed components. Here, generators are of the form $\mathbf{x} = \{x\}$, where x is an intersection point of the $\boldsymbol{\beta}$-circle and one $\boldsymbol{\alpha}$-arc. For any generator $\mathbf{x}$, we can identify the unique site $s(\mathbf{x})$ of the tangle Heegaard diagram on which x is located. We denote by $\mathbb{T}^s$ the set of all generators that lay on the site s. Therefore, we have a partition

$$\mathbb{T} = \bigsqcup_{s \text{ site of } T} \mathbb{T}^s.$$

Domains, sets $\pi_2(\mathbf{x}, \mathbf{y})$, and periodic domains are defined as in the closed 3-manifold case, and admissible tangle Heegaard diagrams are consequentially defined. Without loss of generality, we restrict ourselves to admissible diagrams, as Lemma II.2.8 of [Zib17] shows that any non-admissible diagram can be made admissible. The Maslov index $\mu(\phi)$ for a domain and the count function $c(\cdot)$ are defined in the same way as in the closed case.

We move now to the setting of peculiar Heegaard diagrams. Here, given a domain ϕ, we define $n_y(\phi)$ to be the multiplicity of it at a basepoint $y = p_i, q_j, z_k, w_l$. We set moreover

$$n_p(\phi) = \sum_{i=1}^{4} n_{p_i}(\phi),$$
$$n_q(\phi) = \sum_{j=1}^{4} n_{q_j}(\phi).$$

We now have all the necessary components to define a grading on the domains of a peculiar Heegaard diagram, known as the *Alexander grading*. It should be noted that this grading, along with others, is required for defining the *peculiar module of a 4-ended tangle* T, denoted $\mathrm{CFT}^{\partial}(T)$. While we will not delve into these gradings, it is worth briefly discussing this one, as it is required as input in [`nicepy`] when working with tangles.

Definition 3.41 (Alexander grading)**.** Let T be a 4-ended tangle with m closed components and consider an admissible peculiar Heegaard diagram for T. Call t_1, t_2 the open components and $t_3, \dots, t_{m+2}$ the closed components and assign an orientation to the open components.

Moreover, let $\{(i_1, o_1), (i_2, o_2)\}$ be an ordered partition of $\{1, 2, 3, 4\}$ into pairs, constructed as follows. We associate numbers from 1 to 4 to the tangle ends (starting from north-west and going counter-clockwise); then i_1 is the number corresponding to the inward pointing end of the string t_1 and o_1 the number of the outward pointed end. The same for the second couple and the open component t_2.

Let $\phi \in \pi_2(\mathbf{x}, \mathbf{y})$ for two generators $\mathbf{x}, \mathbf{y}$. We define the *Alexander grading relative to the open components of* ϕ, denoted by $A_{t_k}(\phi)$ for $k = 1, 2$, as

$$A_{t_k}(\phi) := n_{p_{o_k}}(\phi) + n_{q_{o_k}}(\phi) - n_{p_{i_k}}(\phi) - n_{q_{i_k}}(\phi).$$

We define the *Alexander grading relative to the closed components of* ϕ, denoted by $A_{t_h}(\phi)$ for $h = 3, \dots, m+2$ as

$$A_{t_h}(\phi) := n_{w_h}(\phi) - n_{z_k}(\phi).$$

3.5.1 Peculiar modules for 4-ended tangles

This subsection presents an intermediate step in the construction of HFT, specifically, the peculiar module for a 4-ended tangle T, denoted by $\mathrm{CFT}^{\partial}(T)$.

As a reference, see Section III.1 of [Zib17].

Definition 3.42 (Quiver)**.** We call a *quiver* an oriented graph that allows loops and multiple arrows between two vertices.

We are going to work with the following quiver, which we denote by $\mathcal{Q}$.

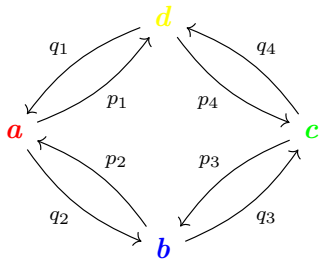

Definition 3.43 (Peculiar algebra $\mathcal{A}^{\partial}$)**.** We define the *peculiar algebra* $\mathcal{A}^{\partial}$ to be $\mathbb{F}_2[\mathcal{Q}]$, the *path algebra* (also called *quiver algebra*) over $\mathcal{Q}$, with relations $p_i q_i = 0 = q_i p_i$. Namely, this is described as

$$\mathcal{A}^{\partial} = \frac{\mathbb{F}_2\left[\mathcal{Q}\right]}{p_i q_i = 0 = q_i p_i}.$$

This is the vector space $\mathbb{F}_2$ generated by all paths in $\mathcal{Q}$, where the multiplication $\mu_{\mathcal{A}^{\partial}}$ is defined as the bilinear extension of the concatenation of paths to the entire vector space. By "concatenating", we mean that given two paths v_1, v_2, then

$$\begin{aligned}\mu_{\mathcal{A}^{\partial}}(v_1, v_2) = & \\ &= v_2 \cdot v_1 \\ &= \begin{cases} v_2 \text{ concatenated } v_1 & \text{if the head of } v_1 \text{ coincides with the tail of } v_2 \\ 0 & \text{otherwise.} \end{cases}\end{aligned}$$

Remark in particular that there exists a constant path on any of the vertices, which we denote by the letter ι; for instance

$$\iota_a \circlearrowright a.$$

We call $\mathcal{I}^\partial$ the ring of idempotents of $\mathcal{A}^\partial$, generated by the idempotent elements of $\mathcal{A}^\partial$, i.e.

$$\mathcal{I}^\partial = \mathbb{F}_2\langle \iota_a, \iota_b, \iota_c, \iota_d \rangle$$

To simplify the notation a bit, we can denote the product in $\mathcal{A}^\partial$ as follows

$$p_i \cdot p_{i+1} \cdot \dots \cdot p_{i+n} = p_{i(i+1)\dots(i+n)}$$
$$q_j \cdot q_{j-1} \cdot \dots \cdot q_{j-m} = q_{j(j-1)\dots(j-m)}$$

where we take the indices modulo 4 and with an offset of 1.

Moreover, we set

$$p = p_1 + p_2 + p_3 + p_4$$
$$q = q_1 + q_2 + q_3 + q_4.$$

With this new notation, the relations $pq = 0 = qp$ hold, and we have $p^2 = p_{12} + p_{23} + p_{34} + p_{41}$, as an example. Furthermore, we can now omit the indices $1, 2, 3, 4$ and write, for instance, $a \xrightarrow{p^3} b$, which means "the only composition of 3 p-maps that links a and b, i.e. p_{341}.

Definition 3.44 (Curved chain complex over $\mathcal{A}^\partial$)**.** A *curved chain complex over* $\mathcal{A}^\partial$ is defined by a pair (X, ∂), where

- X is a left $\mathcal{I}^\partial$-module, and
- ∂ is a morphism $X \xrightarrow{\partial} \mathcal{A}^\partial \otimes_{\mathcal{I}^\partial} X$ such that $\partial^2 = \left(p^4 + q^4\right) \otimes \mathrm{id}_X$, where we define ∂^2 as the following composition of maps

$$X \xrightarrow{\partial} \mathcal{A}^\partial \otimes_{\mathcal{I}^\partial} X \xrightarrow{\mathrm{id}_{\mathcal{A}^\partial} \otimes \partial} \mathcal{A}^\partial \otimes_{\mathcal{I}^\partial} \mathcal{A}^\partial \otimes_{\mathcal{I}^\partial} X \xrightarrow{\mu_{\mathcal{A}^\partial} \otimes \mathrm{id}_X} \mathcal{A}^\partial \otimes_{\mathcal{I}^\partial} X.$$
$$\partial^2$$

We denote by $\mathrm{Mod}^{\mathcal{A}^\partial}_{p^4+q^4}$ the category of all the curved chain complexes over $\mathcal{A}^\partial$: the objects are curved chain complexes and, given two curved chain complexes $(X_1, \partial_1), (X_2, \partial_2)$ the morphisms between them are chain maps, i.e. maps $f : X_1 \to X_2$ that commute with the differentials (meaning $\partial_2 \circ f = f \circ \partial_1$).

Example 3.45 (A first curved chain complex)**.** We can see a first example of a curved chain complex (X, ∂), where X is

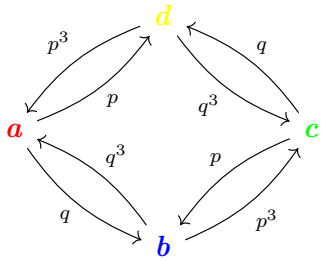

We can see that it is a curved chain complex. Firstly, we have that for all vertices $x \neq y$ holds

$$\sum_z (x \to z \to y) = 0 :$$

in fact, either we have $x \xrightarrow{p^m} z \xrightarrow{q^n} y$ or $x \xrightarrow{q^n} z \xrightarrow{p^m} y$; hence the composition is zero. Secondly, we have that for any vertex x holds

$$\sum_z (x \to z \to x) = p^4 + q^4 :$$

in fact, for any vertex we have one arrow pair whose composition is p^4 and one whose composition is q^4.

We can still slim the notation a bit without adding confusion. Let n, m be positive integers such that $n + m = 4$; then for any two generators x, y we denote

and

With this notation, the last example is represented as

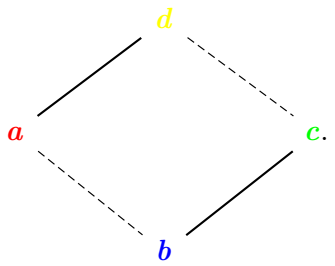

Example 3.46. Using similar arguments to above, one can prove that another example of curved chain complex is the following

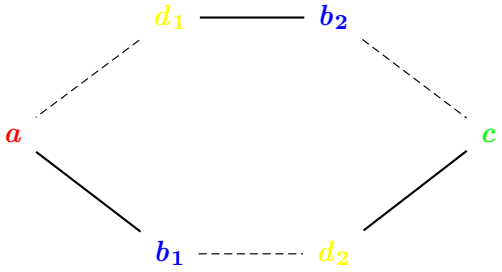

We have two main results that help us to work with curved chain complex: the Cancellation Lemma and the Clean-Up Lemma. This two lemmas allow us to "simplify" curved chain complexes. The proof of both can be found in [Zib20], Lemma 1.22 and Lemma 1.24.

Lemma 3.47 (Cancellation Lemma ([Zib20, Lemma 1.22]))**.** *Let (X, ∂) be a curved chain complex of the following form*

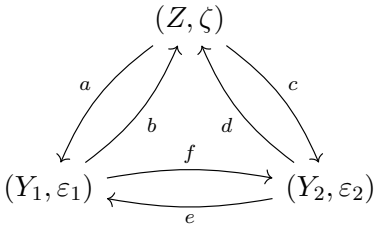

where $(Z, \zeta), (Y_1, \varepsilon_1)$ and (Y_2, ε_2) are pre-curved chain complexes, i.e. a curved chain complex for which we do not require that $\partial^2 = (p^4 + q^4) \cdot \mathrm{id}$, and f is an isomorphism with inverse g.

Then (X, ∂) is chain homotopic to the curved chain complex $(Z, \zeta + bgc)$.

Lemma 3.48 (Clean-Up Lemma ([Zib20, Lemma 1.24]))**.** *Let (X, ∂) be a curved chain complex. Then, for any morphism $h \in Mor((X, \partial), (X, \partial))$ with the properties that*

- $h^2 = 0$,
- $h(h\partial + \partial h) = 0$,
- $(h\partial + \partial h)h = 0$,

it holds that (X, ∂) is chain isomorphic to $(X, \partial + (h\partial + \partial h))$.

In Definition III.1.11 of [Zib17], the author introduced the *peculiar module of a tangle T*. The construction of this module involves three different gradings, including the Alexander grading presented in Definition 3.41. With these gradings, one can define a class of curved chain complexes called *peculiar modules* that are endowed with additional structures given by the gradings. However, since we are only presenting this topic in broad terms to highlight its Floer Homology structure, we will refer to peculiar modules and curved chain complexes interchangeably, without going into the details of the construction of the former.

Definition 3.49 (The peculiar module $\mathrm{CFT}^{\partial}(T)$)**.** et T be a 4-ended tangle without closed components, and let $\mathcal{H}$ be an admissible peculiar Heegaard diagram for T. Let $\mathbb{T}$ be the set of generators of the diagram.

We define $\mathrm{CFT}^{\partial}(T)$ to be the vector space over $\mathbb{F}_2$ generated by elements in $\mathbb{T}$.

We can turn $\mathrm{CFT}^\partial(T)$ into a left $\mathcal{I}^\partial$-module by defining for any $\mathbf{x} \in \mathbb{T}$ the following multiplication

$$\iota_i \cdot \boldsymbol{x} = \begin{cases} \mathbf{x} & \text{if } s(\mathbf{x}) = i, \\ 0 & \text{otherwise .} \end{cases}$$

Moreover, we need to define a boundary map on $\mathrm{CFT}^\partial(T)$; this is done in similar fashion to the closed case.

Definition 3.50 (Boundary map for $\mathrm{CFT}^\partial(T)$)**.** Given a generator $\mathbf{x}$, we define

$$\mathbf{x} \mapsto \partial\mathbf{x} = \sum_{\mathbf{y}} \left(\sum_{\substack{\phi \in \pi_2(\mathbf{x},\mathbf{y}) \\ \text{s.t. } n_p(\phi), n_q(\phi) \geq 0 \\ \text{and } \mu(\phi)=1}} c(\phi) \cdot \iota_{s(\mathbf{x})} \cdot p^{n_p(\phi)} q^{n_q(\phi)} \cdot \iota_{s(\mathbf{y})} \otimes_{\mathcal{I}^\partial} \mathbf{y} \right).$$

The following result states that we have indeed defined a peculiar module in the sense above presented and that it is an invariant for the tangle T.

Theorem 3.51 ([Zib17, Theorem III.1.12])**.** $\mathrm{CFT}^\partial(T)$ *is indeed a well-defined peculiar module. Furthermore, its chain homotopy type is an invariant of the tangle* T*.*

3.5.2 The multicurve invariant HFT

We now link the algebraic theory developed around $\mathrm{Mod}^{\mathcal{A}^\partial}_{p^4+q^4}$ and CFT^∂ and the more geometric perspective of curves in $\mathcal{S}^2_4$. To do so, we need to talk about *multicurves* on $\mathcal{S}^2_4$.

We discuss this according to what is done in Section 1.2 of [Zib19] and in Section 4.2 of [Aub22].

Definition 3.52 (Loop or immersed curved with local system)**.** A *loop* or *immersed curve with local system* on the 4-punctured sphere $\mathcal{S}^2_4$ is defined as a pair (γ, A), where

- γ is an immersion of an oriented circle into $\mathcal{S}^2_4$, which represents a non-trivial primitive element[1] of $\pi_1(\mathcal{S}^2_4)$;
- $A \in \mathrm{GL}_n(\mathbb{F}_2)$ for some integer n.

We consider γ up to isotopy, A up to matrix similarity and (γ, A) up to simultaneous orientation reversal of γ and inversion of the matrix A. Given a loop (γ, A), we say that γ is the *underlying curve* of the loop and that A is its *local system*.

[1] Recall that an element h of a group G is said to be primitive if it does not exists $g \in G$ such that for some $n \in \mathbb{N}_{\geq 2}$ holds $h = g^n$.

Definition 3.53 (Multicurve)**.** We define a *multicurve* on $\mathcal{S}_4^2$ to be an unordered set of loops with local systems $L = \{(\gamma_i, A_i)\}_{i=1}^k$. Given a multicurve L and a loop γ, we define $A_L(\gamma)$ as the direct sum[2] of the following matrices

$$A_L(\gamma) = \bigoplus_{\gamma=\gamma_i} A_i \oplus \bigoplus_{-\gamma=\gamma_i} A_i^{-1},$$

where with $\gamma = \gamma_i$ we mean that they are isotopic and $-\gamma$ is γ with the orientation reversed. We then say that two multicurves $L = \{(\gamma_i, A_i)\}_{i=1}^k$ and $L = \{(\gamma'_j, A'_j)\}_{j=1}^l$ are *isotopic* if for any loop γ the matrices $A_L(\gamma)$ and $A_{L'}(\gamma)$ are similar.

Remark 3.54. It is clear from the definition how it is possible to go from a multicurve to a collection of immersed curves and vice versa. Hence, we can freely talk about collection of immersed curves instead of multicurve if it is advantageous.

Theorem 3.55 ([Zib19, Theorem 1.11])**.** *We can associate a multicurve $L(X, \partial) = \{(\gamma_i, A_i)\}_{i\in I}$ to any peculiar module (X, ∂) in such a way that if another peculiar module (X', ∂') is given with $L(X', \partial') = \{(\gamma'_j, A'_j)\}_{j\in J}$, then (X, ∂) and (X', ∂') are homotopic if and only if their respective multicurves are the same.*

In other words, we have a 1-to-1 correspondence

$$\frac{\left\{\text{Multicurves on } \mathcal{S}_4^2\right\}}{\text{homotopy}} \quad \overset{\text{1:1}}{\longleftrightarrow} \quad \frac{\left\{\text{Objects in } \mathrm{Mod}^{\mathcal{A}^\partial}_{p^4+q^4}\right\}}{\text{chain homotopy}}.$$

An expanded version of Theorem 3.55 is a key result in [Zib20], as described in its Section 0.2. The theorem establishes an equivalence between the category of peculiar modules and the compact portion of the wrapped Fukaya category of $\mathcal{S}_4^2$. This is a central result for HFT, as it allows peculiar modules to be classified in terms of multicurves.

We can see explicitly how this correspondence works with some illustrative examples; a more detailed explanation can be found in Definition 1.10 of [Zib19].

Let $(X, \partial) \in \mathrm{Mod}^{\mathcal{A}^\partial}_{p^4+q^4}$ be a curved chain complex, and consider the 4-punctured sphere $\mathcal{S}_4^2$ with the sites a, b, c, d as previously defined. We have that every generator in X corresponds to an intersection point on some site: a red generator (labeled "a") is a point on the site a, a blue one is on the site b, and so on. Then we have that a solid line that connects two generators is a segment on the front of $\mathcal{S}_4^2$, and a dashed line is a segment on the back of it. See Figure 3.9 for two examples.

[2]Recall that the direct sum of matrices is defined as

$$\oplus_{i=1}^n A_i = \begin{pmatrix} A_1 & 0 & \dots & 0 & 0 \\ 0 & A_2 & \dots & 0 & 0 \\ 0 & 0 & \dots & 0 & 0 \\ \vdots & \vdots & \ddots & \vdots & \vdots \\ 0 & 0 & \dots & 0 & A_n \end{pmatrix}.$$

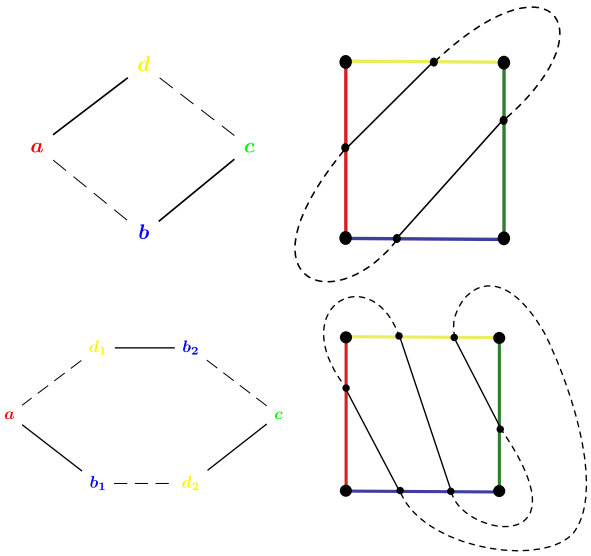

Figure 3.9: Examples of the correspondence between multicurves and curved chain complexes.

We can finally define the invariant HFT in terms of $\mathrm{CFT}^{\partial}(T)$.

Definition 3.56 (HFT)**.** Given an oriented 4-ended tangle T, we define $\mathrm{HFT}(T)$ as the multicurve associated to $\mathrm{CFT}^{\partial}(T)$.

Surprisingly, we can classify the multicurves yielded by HFT with only two families: the *rational curves* and the *special curves* (sometimes also called *irrational curves* in older literature). For this classification, we use the covering space of $\mathcal{S}^2_4$ presented in Section 1.4: given a closed curve $\gamma : \mathcal{S}^1 \to \mathcal{S}^2_4$, we can lift it to a curve $\widetilde{\gamma}$ in $\mathbb{R}^2/\mathbb{Z}^2$ as

$$\begin{array}{ccc} I & \xrightarrow{\widetilde{\gamma}} & \mathbb{R}^2/\mathbb{Z}^2 \\ {\scriptstyle 0\equiv 1}\downarrow & & \downarrow{\scriptstyle \eta} \\ \mathcal{S}^1 & \xrightarrow{\gamma} & \mathcal{S}^2_4. \end{array}$$

Definition 3.57 (Rational and special curves)**.** Let p/q be an element of $\mathbb{Q}\mathrm{P}^1$. We define the *rational curve of slope* p/q to be the primitive loop $\mathfrak{r}(p/q) \subset \mathcal{S}^2_4$ that, under the covering map η, lifts (up to homotopy) to a straight line of slope p/q. We denote it by $\mathfrak{r}_A(p/q)$ if we equip it with the local system A.

Now, let i_1 and i_2 be two distinct tangle ends that lie on a line of slope $p/q \in \mathbb{Q}\mathrm{P}^1$ in $\mathbb{R}^2$ with the lattice given by $\mathbb{Z}^2$. We can divide this line into intervals of equal length with the points of the lattice, and we mark every $(2n)$-th interval of the line for a fixed integer $n > 0$. We consider a small push-off of this line, done in a way that the result intersects only the marked intervals and each of them exactly once. We can define the *special curve of slope* p/q *of length* n *through the punctures* i_1 and

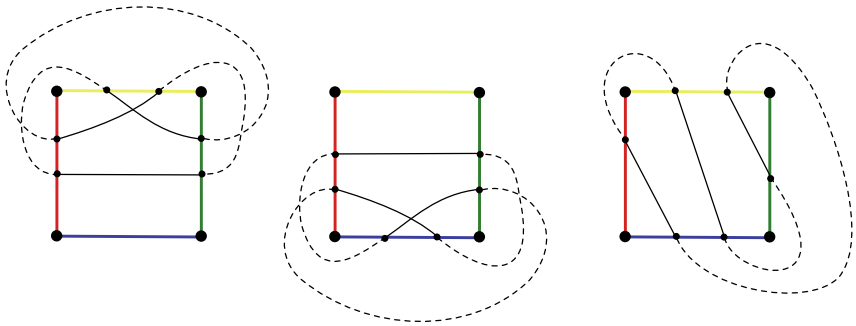

Figure 3.10: Three linear loops. Starting from the left: $\mathfrak{s}_2(0;1,4), \mathfrak{s}_2(0;2,3)$ and $\mathfrak{r}(-2)$.

i_2 to be the primitive loop $\mathfrak{s}_n(p/q; i_1, i_2) \subset \mathcal{S}^2_4$ that, under the covering map η, lifts (up to homotopy) to the curve described above.

If a primitive loop in $\mathcal{S}^2_4$ is either rational or special, we call it *linear with slope* p/q.

The following theorem explains how the multicurves obtained via HFT can be classified by these two families.

Theorem 3.58 ([Zib19, Theorem 0.5])**.** *For a 4-ended tangle T, the underlying curve of each component of* $\mathrm{HFT}(T)$ *is either rational or special. Moreover, if it is special, its local system is equal to an identity matrix.*

We can simplify the notation of the rational and special curves even further. First, we can ignore the data of the local system. In fact, by the above theorem, for special curves the local system is always going to be trivial. For rational curves, it could potentially be non-trivial, but to the author's knowledge, no computation of HFT has yielded a rational curve with a non-trivial local system up to today.

We can simplify the notation even further with the help of the following result: notice that, for each slope p/q and a fixed $n > 0$, there are exactly two choices for the pair of punctures (i_1, i_2). The following theorem tells us that, given any $\mathrm{HFT}(T)$, the number of such components is the same.

Theorem 3.59 ([LMZ20, Theorem 3.9])**.** *Let $i, j, k, l = 1, 2, 3, 4$, $p/q \in \mathbb{Q}\mathrm{P}^1$ and $n \in \mathbb{N}$. Then, for any 4-ended tangle T, the number of components of the form $\mathfrak{s}_n(p/q; i, j)$ and $\mathfrak{s}_n(p/q; k, l)$ in* $\mathrm{HFT}(T)$ *agree.*

We can therefore introduce the following notations for special curves: we denote by $\mathfrak{s}_{2n}(p/q)$ the data of the presence of $\mathfrak{s}_n(p/q; i, j)$ and $\mathfrak{s}_n(p/q; k, l)$.

Furthermore, by recalling the definition of the mirror image $m(\cdot)$ of a tangle, we can explain how it affects the Tangle Floer Homology of a given tangle.

Proposition 3.60 ([Zib20, Proposition 5.4])**.** *Let T be a tangle with Tangle Floer Homology*

$$\mathrm{HFT}(T) = \sum_{i=1}^{n} \mathfrak{r}(p_i/q_i) + \sum_{j=1}^{m} \mathfrak{s}_{2n}(p_j/q_j).$$

Then, it holds

$$\mathrm{HFT}(m(T)) = m\left(\mathrm{HFT}(T)\right) = \sum_{i=1}^{n} \mathfrak{r}(-p_i/q_i) + \sum_{j=1}^{m} \mathfrak{s}_{2n}(-p_j/q_j).$$

3.5.3 Naturality on rational tangles

We can focus on rational tangles in particular, as the HFT invariant exhibits especially nice behavior on them and can even detect them.

In [Zib20], Zibrowius proved the following result.

Theorem 3.61 ([Zib20, Theorem 6.2])**.** *A 4-ended tangle T is rational if and only if* $\mathrm{HFT}(T)$ *consists of single rational component carrying the unique one-dimensional local system. Moreover,* $\mathrm{HFT}(Q_{p/q}) = \mathfrak{r}(p/q)$.

Remark 3.62. This result, justify once more our choice to lose the data of the local system for rational curves.

Moreover, in [Zib19], the author was able to prove a stronger version of the above result, which allows us to know how adding vertical or horizontal (half-) twists to any 4-ended tangle affects HFT. Recall the definition of the two operators τ_1 and τ_2 given in Section 1.4.

Theorem 3.63 ([Zib19, Theorem 2.1])**.** *Let T be a 4-ended tangle and $\tau \in \langle \tau_1, \tau_2 \rangle$. Then*

$$\mathrm{HFT}(\tau T) = \tau\, \mathrm{HFT}(T).$$

Recalling Remark 1.39, we can see a practical example of this last result, as it is going to be a useful argument in Chapter 5. Let T be a tangle and denote its Tangle Floer Homology as

$$\mathrm{HFT}(T) = \sum_{i=1}^{n} \mathfrak{r}(p_i/q_i) + \sum_{j=1}^{m} \mathfrak{s}_{2n}(p_j/q_j).$$

Assume that we want to add a horizontal or vertical half-twists to it. Denote the resulting tangle as T'; if the half-twist is horizontal, then

$$T' = T + Q_{\pm 1}$$

and if it is vertical, then

$$T' = T * Q_{\pm 1}.$$

In the horizontal case, we obtain

$$\mathrm{HFT}\left(T'\right) = \mathrm{HFT}(T + Q_{\pm 1}) = \sum_{i=1}^{n} \mathfrak{r}(p_i/q_i \pm 1) + \sum_{j=1}^{m} \mathfrak{s}_{2n}(p_j/q_j \pm 1).$$

In the vertical case, we obtain

$$\mathrm{HFT}\left(T'\right) = \mathrm{HFT}(T * Q_{\pm 1}) = \sum_{i=1}^{n} \mathfrak{r}\big(p_i/(q_i \pm 1)\big) + \sum_{j=1}^{m} \mathfrak{s}_{2n}\big(p_j/(q_j \pm 1)\big).$$

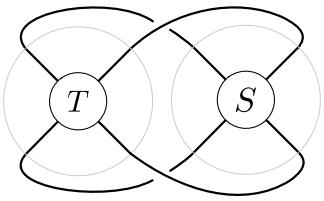

Figure 3.11: Knot obtained as the gluing of two 4-ended tangles.

3.5.4 Motivations from bordered sutured point of view

The construction of this version of Heegaard Floer Homology is based on the theory of *Bordered Sutured Floer Homology*. While we do not delve into this theory in detail, we can use it to motivate our presentation for HFT. As mentioned in Section 1.7, one of the main interesting properties of Bordered Sutured Floer Homology is its gluing property, which is also inherited by HFT. To understand this better, we can consider a particular case of Theorem 0.2 of [Zib20].

Theorem 3.64 ([Zib20, Theorem 0.2])**.** *Let T_1 and T_2 be two 4-ended tangles without closed components and let K be the knot obtained by their gluing as showed in Figure 3.11.*

Then the Knot Floer Homology $\widehat{\mathrm{HFK}}(\mathcal{S}^3, K)$ can be computed from $\mathrm{CFT}^\partial(T_1)$ and $\mathrm{CFT}^\partial(T_2)$.

Further details can be found in the Introduction of [Zib20].

Chapter 4

The Nicefication Algorithm

n this chapter, we will introduce the concept of *nice Heegaard diagrams*, a useful tool for computing Heegaard Floer Homology. The notion of nice Heegaard diagrams was first introduced by Sarkar and Wang in [SW10], and we will adopt their approach in our presentation.

Definition 4.1 (Nice Heegaard diagram)**.** We say that a pointed Heegaard diagram $\mathcal{H} = (\Sigma, \boldsymbol{\alpha}, \boldsymbol{\beta}, z)$ for a closed 3-manifold Y is *nice* if any region that does not contain z is either a bigon or a rectangle.

The main motivation behind our interest in nice Heegaard diagrams is captured by the following two theorems, originally proven by Sarkar and Wang in [SW10]. This chapter aims to prove and generalise these theorems for the cases we are interested in.

Theorem 4.2 (Sarkar-Wang, 2006 ([SW10, Theorem 1.1]))**.** *Given a nice Heegaard diagram of a closed oriented three-manifold Y, we have that its Heegaard Floer Homology $\widehat{\mathrm{HF}}(Y)$ can be computed combinatorially.*

Similarly, for a knot $K \subset \mathcal{S}^3$, we have that its Knot Floer Homology $\widehat{\mathrm{HFK}}(\mathcal{S}^3, K)$ can be computed combinatorially in a nice Heegaard diagram.

Theorem 4.3 (Sarkar-Wang, 2006 ([SW10, Theorem 1.2]))**.** *Every closed oriented 3-manifold Y admits a nice Heegaard diagram.*

Every knot K in $\mathcal{S}^3$ admits a nice Heegaard diagram.

The proof of Theorem 4.3 relies on the *Nicefication Algorithm*, which is capable of transforming any pointed Heegaard diagram into a nice Heegaard diagram using isotopies and handleslides. This algorithm was originally developed by Sarkar and Wang in [SW10] and has been implemented inside [`nicepy`] by the author during the course of this thesis work.

4.1 Holomorphic discs in nice Heegaard diagrams

In this section, we present a proof of Theorem 4.2. The key idea is to consider the count function $c(\cdot)$ in the nice case and show that it is nontrivial only when the

domain ϕ is a special type of empty embedded n-gon.

As a reference, one can look at Section 3 of [SW10].

Let $\mathcal{H} = (\Sigma, \boldsymbol{\alpha}, \boldsymbol{\beta}, z)$ be a nice admissible Heegaard diagram of genus g for a closed 3-manifold Y; choose a product complex structure on $\Sigma \times \mathbb{D}^2$.

Definition 4.4 (Empty embedded $2n$-gon)**.** Let $\mathbf{x} = \{x_1, \dots, x_g\}$ and $\mathbf{y} = \{y_1, \dots, y_g\}$ be generators in $\mathcal{H}$. A domain $\phi \in \pi_2^0(\mathbf{x}, \mathbf{y})$ is called an *empty embedded* $2n$*-gon* if it has the following properties:

1. it only has 0 and 1 as coefficients;
2. it is topologically an embedded disc with $2n$ vertices on its boundary;
3. for each vertex v holds $\mu_v(\phi) = 1/4$ (meaning that, if $\phi_1, \dots, \phi_4$ are the region around v, only one of them has 1 as coefficient in ϕ);
4. for any i, it does not contain x_i or y_i in its interior.

Remark 4.5 ($\mu(\phi) = 1$) for any empty embedded $2n$-gon ϕ)**.** Any empty embedded $2n$-gon $\phi \in \pi_2^0(\mathbf{x}, \mathbf{y})$ is taken into account by the boundary map of $\widehat{\mathrm{CF}}$. In fact, by Remark 3.19 we have that $e(\phi) = 1 - n/2$. Moreover, each of the corners has to be an x_i or an y_i and at every other x_j and y_j the point measure is zero, i.e. $\mu_{x_j}(\phi) = 0 = \mu_{y_j}(\phi)$. Therefore $\mu_{\mathbf{x}}(\phi) + \mu_{\mathbf{y}}(\phi) = (2n)/4 = n/2$ and $\mu(\phi) = e(\phi) + \mu_{\mathbf{x}}(\phi) + \mu_{\mathbf{y}}(\phi) = 1$.

To prove Theorem 4.2, we exploit two other results proven in [SW10]. The first theorem states that in a nice Heegaard diagram, only empty embedded bigons and squares contribute to the boundary map of $\widehat{\mathrm{CF}}$.

Theorem 4.6 ([SW10, Theorem 3.3])**.** *Let $\phi \in \pi_2^0(\mathbf{x}, \mathbf{y})$ be a domain in a nice Heegaard diagram such that $\mu(\phi) = 1$. If ϕ has a holomorphic embedding (i.e. $\widetilde{M}(\phi)$ as at least one point and $c(\phi)$ may be 1), then ϕ is an empty embedded bigon or an empty embedded square.*

The second theorem we present in this section, which differs slightly from the presentation in [SW10], states that every empty embedded bigon and every empty embedded square in a nice Heegaard diagram has a nontrivial count function.

Theorem 4.7 ([SW10, Theorem 3.4])**.** *If $\phi \in \pi_2^0(\mathbf{x}, \mathbf{y})$ is an empty embedded bigon or an empty embedded square, then $\mu(\phi) = c(\phi) = 1$.*

Therefore, we can already prove Theorem 4.2 as a consequence of Theorems 4.6 and 4.7.

Proof of Theorem 4.2 ([SW10])*.* Let ϕ be a domain in a nice Heegaard diagram with $\mu(\phi) = 1$. If ϕ does not have a holomorphic embedding, then $c(\phi) = 0$ and ϕ is not detected by the boundary map of $\widehat{\mathrm{CF}}$. If ϕ has some holomorphic embedding, then by Theorem 4.6 we obtain that ϕ is either an empty embedded bigon or an empty embedded square and by Theorem 4.7 we get $c(\phi) = 1$.

Therefore, in a nice Heegaard diagram, the count function is combinatorial, and consequently, the computation of $\widehat{\mathrm{HF}}$ can also be done combinatorially: it is sufficient to count the empty embedded bigons and empty embedded squares present in the diagram. □

We devote the rest of this section to the proofs of Theorems 4.6 and 4.7.

In order to prove Theorem 4.6, we need to discuss the consequences for a domain ϕ to have at least one holomorphic embedding u. We have the following proposition, whose proof can be found in [SW10].

Proposition 4.8 ([SW10, Proposition 2.4])**.** *Let ϕ be a domain in $\pi_2^0(\mathbf{x}, \mathbf{y})$ for some generators $\mathbf{x}$ and $\mathbf{y}$. If ϕ has a holomorphic embedding, then ϕ is a positive domain.*

In particular, if $c(\phi) \neq 0$, then ϕ is a positive domain.

Moreover, as one can read in Section 2.3 of [SW10], also the following lemma holds.

Lemma 4.9 ([SW10])**.** *If ϕ has a holomorphic embedding u, then the number of branch points of $p_2 \circ u$ is given by $\mu_{\mathbf{x}}(\phi) + \mu_{\mathbf{y}}(\phi) - e(\phi)$.*

In such situation, the Maslov index can be computed in a more practical way. In fact, as one can deduce by manipulating the formula given in the statement of Proposition 4.2 of [Lip06] and the formulas deducted in its proof, it holds

$$\begin{aligned} \mu(\phi) &= 2e(\phi) + g - \chi(S) \\ &= e(\phi) + b + \frac{1}{2}(g - t), \end{aligned} \tag{¤}$$

where

- g is the genus of the Heegaard diagram;
- b denotes the number of branch points of $p_1 \circ u$;
- t denotes the number of trivial discs (Definition 3.13); notice that they correspond to the coordinates x_i of $\mathbf{x}$ with $\mu_{x_i}(\phi) = 0$.

With this acquired knowledge, we can prove Theorem 4.6.

Proof of Theorem 4.6 ([SW10])*.* Let $\phi = \sum_i a_i \phi_i$ be a domain, where the ϕ_i's are regions that do not contain the basepoint. Let u be one holomorphic embedding for ϕ; then for Proposition 4.8, we have that $a_i \geq 0$, for any i. Moreover, by the niceness of the diagram, we have that each ϕ_i is a bigon or a square; therefore for Remark 3.19 we have $e(\phi_i) \geq 0$ and hence $e(\phi) = \sum_i a_i \cdot e(\phi_i) \geq 0$. So, by Lipshitz's formula

$$1 = \mu(\phi) = e(\phi) + \mu_{\mathbf{x}}(\phi) + \mu_{\mathbf{y}}(\phi),$$

we obtain that $0 \leq \mu_{\mathbf{x}}(\phi) + \mu_{\mathbf{y}}(\phi) \leq 1$. We are now going to see that there are only two possibilities for the values of $\mu_{\mathbf{x}}(\phi)$ and $\mu_{\mathbf{y}}(\phi)$: either $\mu_{\mathbf{x}}(\phi) = \mu_{\mathbf{y}}(\phi) = 1/2$ or $\mu_{\mathbf{x}}(\phi) = \mu_{\mathbf{y}}(\phi) = 1/4$. After proving this, we will use Lipshitz's cylindrical reformulation to understand what bordered surface maps into $\Sigma \times \mathbb{D}^2$ and represents ϕ, proving that it is either a "bigon" or a "square".

We need the following definition in order to proceed with the proof.

Definition 4.10. We say that ϕ *hits the* $\boldsymbol{\alpha}$*-circle* α_i if $\partial\phi$ is non-zero on some part of α_i.

We have the following observations.

Observation 4.11.

1. For any $x_i \in \mathbf{x}$ and $y_i \in \mathbf{y}$, we can assume that $x_i, y_i \in \alpha_i$.
2. Since $\phi \neq \Sigma$ (because ϕ does not contain the basepoint z), it has to hit at least one $\boldsymbol{\alpha}$-circle; without loss of generality, assume that ϕ hits α_1. Therefore, we can deduce that $\mu_{x_1}(\phi), \mu_{y_1}(\phi) \geq 1/4$: in fact, by definition, if $\phi \in \pi_2^0(\mathbf{x}, \mathbf{y})$, then $\partial\left(\partial\phi_{|\alpha}\right) = \mathbf{y} - \mathbf{x}$; since $\partial\phi_{|\alpha_1} \neq 0$, we have that x_1 and y_1 are vertices of ϕ and that $\mu_{x_1}(\phi), \mu_{y_1}(\phi) \geq 1/4$ (they are vertices at least one time for ϕ).
3. Assume that ϕ does not hit α_i, for some $i \geq 2$. Then $x_i = y_i$, otherwise it would not be true that $\partial\left(\partial\phi_{|\alpha}\right) = \mathbf{y} - \mathbf{x}$.

   Moreover, $x_i = y_i$ must lie outside the domain ϕ. In fact, if it were to lie on the boundary of ϕ, we would have $\mu_{x_i}(\phi) = \mu_{y_i}(\phi) \geq 1/2$. Similarly, if $x_i = y_i$ were to lie in the interior of ϕ, we would have $\mu_{x_i}(\phi) = \mu_{y_i}(\phi) = 1$. In both cases, we would have $\mu_{x_i}(\phi) = \mu_{y_i}(\phi) \geq 1/2$ and hence

   $$1 < \mu_{\mathbf{x}}(\phi) + \mu_{\mathbf{y}}(\phi) = \mu_{x_1}(\phi) + \mu_{y_1}(\phi) + \mu_{x_i}(\phi) + \mu_{y_i}(\phi),$$

   which is an absurd.
4. ϕ can hit at most two $\boldsymbol{\alpha}$-circles: if it were to hit more than 2, we would have that $\mu_{\mathbf{x}}(\phi), \mu_{\mathbf{y}}(\phi) \geq 3/4$.
5. Remark also that $e(\phi) \in 1/2\mathbb{N}$ (since Euler measure is additive and $e(\phi) = 1/2$ for ϕ a bigon and $e(\phi) = 0$ for ϕ a square, see Remark 3.19).

Therefore, we can only have the following cases regarding ϕ.

- **Case 1**: ϕ hits two $\boldsymbol{\alpha}$-circles; without loss of generality we assume ϕ to hit α_1 and α_2. In such case, we have that the following properties hold:
  - $\mu_{x_1}(\phi) = \mu_{x_2}(\phi) = \mu_{y_1}(\phi) = \mu_{y_2}(\phi) = 1/4$;
  - ϕ consists of squares, since for Lipshitz's formula $e(\phi) = 0$;
  - there are $(g-2)$ trivial discs (corresponding to $x_3 = y_3, \ldots, x_g = y_g$).
- **Case 2**: ϕ hits only one $\boldsymbol{\alpha}$-circle; without loss of generality we assume ϕ to hit α_1. In such case, we have two possible sub-cases, distinguishing on the sum $\mu_{\mathbf{x}}(\phi) + \mu_{\mathbf{y}}(\phi)$.

* **Sub-case 2a**: $\mu_{\mathbf{x}}(\phi) + \mu_{\mathbf{y}}(\phi) = 1/2$. In this case, we have that:
  - $\mu_{x_1}(\phi) = \mu_{y_1}(\phi) = 1/4$;
  - ϕ consists of squares and exactly one bigon (since for Lipshitz's formula $e(\phi) = 1/2$);
  - there are $(g-1)$ trivial discs (corresponding to $x_2 = y_2, \dots, x_g = y_g$).
* **Sub-case 2b**: $\mu_{\mathbf{x}}(\phi) + \mu_{\mathbf{y}}(\phi) = 1$. In this case, we have that:
  - $\mu_{x_1}(\phi) = \mu_{y_1}(\phi) = 1$;
  - ϕ consists of squares (since for Lipshitz's formula $e(\phi) = 0$);
  - there are $(g-1)$ trivial discs (corresponding to $x_2 = y_2, \dots, x_g = y_g$).

Our aim will now be to understand the surface S which maps to $\Sigma \times \mathbb{D}^2$ (using the cylindrical reformulation by Lipshitz) in these three cases.

Observation 4.12. We can make some observations on the three cases found, reducing ourselves to look at only the first two of them.

- Let us consider the first case. This corresponds to a map from S to Σ, where S has $g-2$ trivial disc components and, using ($\natural$), $\chi(S) = g-1$ (recall that $e(\phi) = 0$).

  Let $F = S \setminus \{\text{ trivial discs }\}$. Then F is a double branched cover over $\mathbb{D}^2$, and we claim that $\chi(F) = 1$ and it has one branch point. To see that $\chi(F) = 1$, one can prove that "to remove a disc" from some surface makes the Euler characteristic of the surface to go down by one (using the Inclusion-Exclusion principle for $\chi(\cdot)$); since we are removing one disc for every trivial disc component, we get that $\chi(F) = (g-1) - (g-2) = 1$. To see that F has 1 branch point, recall that for Lemma 4.9 we have that the number of branch points is given by $\mu_{\mathbf{x}}(\phi) + \mu_{\mathbf{y}}(\phi) - e(\phi) = 1$.

  Therefore F is a disc with 4 marked points on its boundary (which correspond to x_1, y_1, x_2, y_2). We then say that F is a *square* and we call the marked points *corners of F*.

- Consider now the other two cases. In both, S has $(g-1)$ trivial disc components and we call again $F = S \setminus \{\text{ trivial discs }\}$. In this case, F is just a single cover over $\mathbb{D}^2$ and the number of branch points has to be 0.

  Consider Sub-case 2b. If this case were possible, we could use Lemma 4.9 to conclude that the number of branch points would be 1, which is impossible. Therefore, the third case is not possible.

  Consider then Sub-case 2a. Here, F is a disc with 2 marked points on its boundary (corresponding to x_1 and y_1). We then say that F is a *bigon* and we call the marked points *corners of F*.

We have then proven that only Case 1 and 2a can occur, we will refer to them as Case 1 and Case 2.

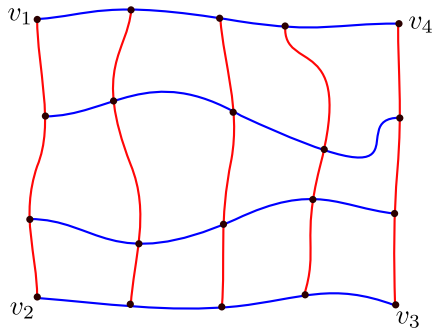

Figure 4.1: Pre-image of $\boldsymbol{\alpha}$-edges and $\boldsymbol{\beta}$-edges for a square.

We want now to study the map $f = p_1 \circ u_{|F} : F \to \Sigma$. In both the cases, ϕ is the image of F via f and the trivial discs are mapped to $x_3 = y_3, \ldots, x_g = y_g$ (and also $x_2 = y_2$ for the second case), that are outside of ϕ. Notice that, for both cases, f has no branch points; therefore, it is a local diffeomorphism even at the boundary of F. We can also establish that every corner v of F has exactly one preimage under f. To see this, note that in the non-trivial x_i's we have $\mu_{x_i}(\phi) = \mu_{y_i}(\phi) = 1/4$, which implies that the preimages of each corner under f are uniquely determined.

All is left to prove is that f is an embedding, i.e. that is not only a local diffeomorphism but an actual diffeomorphism. Once we establish this, we will also be able to conclude that ϕ is an embedded square (in Case 1) or an embedded bigon (in Case 2). We will proceed to prove this by examining each case separately.

Case 1. Here we have a map $f : F \to \Sigma$, where F is a square (i.e. a disc with 4 marked points on the boundary), and we denote the corners by v_1, v_2, v_3, v_4.

In order to prove that f is an embedding, i.e., not only a local diffeomorphism but an actual diffeomorphism, we first study the preimage of the $\boldsymbol{\alpha}$- and $\boldsymbol{\beta}$-edges of the boundary and the interior of ϕ under f. Exploiting the fact that f is a local diffeomorphism, we see that these preimages are 1-manifolds with boundary; we can therefore still call them $\boldsymbol{\alpha}$- and $\boldsymbol{\beta}$-edges. Furthermore, also in the preimage the $\boldsymbol{\alpha}$-edges are only allowed to intersect $\boldsymbol{\beta}$-edges and vice versa. Moreover, at any corner v_i, there is an intersection between an $\boldsymbol{\alpha}$-edge and a $\boldsymbol{\beta}$-edge.

Note that any preimage of a square region is still a square region. Therefore, the $\boldsymbol{\alpha}$- and $\boldsymbol{\beta}$-edges cut F into squares. In particular, this means that no edge can form a closed loop γ: if that were the case, we would have that the Euler measure of $A = F \setminus \{\text{region enclosed by } \gamma\}$ is negative and hence A could not be tiled by squares.

Similarly, no edge can intersect an edge of the same colour more than once in the preimage. This holds in particular on the border of F, meaning that an edge cannot "start" and "finish" on the same edge. Therefore, we have that the edges are straight lines inside F; we can consider the $\boldsymbol{\alpha}$-edges to be vertical edges that cut F into vertical rectangles and the $\boldsymbol{\beta}$-edges to be horizontal edges that cut F into horizontal rectangles, as shown in Figure 4.1.

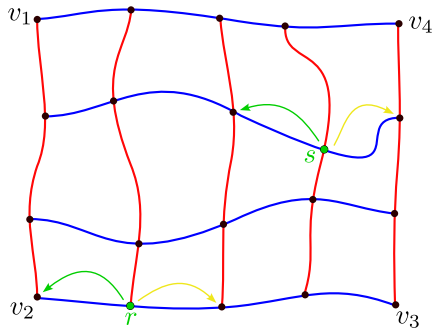

Figure 4.2: Points found with the "walk" on β_i, finishing in the wrong case (we reach the border first starting from s) in yellow and in the right case (we reach the border first starting from r) in green.

Let us call *vertices* the intersection points between $\boldsymbol{\alpha}$- and $\boldsymbol{\beta}$-edges, including the corners. Based on the observations made above, we can reduce our proof to showing that distinct vertices are mapped to distinct points by f, which would imply that f is an embedding.

Suppose $r, s \in F$ are distinct vertices and assume, for the sake of contradiction, that $f(r) = f(s)$. We consider the following two cases:

(a) At least one of r or s lies on ∂F.

(b) Both r and s lie in the interior of F.

We only prove the contradiction in case (a), as case (b) can be reduced to case (a).

Suppose that $r \in b_r \subset \partial F$ and b_s is the $\boldsymbol{\beta}$-edge on which s lies. The case where $r \in a_r \subset \partial F$ for a_r an $\boldsymbol{\alpha}$-arc can be proven similarly. Let β_i be the $\boldsymbol{\beta}$-circle in Σ containing $f(r) = f(s)$, and we select an orientation for β_i and explore it until we reach an intersection point with some $\boldsymbol{\alpha}$-circle. We examine the preimages of that point via f, which are at least 2 since we are virtually moving from both r and s on the $\boldsymbol{\beta}$-edges b_r, b_s in F. If at least one of them is situated in an $\boldsymbol{\alpha}$-edge $a \subset \partial F$, we stop; otherwise, we proceed to explore the intersection points on β_i following the orientation. At some point, we will encounter such a point, and we call t, u to be two preimages of such an intersection point on β_i such that $t \in a \subset \partial F$. We have two cases: $t \in b_r$ or $t \in b_s$. If the second one is the case, we can repeat the walk on β_i by reversing the chosen orientation. Notably, $t \in b_r$ is a corner; therefore, we have found $f(t) = f(u)$ for two distinct vertices, one of which is a corner. This contradicts the embedding assumption near the corners. ↯

See Figure 4.2 for a visual illustration.

We still need to show how to reduce case (b) to case (a). Assume both r and s are in the interior of F. Let a_r and a_s be the $\boldsymbol{\alpha}$-edges on which they lie, respectively, and let α_i be the $\boldsymbol{\alpha}$-circle in Σ that contains $f(r) = f(s)$. As before, we choose an orientation and examine successive points of intersection with $\boldsymbol{\beta}$-circles. For each

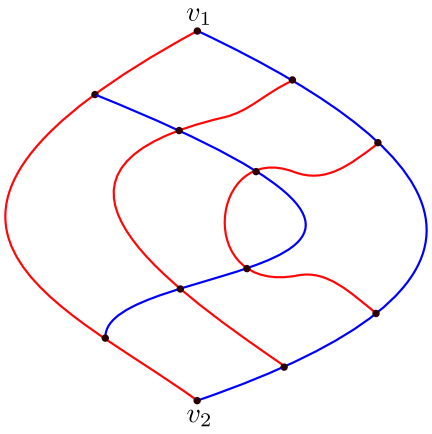

Figure 4.3: Pre-image of $\boldsymbol{\alpha}$-edges and $\boldsymbol{\beta}$-edges for a bigon.

intersection point, we have at least two preimages in F: one on a_r and one on a_s. We explore α_i until one of the preimages of some intersection point falls on ∂F, then we proceed as in case (a).

Case 2.

In this case, we consider a map $f : F \to \Sigma$, where F is a bigon (i.e., a disk with two marked points on the boundary), and we refer to the corners as v_1 and v_2.

As before, we establish the setup in which the preimages of $\boldsymbol{\alpha}$ and $\boldsymbol{\beta}$-edges are 1-manifolds with borders, and the edges of different colours can intersect only each other. The points of intersection are referred to as vertices, and each corner v_i we have an intersection between an $\boldsymbol{\alpha}$-edge and a $\boldsymbol{\beta}$-edge. Similarly, we still cannot have any closed loops, and the tiling on $\phi \subset \Sigma$ induces a tiling with squares and a single bigon on F.

Differing from the previous case, the boundary of F consists of one $\boldsymbol{\alpha}$-edge $\bar{a}$ and one $\boldsymbol{\beta}$-edge $\bar{b}$, and the remaining edges must "start" and "end" F on the same border edge of the other colour. However, their entry and exit points are nested. For example, the $\boldsymbol{\alpha}$-edges of F that are not $\bar{a}$: if we look at the connected regions of $F \setminus \{a \mid a \text{ is a } \boldsymbol{\alpha}\text{-edge different than } \bar{a}\}$, then only one region can be a bigon, the closest to $\bar{b}$. Thus, the tiling of F is as shown in Figure 4.3, with a bigon in the centre and squares surrounding it.

As in the previous case, to show that f is an embedding it is enough to show that it is an embedding restricted to vertices; this is done in the same fashion of Case 1.

Hence, both in Case 1 and Case 2, f is an embedding and the theorem is proved. □

Proof of Theorem 4.7 ([SW10]). Let $\phi \in \pi_2^0(\mathbf{x}, \mathbf{y})$ be an empty embedded square; then by Remark 4.5 it holds $\mu(\phi) = 1$. We want to prove that ϕ admits a unique holomorphic embedding u, which would imply that $c(\phi) = 1$.

To begin with, we construct a branched cover F of $\mathbb{D}^2$ that is mapped diffeomorphically onto ϕ. We start by considering a disc F with four marked points on its

boundary. Given a complex structure on Σ, we can then induce a holomorphic structure on F. The cross-ratio of the four marked points on the boundary determines a unique one-parameter family of branch points in $\mathbb{D}^2$ that gives that cross-ratio. Hence, there is a holomorphic branched cover $g : F \to \mathbb{D}^2$ satisfying the boundary conditions, which is unique up to re-parametrisation: therefore, we proved that ϕ has a holomorphic representative u. Additionally, as shown in the proof of Theorem 4.6, we have established that u uniquely determines the topological type of F. Hence, u is the unique holomorphic embedding of ϕ.

The case for $\phi \in \pi_2^0(\mathbf{x}, \mathbf{y})$ an empty embedded bigon is done analogously with F a disc with two marked points on its boundary.

□

4.2 The nicefication algorithm

We see now how we can construct a nice Heegaard diagram starting from a generic admissible one. For this purpose, we only need to use isotopies and handleslides on the $\boldsymbol{\beta}$-curves. The algorithm presented was developed by Sarkar and Wang in Section 4 of their paper [SW10], and we are going to follow their exposition closely. Some changes were made to the algorithm for implementation purposes, and these will be discussed in Section 4.5.

From here on, we call *good regions* bigons and squares and *bad regions* all the others. Schematically, the algorithm is the following:

Step 1: killing all non-disc regions;

Step 2: making all but one region to be bigons and squares.

Let $\mathcal{H} = (\Sigma, \boldsymbol{\alpha}, \boldsymbol{\beta}, z)$ be a pointed Heegaard diagram. In this section, following the notation adopted in [SW10], we will denote with D and D_i the regions of the diagram.

4.2.1 Step 1: killing all non-disc regions

We want to only have disc regions in our diagram. We divide this first step in two sub-steps.

Sub-step 1.1: making any circle intersects some other circle

First of all, we want to ensure that any $\boldsymbol{\alpha}$-circle intersects at least one $\boldsymbol{\beta}$-circle and that any $\boldsymbol{\beta}$-circle intersects at least one $\boldsymbol{\alpha}$-circle.

Let α_i be an $\boldsymbol{\alpha}$-circle that does not intersect any $\boldsymbol{\beta}$-circle. We can then find an arc c that connects α_i to some β_j, satisfying the following requests:

1. c intersects β_j only at its end;
2. c does not intersect any other $\boldsymbol{\beta}$-circle.

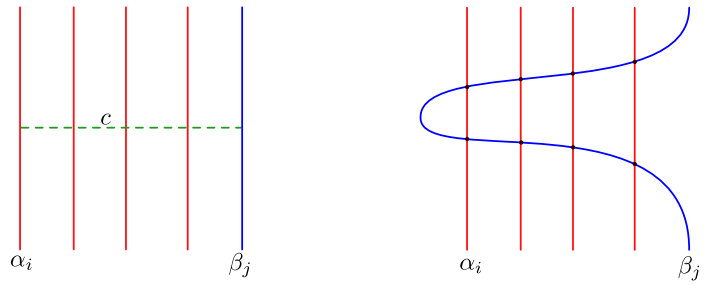

Figure 4.4: Making all the $\boldsymbol{\alpha}$-circles intersect some $\boldsymbol{\beta}$-circle.

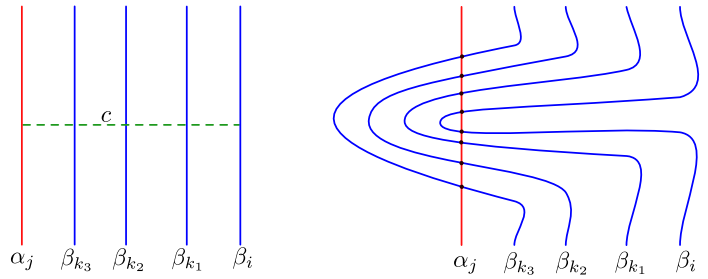

Figure 4.5: Making all the $\boldsymbol{\beta}$-circles intersect some $\boldsymbol{\alpha}$-circle.

Then, we perform a finger move on β_j along c to make itα_i intersect it. See Figure 4.4 for a visual representation.

Let now β_i be a $\boldsymbol{\beta}$-circle that does not intersect any $\boldsymbol{\alpha}$-circle. We find an arc c that connects β_i to some α_j, satisfying the following requests:

1. c intersects α_j only at its end;
2. c does not intersect any other $\boldsymbol{\alpha}$-circle.

Let $\beta_{k_1}, \dots, \beta_{k_n}$ be the others $\boldsymbol{\beta}$-circles intersected by c, in addition to β_i. Then, we perform $n+1$ "nested" finger moves along c, to make β_i intersect α_j: one on β_i and the others on the β_k's. See Figure 4.5 for a visual idea.

performing these two moves for all the circles that do not intersect any other circle ensures that every $\boldsymbol{\alpha}$-circle intersects at least one $\boldsymbol{\beta}$-circle and every $\boldsymbol{\beta}$-circle intersects at least one $\boldsymbol{\alpha}$-circle.

Sub-step 1.2: making all the regions discs

We can observe that since $\Sigma \setminus \boldsymbol{\alpha}$ is a punctured sphere, all the regions are planar surfaces. Let D be a non-disc region, i.e. a region that has more than one boundary component. Since we already executed the previous sub-step, every boundary component has to contain both $\boldsymbol{\alpha}$ and $\boldsymbol{\beta}$-edges (if not, there would be a circle that does not intersect any other circle). To eliminate the excess boundary components, we perform some finger moves on $\boldsymbol{\beta}$-circles, as shown in Figure 4.6.

After sufficiently many iterations, we obtain a Heegaard diagram with only disc regions.

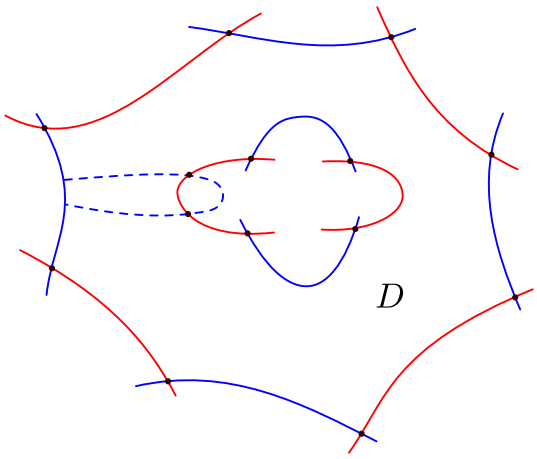

Figure 4.6: Killing the non-disc regions. The dotted arcs indicate the finger moves that we need to do on the $\boldsymbol{\beta}$-circles.

4.2.2 Step 2: making all but one region bigons or squares

Let now $\mathcal{H} = (\Sigma, \boldsymbol{\alpha}, \boldsymbol{\beta}, z)$ be a pointed Heegaard diagram with only disc regions; we are now going to make all the regions but one bigons or squares, using finger moves and handleslides. It is important to remark that with the following algorithm we generate only disc regions in our diagram.

We are going to need some definitions for this step of the algorithm.

Definition 4.13 (Distance of a region)**.** Given a region D of $\mathcal{H}$, let $z' \in D$ be a point in its interior. We define the *distance of* D, denoted by $d(D)$, to be the smallest number of intersection points between the $\boldsymbol{\beta}$-circles and an arc connecting z and z' in the complement of the $\boldsymbol{\alpha}$-circles.

In particular, we call D_0 the region that contains the basepoint z; this is the only region of distance 0.

Remark that the definition of distance is well posed, as by the definition of Heegaard diagram we have that $\Sigma \setminus \boldsymbol{\alpha}$ is connected.

Definition 4.14 (Badness of a region)**.** For a $2n$-gon disc region D, we define the *badness of* D, denoted by $b(D)$, to be $b(D) = \max\{n-2, 0\}$.

Definition 4.15 (Distance of $\mathcal{H}$)**.** We define the *distance of the diagram* to be the maximum distance of a bad region in the diagram. We denote it by $d(\mathcal{H})$.

Definition 4.16 (Distance d_* complexity)**.** Consider a distance d_*, $0 < d_* \leq d(\mathcal{H})$. We define the *distance* d_* *complexity of* $\mathcal{H}$, denoted by $c_{d_*}(\mathcal{H})$ to be the tuple

$$c_{d_*}(\mathcal{H}) = \left(\sum_{i=1}^{m} b(D_i), -b(D_1), -b(D_2), \ldots, -b(D_m) \right),$$

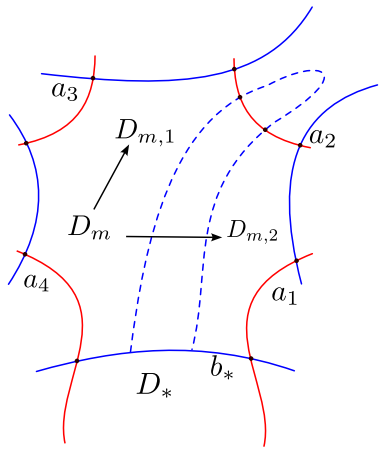

Figure 4.7: Initial finger move done on b_*, exiting from D_m through a_2.

where $D_1, \dots, D_m$ are all the bad regions of distance d_*, ordered such that $b(D_1) \geq b(D_2) \geq \cdots \geq b(D_m)$

We call the first term the *total badness of distance d_* of $\mathcal{H}$* and we denote it by $b_{d_*}(\mathcal{H})$. If there are no distance d_* bad regions, then $c_{d_*}(\mathcal{H}) = (0)$. We order the set of distance d_* complexities lexicographically.

The algorithm is based on the following result, which states in details how we can simplify our diagram to a nicefied version of it only by finger moves and handleslides.

Theorem 4.17. *For a distance d pointed Heegaard diagram $\mathcal{H}$ with only disc regions, if $c_d(\mathcal{H}) \neq (0)$, we can modify $\mathcal{H}$ by isotopies and handleslides to get a new Heegaard diagram $\mathcal{H}'$ with only disc regions, satisfying $d(\mathcal{H}') \leq d(\mathcal{H})$ and $c_d(\mathcal{H}') < c_d(\mathcal{H})$.*

To prove the above theorem, we demonstrate how a full cycle of the algorithm operate, showing that indeed we can get a new diagram $\mathcal{H}'$ such that $c_d(\mathcal{H}') < c_d(\mathcal{H})$.

We order the bad regions of distance d as in the definition of $c_d(\mathcal{H})$. Now we look at the *worst region* of the diagram, i.e. the region of distance d with the smallest badness, which we denote by D_m. Since it is a bad region, it is a $(2n)$-gon with $n \geq 3$.

Pick an adjacent region D_* with distance $d-1$ having a common $\boldsymbol{\beta}$-edge with D_m (remark that by how the assignment of the distance is done, we can only have that regions that are neighbours via a $\boldsymbol{\beta}$-edge can only have distance $d-1, d$ or $d+1$). Let b_* be (one of) their common $\boldsymbol{\beta}$-edge(s). We order the $\boldsymbol{\alpha}$-edges of D_m counterclockwise starting at b_* and we denote them by $a_1, a_2, \dots, a_n$. We try now to make a finger move on b_* into the D_m and out of D_m through a_2, as demonstrated in Figure 4.7 for D_m an octagon.

If we reach a square region of distance $\geq d$, we push through with our finger, going outside of this region via the opposite $\boldsymbol{\alpha}$-edge, as in Figure 4.8. Note that doing a finger move through regions of distance $\geq d$ does not change the distance of any of the bad regions, since they all have distance $\leq d$: therefore the minimal

path connecting the basepoint of the diagram to a bad regions cannot pass through this square region, otherwise we would have that the distance of such bad region is strictly greater than d.

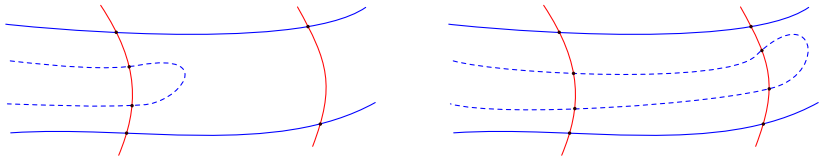

Figure 4.8: When a square region of distance $\geq d$ is reached (figure on the left), we push through it (figure on the right).

We continue to push up our finger through all the squares of distance $\geq d$, until we reach one of the following four cases:

1. a bigon region is reached;
2. a region with distance $\leq d-1$ is reached;
3. a bad region with distance d other than D_m, i.e., D_i with $i < m$, is reached;
4. we come back to D_m.

We now study each case, proving how we can obtain a new diagram $\mathcal{H}'$ such that the statement of Theorem 4.17 holds for each one of them. It is important to remark that the above cases are all the possible cases that we can encounter.

Case 1: a bigon region is reached

This is the case in which we reached a bigon that can have any distance. Remark that all regions in between D_m and this bigon are square regions with distance $\geq d$. We stop the finger move inside the bigon region, dividing it into a square and a new bigon, as illustrated in Figure 4.9.

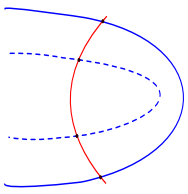

Figure 4.9: A bigon is reached by the finger move.

Denote the new Heegaard diagram obtained by $\mathcal{H}'$. We have $b(D_{m,1}) = b(D_m) - 1$ and $D_{m,1}$ is still a region of distance d. Since $D_{m,2}$ is a square (which is a good region), we get $b_d(\mathcal{H}') = b_d(\mathcal{H}) - 1$. We have also increased the badness of D_*, but it is a distance $d-1$ region and hence is not a problem. Notice that we did not increase the distance of any other bad region since we did not pass through any region of

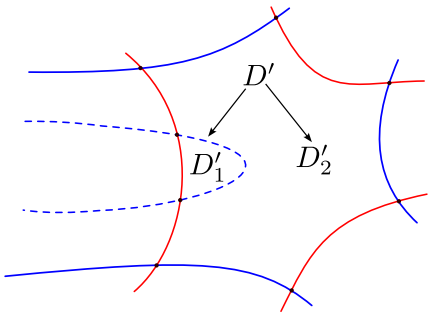

Figure 4.10: A smaller distance region is reached.

distance $\leq d-1$ and all bad regions has distance $\leq d$. Therefore $d(\mathcal{H}') \leq d(\mathcal{H})$ and $c_d(\mathcal{H}') < c_d(\mathcal{H})$; hence the theorem is proved in this case.

Case 2: a region with distance $\leq d-1$ is reached

Let D' be the region with distance $< d$ that we have reached with our finger; denote $d(D') = d'$. Notice that D' might be a bigon or also a square region. Let $\mathcal{H}'$ be the new Heegaard diagram obtained by performing the finger move. We call the new generated regions as in Figure 4.10.

As in the previous case, we have that $b(D_{m,1}) = b(D_m) - 1$ and that $D_{m,2}$ is a good region. Our finger move splits D' into two regions: the bigon region D'_1 and the other region D'_2. The latter is going to be a bad region if D' was not a bigon; hence, when D' is a square or a bad region, D'_2 will be a bad region of distance $d' < d$. We have increased the badness of D_* (which is a distance $d-1$ region) and we might have increased the distance d' complexity (as we replaced D' with a worse region, and hence the total badness of distance d' may be increased), but we have $d(\mathcal{H}') \leq d(\mathcal{H})$ and $c_d(\mathcal{H}') < c_d(\mathcal{H})$. Therefore, Theorem 4.17 is proved also in this second case.

Case 3: a bad region with distance d other than D_m is reached

The third case is the most challenging of the four because it does not reduce the total badness of distance d but merely shifts it to another region with a larger badness, which will then appear first in $c_d(\mathcal{H}')$ with respect to $c_d(\mathcal{H})$. The process can be similar to the second case; however, we need to be more careful in proving the theorem.

Let D_i be the distance d bad region that we have reached, with $i < m$. Denote by $D_{i,1}$ and $D_{i,2}$ the two parts of D_i separated by our finger move as in Figure 4.11. $D_{i,1}$ is a bigon and hence a good region, while $D_{i,2}$ is a bad region of distance d. We have $b(D_{i,2}) = b(D_i) + 1$ and $b(D_{m,1}) = b(D_m) - 1$, thus the total badness of distance d remains the same. But we are decreasing the distance d complexity since

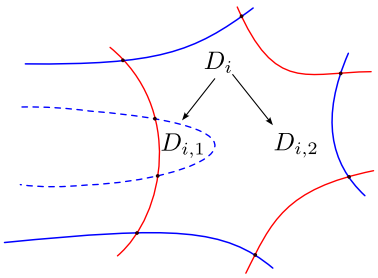

Figure 4.11: Another distance d bad region is reached.

we are moving the badness from a later bad region to an earlier one:

$$\begin{aligned} c_d(\mathcal{H}') &= (b_d(\mathcal{H}), -b(D_1), \dots, -b(D_i) - 1, \dots, -b(D_m) + 1) \\ &< (b_d(\mathcal{H}), -b(D_1), \dots, -b(D_i), \dots, -b(D_m)) = c_d(\mathcal{H}). \end{aligned}$$

Remark that the position of D_i inside $c_d(\mathcal{H})$ may have changed since the badness increased, but it could only may have moved more "to the left" of the tuple. We have also increased the badness of D_*, but it is a distance $d-1$ region and hence it is not a problem. For the new Heegaard diagram $\mathcal{H}'$, we have $d(\mathcal{H}') = d(\mathcal{H})$ and $c_d(\mathcal{H}') < c_d(\mathcal{H})$ and therefore the Theorem's statement is proved.

Case 4: we come back to D_m

This case is very different from the previous three. We divide it into two sub-cases, according to which edge the finger move is coming back through.

Sub-case 4.1: we come back through an adjacent edge

This sub-case is drawn in Figure 4.12. Without loss of generality, we assume that the finger comes back via a_1.

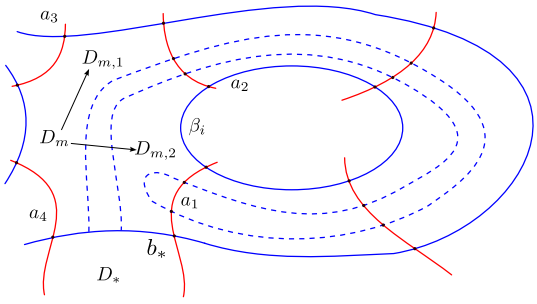

Figure 4.12: Coming back via an adjacent edge with the finger. The finger path is denoted by the dotted arc.

In this case, we see the full copy of some $\boldsymbol{\beta}$-circle, say β_i, one the right side along our long finger: in fact, we have pushed through linked squares and doing this it is not possible to "change" the $\boldsymbol{\beta}$-circle that we have on the right, as it would mean that we passed through an hexagon (or a region with more edges). Suppose $b_* \subset \beta_j$.

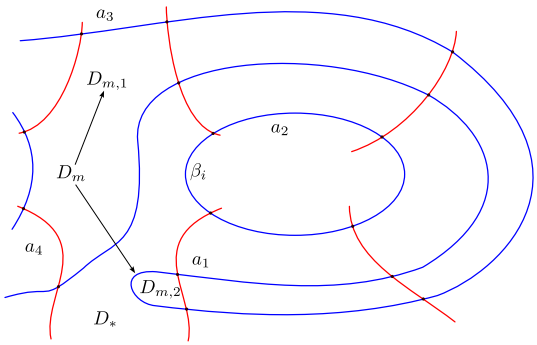

Figure 4.13: Coming back via an adjacent edge, performing the handleslide. The dotted arc denotes β_i after the handleslide.

Note that $i \neq j$: otherwise we would have had $b_* \subset \beta_i$ and we would have reached either D_m or D_* at an earlier time as we would have passed by the entirety of β_i. Now, instead of doing the finger move, we perform a handleslide of β_j over β_i, as it is displayed in Figure 4.13.

Notice that after the handleslide, we are not increasing the distance of any bad region. In fact, that would happen only if the basepoint was "inside" of β_i, but this is not possible: if this was to be true, then we would find that D_* was inside of β_i, but this is a contradiction.

As in the previous cases, we have increased the badness of D_*; this is not a problem since it is a distance $d-1$ region. Moreover, $D_{m,2}$ is a bigon region and $b(D_{m,1}) = b(D_m) - 1$. Thus, for the new Heegaard diagram $\mathcal{H}'$ after the handleslide, the total badness of distance d is decreased by 1; we have $d(\mathcal{H}') \leq d(\mathcal{H})$ and $c_d(\mathcal{H}') < c_d(\mathcal{H})$. Hence, the theorem is proved also in this case.

Sub-case 4.2: we come back through a non-adjacent edge

Suppose that we return through a_k with $3 < k \leq n$ (recall that D_m is a $(2n)$-gon). Then, instead of the finger move through a_2, we do a finger move on b_* through a_3 as it is drawn in Figure 4.14.

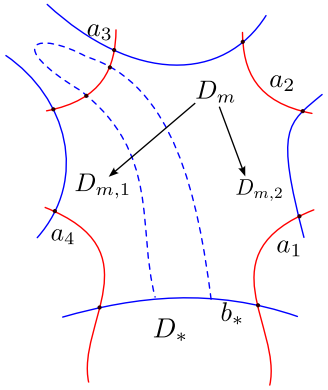

Figure 4.14: Finger move done on b_*, exiting from D_m through a_3.

If we reach one of the first three cases, we can do the finger move and we are still decreasing the distance d complexity. In fact, we have that $b(D_{m,1}) = b(D_m) - 2$ and $b(D_{m,2}) = 1$, therefore the total complexity of distance d is going down by a factor of 1; we are increasing the badness of D_*, but it is a distance $d-1$ region.

Suppose instead that we come back to D_m via some $\boldsymbol{\alpha}$-edge a_i. We claim that $3 < i < k$. Certainly we can not come back via a_3, as we only push through squares and we go out from them via the only other $\boldsymbol{\alpha}$-edge that they have. The finger can not come back via a_k since the chain of squares from a_k is connected to a_2. The last possibility to discard is that either $i > k$ or $i < 3$. If that was the case, we could get two simple closed curves c_1 and c_2, as shown in Figure 4.15.

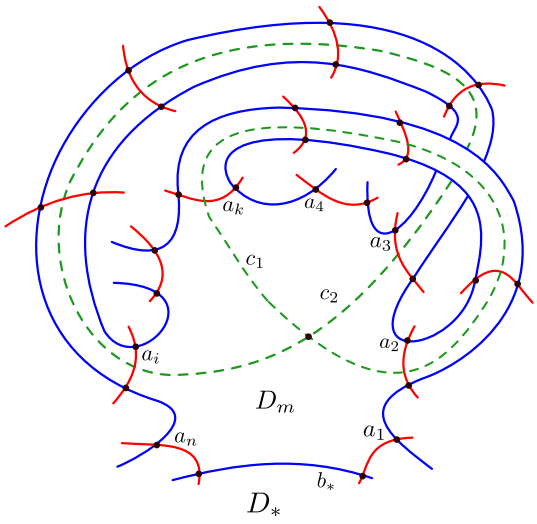

Figure 4.15: There are no crossing fingers. The fingers are not showed here. Instead, the two dotted green circles denote the cores of the two fingers.

Then c_1 and c_2 intersect transversely at exactly one point and they are in the complement of the $\boldsymbol{\beta}$-circles. The complement of the $\boldsymbol{\beta}$-circles is a punctured sphere, attach discs to the holes to get a sphere: then, as homology classes, we get $[c_1] \cdot [c_2] = 1$. But $H_1\left(S^2\right) \cong 0$: this is a contradiction $\lightning$. Thus we must have $3 < i < k$.

Now, instead of the finger move through a_3, we do another finger move through a_4. Iterating the same arguments as above, we see that we either end up with a finger which does not come back, or we get some finger that starts at a_j and comes back via a_{j+1}. Then:

- if the finger does not come back, we reduce it to the previous cases and the theorem follows;
- if there is a finger which starts at a_j and comes back at a_{j+1}, we went around a full $\boldsymbol{\beta}$-circle and we can do a handleslide similar to the one in Sub-case 4.1. In this case, we have that $b\left(D_{m,1}\right) = \max\{n-j-1, 0\}$ and $b\left(D_{m,2}\right) = \max\{j-2, 0\}$; hence $b\left(D_{m,1}\right) + b\left(D_{m,2}\right) \leq (n-j-1) + (j-2) = n-3$ and

we decreased the total badness of distance d. We increased the badness of D_*, but it is a distance $d-1$ region. Thus, the new Heegaard diagram $\mathcal{H}'$ obtained with the handleslide, is such that $d(\mathcal{H}') \leq d(\mathcal{H})$ and $c_d(\mathcal{H}') < c_d(\mathcal{H})$.

Thus, Theorem 4.17 was proved.

4.3 Admissibility of the nicefied diagram

We now show that if we start with an admissible Heegaard diagram, then the algorithm yields an admissible nice Heegaard diagram. The algorithm uses isotopies and handleslides, therefore it is sufficient to show that they leave the admissible property unaltered.

As a reference, one can look at section 4.2 of [SW10].

We start by proving that isotopies do not affect the admissibility. Let $\mathcal{H}$ and $\mathcal{H}'$ be the Heegaard diagrams before and after the isotopy; we denote the regions modified by the isotopy as in Figure 4.16.

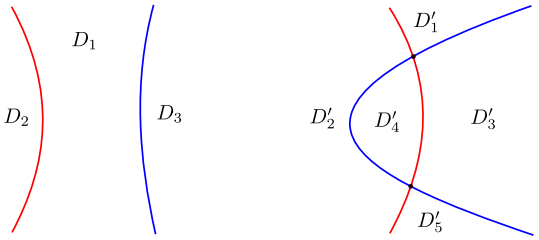

Figure 4.16: Isotopy of a $\boldsymbol{\beta}$-circle.

Suppose $\mathcal{H}$ is admissible. Consider a periodic domain ϕ' in $\mathcal{H}'$, described as

$$\phi' = c_1 D'_1 + c_2 D'_2 + c_3 D'_3 + c_4 D'_4 + c_5 D'_5 + \cdots .$$

Our goal is to prove that ϕ' has both positive and negative coefficients. We have the following properties.

- $c_2 - c_1 = c_4 - c_3 = c_2 - c_5$. To see this, we think of the $\boldsymbol{\alpha}$-circle as if it goes from top to down; we can divide it in three pieces, the first between D'_1 and D'_2, the second between D'_3 and D'_4 and the third between D'_5 and D'_2. Since ϕ' is a periodic domain, we have that the coefficients of this particular $\boldsymbol{\alpha}$-circle has to be the same on the border of ϕ', hence we obtain exactly the relations stated above;

- repeating the same argument on the $\boldsymbol{\beta}$-circle, we obtain $c_1 - c_3 = c_2 - c_4 = c_5 - c_3$.

Hence $c_1 = c_5$ and $c_4 = c_2 + c_3 - c_1$. Notice that the regions are all the same before and after the isotopy except for those in Figure 4.16; therefore,

$$\phi = c_1 D_1 + c_2 D_2 + c_3 D_3 + \cdots$$

is a periodic domain for $\mathcal{H}$. In fact, the if a is the multiplicity of the $\boldsymbol{\alpha}$-circle in all ϕ, then we need that $a = c_2 - c_1$, and this is true since we have that $a = c_2 - c_1 = c_4 - c_3 = c_2 - c_5$ in ϕ'. Same goes for the $\boldsymbol{\beta}$-circle.

Since $\mathcal{H}$ is admissible, ϕ has both positive and negative coefficients, and so does ϕ' as we only added coefficient with respect to ϕ. Hence $\mathcal{H}'$ is admissible.

We now want to prove the same thing for a handleslide; let us consider the one indicated in Figure 4.17.

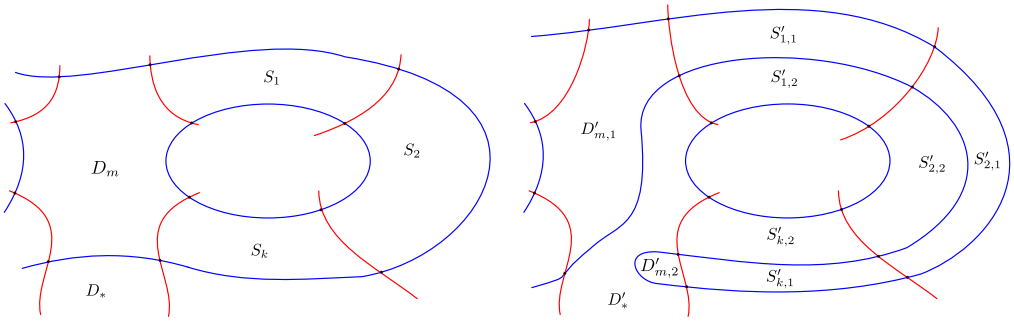

Figure 4.17: Handleslide of a $\boldsymbol{\beta}$-circle: before (on the left) and after (right).

Suppose that $\mathcal{H}$ is admissible. Let the following be a periodic domain in $\mathcal{H}'$

$$\phi' = c_* D'_* + c_1 D'_{m,1} + c_2 D'_{m,2} + c_{1,1} S'_{1,1} + c_{1,2} S'_{1,2} + \cdots + c_{k,1} S'_{k,1} + c_{k,2} S'_{k,2} + \cdots$$

By looking at the coefficients for the $\boldsymbol{\beta}$-circle that we modified, we get

$$c_1 - c_* = c_{1,1} - c_{1,2} = \cdots = c_{k,1} - c_{k,2} = c_2 - c_*.$$

Denote $c_0 = c_1 - c_*$, then we have the relations $c_{i,1} = c_{i,2} + c_0$ and $c_1 = c_2$. We can then claim that

$$\phi = c_* D_* + c_1 D_m + c_{1,1} S_1 + \cdots + c_{k,1} S_k + \cdots$$

is a periodic domain for $\mathcal{H}$. To see this, we just need to check the relations on the $\boldsymbol{\alpha}$-edges that we modify with the handleslide. Indeed we have that the differences $c_1 - c_{1,1}$ and $c_1 - c_{k,1}$ are correct because we have them also in $\mathcal{H}'$ (since $c_1 = c_2$). Checking the same for $c_{i,1} - c_{j,1}$ and $c_1 - c_*$ is immediate.

Since $\mathcal{H}$ is admissible, ϕ has both positive and negative coefficients. Hence ϕ' has both positive and negative coefficients, so $\mathcal{H}'$ is admissible.

Remark 4.18. A stronger statement actually holds: in fact, it can be shown that nice Heegaard diagrams are always admissible (as reference, one can see [LMW08], Corollary 3.2).

4.4 Generalisations of the algorithm

The Nicefication Algorithm presented in Section 4.2 is designed specifically for closed Heegaard diagrams. However, we can extend it to work with different types of Heegaard diagrams by introducing some generalisations. In the following subsections, we will explore these generalisations one by one, ultimately arriving at a version of the Nicefication Algorithm that is tailored to peculiar Heegaard, our main interest.

4.4.1 Algorithm for bordered Heegaard diagrams

In this subsection, we see how the algorithm can be adapted to the case of bordered Heegaard diagrams. As reference, one can look at Chapter 8 of [LOT18].

Recall that in the bordered setting, we allow Heegaard diagrams to have one border component on which we put a basepoint z: let D_z be the region with the basepoint on its boundary.

We need to generalise the notion of nice Heegaard diagram for this setting.

Definition 4.19 (Nice bordered Heegaard diagram)**.** We call a bordered Heegaard diagram $(\Sigma, \boldsymbol{\alpha} = \boldsymbol{\alpha}^c \cup \boldsymbol{\alpha}^a, \boldsymbol{\beta}, z)$ *nice* if every region in Σ except for D_z is a bigon or a square. For a boundary region A, this means that it has two $\boldsymbol{\alpha}$-arcs, one $\boldsymbol{\beta}$-arc and one arc of $\partial\Sigma$ as boundary.

Remark 4.20 (No bigons on the boundary)**.** We do not allow boundary regions to have one $\boldsymbol{\alpha}$-arc and one arc of $\partial\Sigma$ as boundary (i.e. to be "bigons"), as it would mean that there is an $\boldsymbol{\alpha}$-arc whose does not intersect any $\boldsymbol{\beta}$-circle.

Then we have a similar result to Theorem 4.3.

Proposition 4.21 ([LOT18, Proposition 8.2])**.** *Let $(\Sigma, \boldsymbol{\alpha}, \boldsymbol{\beta}, z)$ be a bordered Heegaard diagram. Then, it can be turned into a nice bordered Heegaard diagram via*

- *isotopies of the $\boldsymbol{\beta}$-circles not crossing $\partial\Sigma$,*
- *handleslides of $\boldsymbol{\beta}$-circles over other $\boldsymbol{\beta}$-circles.*

Proof. It is clear that, if we are able to fix the bordered diagram around the boundary, then we can simply apply the nicefication algorithm as it is done in the closed case in order to obtain a nice bordered Heegaard diagram.

We then introduce what we could call a "initial finger move around the border", done as follows. Denote the endpoints of the $\boldsymbol{\alpha}$-arcs as in Figure 4.18, with the indices increasing if you go around the border counter-clockwise and with the basepoint z between a_1 and a_{4k}. Observe now the boundary of D_z; we start from the endpoint a_1 and move along the $\boldsymbol{\alpha}$-arc, going away from $\partial\Sigma$, until we reach the first $\boldsymbol{\beta}$-edge of D_z and we call it b. We now operate the following finger move on b: we push it staying close to the border through the $\boldsymbol{\alpha}$-arc ending in a_1, then through the one ending in a_2 and so on, up to intersecting the one ending in a_{4k}. Then, in the resulting diagram, the boundary regions other than D_z are all rectangles.

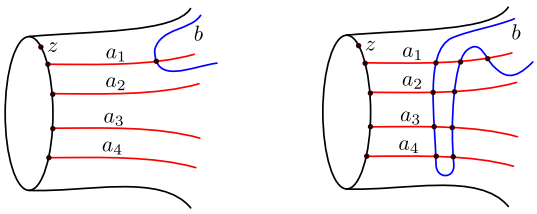

Figure 4.18: Initial finger move around the boundary to make all the boundary regions (except D_z) squares.

We can now apply the Nicefication Algorithm, obtaining a nice bordered Heegaard diagram.

□

Additionally, it is worth noting that the resulting diagram satisfies the conditions of Corollary 3.2 of [LMW08], which implies that it is admissible.

4.4.2 Algorithm for sutured Heegaard diagrams

To generalise the algorithm to the sutured case, we need to adapt it to allow multiple basepoints. This can be achieved quite easily. In this case, we still define the distance of a region D as the smallest number of intersection points between the $\boldsymbol{\beta}$-circles and an arc $c \subset \Sigma \setminus \boldsymbol{\alpha}$ connecting a point in the interior of D and a region containing one of the basepoints z_i. We can then define the distance complexities in the same way as before, and they will still be well-defined.

We can then apply the algorithm as presented in Section 4.2; in particular, we can prove that the distance complexity is strictly decreasing in the same way as for the closed case. Therefore, the algorithm works as before.

4.4.3 Algorithm for bordered sutured Heegaard diagrams

We can combine the generalisations we saw for the bordered and sutured cases to obtain a generalised version of the algorithm for bordered sutured Heegaard diagrams.

As reference, one can look at Section 4.7 of [Zar11].

We first need to define nice Heegaard diagrams in this setting.

Definition 4.22 (Nice bordered sutured Heegaard diagrams)**.** A bordered sutured Heegaard diagram $(\Sigma, \boldsymbol{\alpha}, \boldsymbol{\beta}, \mathcal{Z}_\alpha, \phi_\alpha, \mathcal{Z}_\beta, \phi_\beta)$ is called *nice* if every region in Σ is either:

- a *multiplicity zero region*, which is defined as a region adjacent to $\partial\Sigma \setminus (\phi_\alpha(Z_\alpha) \cup \phi_\beta(Z_\beta))$ (i.e. it has inside one "tick" as we defined them in Subsection 2.6.2),
- a bigon, none of whose sides are in $\phi_\alpha(Z_\alpha) \cup \phi_\beta(Z_\beta)$,
- a square, whose at most one of the sides is in $\phi_\alpha(Z_\alpha) \cup \phi_\beta(Z_\beta)$.

Moreover, we request that every connected component of $\Sigma \setminus \boldsymbol{\alpha}$ contains at least one multiplicity zero region.

Then, we can generalise the Nicefication Algorithm as we did for the last two cases.

Proposition 4.23 ([Zar11, Proposition 4.7.2])**.** *Any bordered sutured Heegaard diagram can be nicefied via*

- *isotopies of the $\boldsymbol{\beta}$-circles not crossing $\partial\Sigma$,*
- *isotopies of $\boldsymbol{\beta}$-arcs that do not move the endpoints and do not cross $\partial\Sigma$,*
- *handleslides of any $\boldsymbol{\beta}$-curve over a $\boldsymbol{\beta}$-circle,*
- *stabilisations.*

Proof. We start by applying stabilisations, in order to ensure that any connected component of Σ has both $\boldsymbol{\alpha}$- and $\boldsymbol{\beta}$-curves.

Then, for any boundary component, we apply to some $\boldsymbol{\beta}$-curve the "initial finger move around the border" that we described in Subsection 4.4.1.

Now we can apply the Nicefication Algorithm as first presented, obtaining a nice bordered sutured Heegaard diagram. In particular, the distance of a region D is defined as the smallest number of intersection points between the $\boldsymbol{\beta}$-circles and an arc $c \subset \Sigma \setminus \boldsymbol{\alpha}$ connecting a point in the interior of D and one multiplicity zero region; since we required that every connected component of $\Sigma \setminus \boldsymbol{\alpha}$ contains at least one multiplicity zero region, this notion is well-defined also in this case. □

4.4.4 Algorithm for peculiar Heegaard diagrams

We conclude this section with the generalisation of the Nicefication Algorithm to the case of 4-ended tangles, i.e. the case of peculiar Heegaard diagrams.

As a reference, one can see Section 5.1 of [Zib20].

We first need to define nice Heegaard diagrams in this setting. Recall that we denote by $(\Sigma, \boldsymbol{\alpha} = \boldsymbol{\alpha}^c \cup \{\mathcal{S}\}, \boldsymbol{\beta}, \{p_i\}_{i=1}^4, \{q_j\}_{j=1}^4, \{z_k\}_{k=1}^m, \{w_l\}_{l=1}^m)$ a peculiar Heegaard diagram for a 4-ended tangle with m closed components.

Definition 4.24 (Nice peculiar Heegaard diagram)**.** Consider a peculiar Heegaard diagram $(\Sigma, \boldsymbol{\alpha}, \boldsymbol{\beta}, \{p_i\}_{i=1}^4, \{q_j\}_{j=1}^4, \{z_k\}_{k=1}^m, \{w_l\}_{l=1}^m)$ for some 4-ended tangle T with m closed components. We need to pick some *special basepoints*: one p_i and one q_j for some $i, j \in \{1, 2, 3, 4\}$ and one between z_k and w_k for each closed component of T. We call a region that does contain a special basepoint a *multiplicity zero region.*

We say that a peculiar Heegaard diagram is *nice* with respect to the choice of the special basepoints above if any region that is not a multiplicity zero region is either a square or a bigon.

Remark 4.25. It should be noted that, based on the definition just provided, there exists at least one multiplicity zero region within each connected component of $\Sigma \setminus \boldsymbol{\alpha}$.

Thus, this can be considered a special instance of a multi-pointed closed Heegaard diagram. As previously mentioned, the Nicefication Algorithm can be adapted to this scenario, resulting in the following outcomes.

Proposition 4.26. *Every 4-ended tangle T admits a nice peculiar Heegaard diagram for any choice of special basepoints.*

In particular, any peculiar Heegaard diagram with a choice of special basepoints can be made nice with a series of

- *isotopies of the $\boldsymbol{\beta}$-circles,*
- *handleslides of $\boldsymbol{\beta}$-circles over other $\boldsymbol{\beta}$-circles.*

In particular, as we proved for closed Heegaard diagrams with Theorem 4.2, also in this case the Heegaard Floer invariant can be computed combinatorially.

Theorem 4.27 ([Zib20, Corollary 5.7])**.** *Let T be a 4-ended tangle and let $\mathcal{H}$ be a nice peculiar Heegaard diagram with some choice of special basepoints for T.*

Then, $\mathrm{HFT}(T)$ *can be computed combinatorially via $\mathcal{H}$.*

The above theorem has been proved in [Zib20] and the Mathematica Software [`PQM.m`] is an implementation of the algorithm that proves the theorem.

4.5 Modifications done to the algorithm

When we have a nice Heegaard diagram, we can compute the needed flavor of Heegaard Floer Homology combinatorially. In the case of 4-ended tangles, presented in Section 3.5, it exists the [`PQM.m`] Mathematica Software, developed by Claudius Zibrowius in 2017, of which the up-to-date version can be found on his personal website. This software takes as input a nice Heegaard diagram for a 4-ended tangle with some other data related to the tangle (the $\boldsymbol{\alpha}$-arcs sites, the Alexander grading of the tangle and the multiplicity zero regions of the diagram) and computes the peculiar module CFT^{∂} of the tangle.

During the implementation of the Nicefication Algorithm, some changes were done with the goal to optimise the final result in the sense of the [`PQM.m`] Software, i.e. aiming to minimise the number of generators of the final result and therefore the running time required to compute the CFT^{∂}. The main changes done are the following two:

1. introduction of general handleslides as a move done by the algorithm;
2. exploration of all the possible moves that we can do on the worst region D_m, comparison of them and choice of the best one to do.

We now discuss these changes in details.

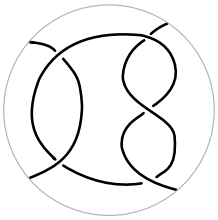

Figure 4.19: $(2,-3)$ Pretzel tangle.

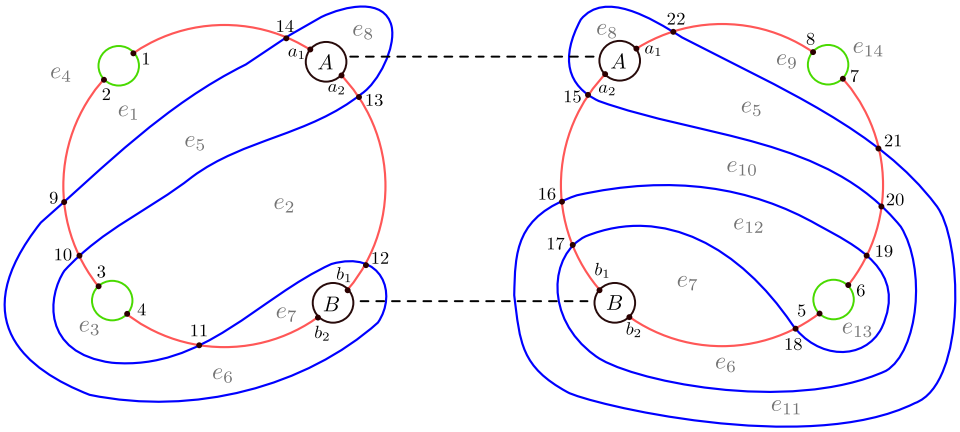

Figure 4.20: Tangle Heegaard diagram for the $(2,-3)$ Pretzel tangle.

4.5.1 General handleslides

With "general handleslides", we mean handleslides as defined in Section 2.2; in fact, these are not considered by the algorithm as it was presented in Section 4.2. This move was introduced in the software during its validation via computation of nice diagrams for Pretzel tangles (whose HFT are known) for the reasons that are now explained.

We define the $(2n,-2m-1)$-Pretzel tangle to be the sum of two rational tangles: $Q_{1/(2n)} + Q_{-1/(2m+1)}$ for $m,n \in \mathbb{Z}_{>0}$. Consider, for instance, the $(2,-3)$ Pretzel tangle shown in Figure 4.20. The construction of its Heegaard diagram as explained in Section 2.6 results in the diagram shown in Figure 4.20.

Then, we transform the diagram into a peculiar one by removing the sutures as described in Section 2.6, obtaining the diagram shown in Figure 4.21.

We then place the two special basepoints, making e_1 and e_3 the two multiplicity zero regions. There are two bad regions in the diagram, e_5 and e_6, which are two octagons of distance 1.

Applying the algorithm as presented in [SW10], we can nicefy the diagram in four cycles, requiring a finger move and a handleslide for each bad region. The final result has a total of 126 generators. However, if we allow general handleslides, we can nicefy the diagram with only two cycles using two general handleslides, resulting in a total of 82 generators.

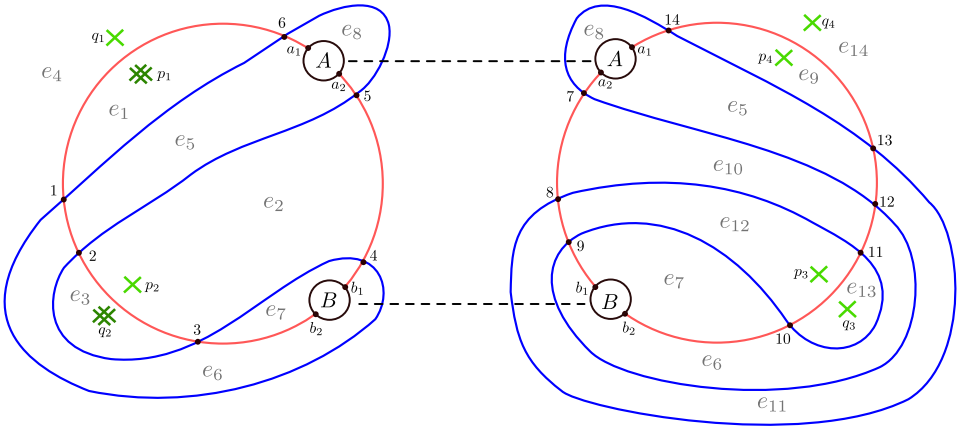

Figure 4.21: Peculiar Heegaard diagram for the $(2,-3)$ Pretzel tangle (the double crosses in a darker green colour denote the special basepoints).

The advantage of using general handleslides was also observed in more complex cases where the difference in the number of generators of the final result had a greater impact on the running time required by the [PQM.m] package.

We can further appreciate the efficiency of the general handleslides by observing how they can affect the distance complexities of a diagram. Note that for the diagram $\mathcal{H}$ in Figure 4.21, the distance 1 complexity (which is the only non-trivial complexity) is

$$c_1(\mathcal{H}) = (4, (-2, \text{ Region 5}), (-2, \text{ Region 6}))\,.$$

After the first general handleslide, we obtain the diagram $\mathcal{H}'$, with complexity

$$c_1(\mathcal{H}') = (2, (-2, \text{ Region 5}))\,;$$

and after the second handleslide we obtain the nice diagram $\mathcal{H}''$, whose has only trivial distance complexities. Therefore, using a general handleslide allows us to reduce the maximum distance badness by a factor of 2, which was not achievable with any of the moves in the original algorithm.

Remark 4.28 (Effect of a general handleslide on the "overall niceness" of the diagram)**.** Let $\mathcal{H}$ be a Heegaard diagram of distance d_*. We want to understand how a general handleslide modifies in general $\mathcal{H}$ from the point of view of its niceness, i.e. how it modifies the complexities $c_d(\mathcal{H})$ for all the possible d's.

The first thing to note is that a general handleslide does not generate any bad regions. This is because a handleslide only generates squares near the $\boldsymbol{\beta}$-circle that we are sliding on, and it leaves the badness of the regions that it cuts through unchanged.

The critical point is the distance of the regions that the handleslide cuts through. If their distance is determined by arcs that are cut by the handleslide, then they may increase by 1. This may also increase the distance of other regions of the diagram with analogous arguments. However, we need not worry about this case as we will

introduce a new algorithm in the next subsection for comparing different Heegaard diagrams which will avoid this scenario.

Therefore, the general handleslides were included in the pool of possible moves of the algorithm.

4.5.2 Comparison of possible moves

We now have all the possible moves that we can make: finger moves, handleslides and general handleslides. Our goal is to obtain the best possible nice Heegaard diagram, i.e. the one with the fewest generators, using these moves. As mentioned above, at every iteration of the algorithm, we try to perform all the possible moves on the worst region of the diagram and generate all the corresponding Heegaard diagrams.

The best choice would be to try all the possible threads generated by the different moves at every cycle and then compare all the final nice diagrams obtained. However, this would not be computationally feasible, and we need to compromise. In this first version of the [`nicepy`] software, the decision is to try to get the best possible diagram after every iteration of the algorithm.

We could adopt two different points of view: on the one hand, we could decide to minimise the number of generators, hence choosing to continue to execute the algorithm on the diagram that has the fewest generators; on the other hand, we could choose to minimise the number of cycles needed by the algorithm to get a nice Heegaard diagram, thereby reducing the number of moves that are done on the initial diagram.

It is unclear at the moment which of the two perspectives is better or what a good balance between them would be. Therefore, for now, the choice made is to minimise the number of cycles of the nicefication algorithm. However, this is still an open question that will be analysed in the future.

Therefore, before running the algorithm, we need a tool that helps us compare all these moves and understand which one is better in the sense described above.

Definition 4.29 (Total complexity)**.** Consider a Heegaard diagram $\mathcal{H}$ of distance d_*. We define its *total complexity* as

$$tc(\mathcal{H}) = \sum_{d=1}^{d_*} 3^d \cdot b_d(\mathcal{H}),$$

where $b_d(\mathcal{H})$ is the total badness of distance d defined in Section 4.2.

The total complexity is convenient when we want to compare multiple Heegaard diagrams obtained by applying some move to a common initial diagram and it is a more direct way to compare the effectiveness of these different moves in the attempt to nicefy the diagram.

We quickly describe how the total complexity is affected in the various scenarios that occur in the algorithm. We use the same notation used when presenting the

algorithm, i.e. $\mathcal{H}$ is the diagram before applying the move, $\mathcal{H}'$ is the diagram obtained after the move is done, D_m is the worst region of distance d_* that we want to modify, $D_{m,1}$ and $D_{m,2}$ are the two regions in which D_m is split by the move, D_* is the neighbour region of distance $d_* - 1$ and D'_* is this same region after the move is done.

- In Case 1 (finger move ending in a bigon), we have $b(D_{m,1})+b(D_{m,2}) \leq b(D_m)-1$ and $b(D'_*) = b(D_*) + 1$; hence
$$tc(\mathcal{H}') \leq tc(\mathcal{H}) - 3^{d_*} + 3^{d_*-1}.$$
Therefore, in this case holds $tc(\mathcal{H}') < tc(\mathcal{H})$.

- In Case 2 (finger move ending in a region D' of smaller distance $d' < d_*$), we have $b(D_{m,1}) + b(D_{m,2}) \leq b(D_m) - 1$, $b(D') = b(D') + 1$ and $b(D'_*) = b(D_*) + 1$; hence
$$tc(\mathcal{H}') = tc(\mathcal{H}) - 3^{d_*} + 3^{d_*-1} + 3^{d'} \leq tc(\mathcal{H}) - 3^{d_*} + 2 \cdot 3^{d_*-1}.$$
Therefore, in this case holds $tc(\mathcal{H}') < tc(\mathcal{H})$.

- In Case 3 (finger move ending in another bad region D' of distance d_*), we have $b(D_{m,1}) + b(D_{m,2}) \leq b(D_m) - 1$, $b(D') = b(D') + 1$ and $b(D'_*) = b(D_*) + 1$; hence
$$tc(\mathcal{H}') \leq tc(\mathcal{H}) - 3^{d_*} + 3^{d_*} + 3^{d_*-1} = tc(\mathcal{H}) + 3^{d_*-1}.$$
This is the worst case in terms of the total complexity, as it is the only case among the ones of the algorithm in which it could increase.

- In Case 4.1 (handleslide), we have $b(D_{m,1}) + b(D_{m,2}) \leq b(D_m) - 1$ and $b(D') = b(D') + 2$; hence
$$tc(\mathcal{H}') \leq tc(\mathcal{H}) - 3^{d_*} + 2 \cdot 3^{d_*-1}.$$
Therefore, in this case holds $tc(\mathcal{H}') < tc(\mathcal{H})$.

Remark 4.30. We do not discuss how tc changes after a general handleslide, as we will only need the knowledge of the above cases to guarantee that the implementation of the algorithm is going to terminate after a finite number of cycles.

We are now ready to execute the algorithm on a Heegaard diagram $\mathcal{H}$ with distance d_*.

The first step of the algorithm is to identify the worst region D_m, which we assume to be a $2n$-gon. Then, the program selects a blue edge b_* that neighbors D_m with a $d_* - 1$ region; let β_* be the $\boldsymbol{\beta}$-circle on which b_* lies. Next, the algorithm attempts to perform a general handleslide on each $\boldsymbol{\beta}$-edge of D_m that is not on β_*, resulting in k new diagrams $\mathcal{H}_1, \ldots, \mathcal{H}_k$ for some $0 \leq k \leq n-1$. After this, the algorithm attempts finger moves on the $\boldsymbol{\alpha}$-edges of D_m that are labeled $a_2, \ldots, an - 1$ as described in the original Nicefication Algorithm, generating s new diagrams $\mathcal{H}k + 1, \ldots, \mathcal{H}_{k+s}$ for some $0 \leq s \leq n - 2$. If a handleslide is successful, it is not considered as a

separate move since it has already been taken into account as a general handleslide. Additionally, the algorithm does not attempt finger moves on a_1 and a_n since the only way to decrease the badness of the region by using these edges would be to perform a handleslide (a finger move would leave D_m as a $2n$-gon).

Remark 4.31. Among all the diagrams $\mathcal{H}_1, \dots, \mathcal{H}_{k+s}$ there is also the diagram that we would obtain by applying the Nicefication Algorithm as presented originally; we denote it by $\mathcal{H}^\star$.

We now have $k+s$ possible Heegaard diagrams that we need to compare in order to understand which one is the better one. For the comparison, we consider three factors:

- the total complexity of the diagrams $tc(\mathcal{H}_i)$,
- the number of generators of the diagrams,
- the distance d_* complexity c_{d_*}.

The algorithm to compare the different Heegaard diagrams is the following.

– **Step 1**. As first step of the comparison, we exploit the total complexity. We call by $tc_{\min}$ the minimum of all the total complexities, i.e.

$$tc_{\min} = \min\left\{tc\left(\mathcal{H}_1\right), \dots, tc\left(\mathcal{H}_{k+s}\right)\right\}.$$

We call $\mathcal{H}_{i_1}, \dots, \mathcal{H}_{i_t}$ the diagrams with minimal total complexity, i.e.

$$tc_{\min} = tc\left(\mathcal{H}_{i_1}\right) = \dots = tc\left(\mathcal{H}_{i_t}\right).$$

– **Step 2**. We then extract from these diagrams the ones with the minimal number of generators. Let $\#\text{gen}_{\min}$ be this number, we call the diagrams which minimise the number of generators $\mathcal{H}_{i_{j_1}}, \dots, \mathcal{H}_{i_{j_s}}$.

– **Step 3**. Among these diagrams, we take the ones that have the smaller distance d_* complexities, we call

$$c_{d_{*\min}} = \min\left\{c_{d_*}(\mathcal{H}_{i_{j_1}}), \dots, c_{d_*}(\mathcal{H}_{i_{j_s}})\right\}$$

and let $\mathcal{H}_{i_{j_{k_1}}}, \dots, \mathcal{H}_{i_{j_{k_r}}}$ be these diagrams.

– **Step 4**. Two different cases can occur:

(a) $c_{d_{*\min}} < c_{d_*}(\mathcal{H})$ and there are not bad regions of distance greater than d_* in at least one among $\mathcal{H}_{i_{j_{k_1}}}, \dots, \mathcal{H}_{i_{j_{k_r}}}$.

If this is the case, any diagram among $\mathcal{H}_{i_{j_{k_1}}}, \dots, \mathcal{H}_{i_{j_{k_r}}}$ which does not have any bad region of distance greater than d_* is nearer to be a nice Heegaard diagram in the sense of the Nicefication Algorithm as presented in Section 4.2. Thus, we can choose any one among them to continue the nicefication process.

(b) $c_{d_{*\min}} \geq c_{d_*}(\mathcal{H})$ or there is at least one bad region of distance greater than d_* in every diagram $\mathcal{H}_{i_{j_{k_1}}}, \dots, \mathcal{H}_{i_{j_{k_r}}}$. In this case, we cannot conclude as above but we need to take some extra precautions.

We first go back to Step 3: we call $c_{d_{*\min,2}}$ the second lowest distance d_* complexity and we consider the diagrams among $\mathcal{H}_{i_{j_1}}, \dots, \mathcal{H}_{i_{j_s}}$ which have distance d_* complexity $c_{d_{*\min,2}}$. We move to Step 4. If we end in case (a), we obtain a Heegaard diagram which we can feed to the next cycle of the Nicefication Algorithm. If we still end in case (b), we consider $c_{d_{*\min,3}}$, and so on.

If we end in case (b) for all $\mathcal{H}_{i_{j_1}}, \dots, \mathcal{H}_{i_{j_s}}$, we go back to Step 2. We call $\#\text{gen}_{\min,2}$ the second lowest number of generators and we consider the diagrams among $\mathcal{H}_{i_1}, \dots, \mathcal{H}_{i_t}$ which have such number of generators. Then we move to Step 3 and Step 4. If we end in case (a), we obtain a Heegaard diagram which we can feed to the next cycle of the Nicefication Algorithm. If also in this case we always end in case (b), then we consider $\#\text{gen}_{\min,3}$, and so on.

If we end in case (b) for all $\mathcal{H}_{i_1}, \dots, \mathcal{H}_{i_t}$, we go back to step 1. We call $tc_{\min,2}$ the second lowest total complexity and we consider the diagrams among $\mathcal{H}_1, \dots, \mathcal{H}_{k+s}$ which have such total complexity. Then we move to Step 2, Step 3 and Step 4. If we end in case (a), we obtain a Heegaard diagram with which we can feed to the next cycle of the Nicefication Algorithm. If we always end in case (b), then we consider $tc_{\min,3}$, and so on.

Notice that we are going to end in case (a) at some point, as among the $\mathcal{H}_1, \dots, \mathcal{H}_{k+s}$ there is also $\mathcal{H}^\star$ for which the hypothesis of case (a) are satisfied.

We call $\mathcal{H}'$ the diagram obtained with the above algorithm and we continue to run the nicefication process on it.

Remark 4.32. Going back to what we said in Remark 4.28, it is now clear that if the chosen diagram $\mathcal{H}'$ is one obtained via a general handleslide, then the above discussion guarantees that we are indeed proceeding towards a nice Heegaard diagram.

Therefore, we have proven the following proposition.

Proposition 4.33. *The [nicepy] Software, implemented starting from the Nicefication Algorithm and modified as described above, terminates in a finite number of steps.*

Remark 4.34 (On the usefulness of the total complexity)**.** The primary advantage of the total complexity is the ability to compare different Heegaard diagrams generated in one cycle of the algorithm better. It allows us to understand to some extent where and how the badness is redistributed by the modification made.

To better visualise this, consider the diagram locally shown in Figure 4.22. We have that the worst region is an octagon D_m of distance d_*, and we let D_* be the neighbouring region of distance $d_* - 1$.

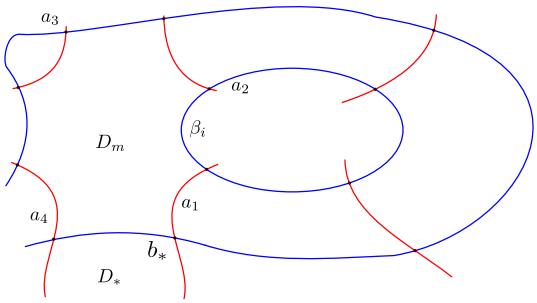

Figure 4.22: Initial situation to study the effectiveness of the total complexity.

Then, we compare two possible moves: one finger move ending in a bigon adjacent to D_m (on the left in Figure 4.23) and one (general) handleslide (on the right in Figure 4.23).

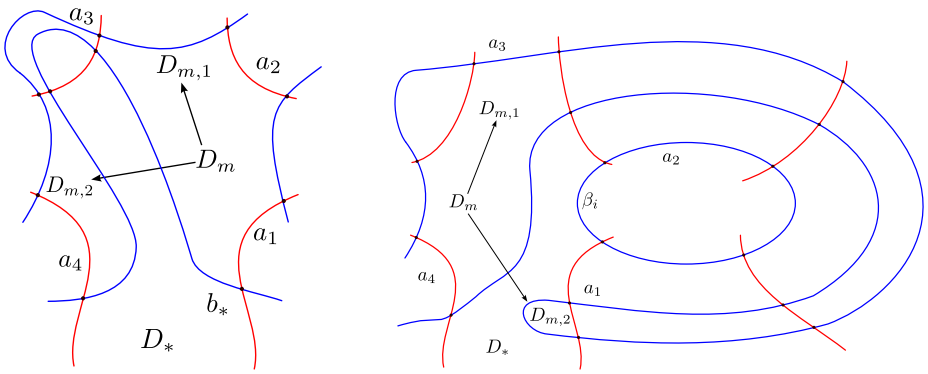

Figure 4.23: Two moves that modify c_{d_*} in the same way but are not equally effective overall.

Then, the difference between these two moves is not detected by c_{d_*}": in fact, in both cases we have that the contribution of the badness of D_m is reduced by one (in one case $D_{m,2}$ is a bigon, in the other it is a square and $b(D_{m,1}) = b(D_m) - 1$). But the difference is clear if we observe c_{d_*-1}: in one case, the badness of D_* increases by one and in the other it increases by two. Hence, in this particular case, we prefer the finger move to the handleslide since it allows us to skip an additional cycle later in the algorithm when we will have to make D_* a good region. The total complexity clearly chooses the right move in this sense, allowing us to reduce the number of cycles that the algorithm needs to end.

Chapter 5

Computations

In the course of this master thesis project, certain families of tangles were studied in order to find patterns in the invariants they yielded. This investigation was meant to be a step towards a more general formula for understanding how HFT behaves under the sum of tangles.

Two families were chosen for this research: the family of the sum of a rational tangle with its mirror image, i.e. $Q_{p/q} + Q_{-p/q}$, and the family of the sum of a rational tangle with a number of full vertical twists, i.e. $Q_{p/q} + Q_{1/(2n)}$. The latter family yielded promising results in terms of a possible pattern that HFT seems to follow, which was presented in the Introduction as Conjecture 0.1. It would be nice to prove this regularity at a theoretical level, which could lead to an explanation of the behaviour of the rational part of HFT under the sum of tangles.

Let us now see the results obtained in detail.

5.1 HFT of $Q_{p/q} + Q_{-p/q}$

We consider a rational tangle $Q_{p/q}$ and its mirror image $Q_{-p/q}$, obtained by swapping all the crossings.

We define the tangle $T_{p/q}$ as the sum $Q_{p/q} + Q_{-p/q}$ for $p/q \in \mathbb{Q}\mathrm{P}^1$ and q odd; see Figure 5.1 for an example. The condition on q ensures that there are no closed components in $T_{p/q}$.

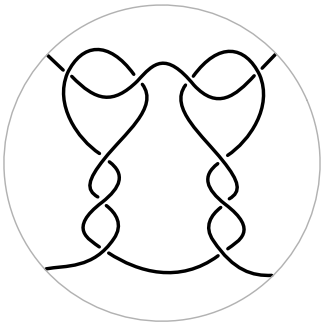

Figure 5.1: $T_{3/7} = Q_{3/7} + Q_{-3/7}$.

We now claim that we can reduce ourselves to the computation of HFT for the set $\mathcal{F} = \{T_{p/q} \mid 0 < 2p < q\}$, in the sense that $\mathrm{HFT}(T_{p/q})$ for a generic $T_{p/q}$ can be deduced from $\mathrm{HFT}(F)$ for some $F \in \mathcal{F}$.

To prove this, consider the following intermediate remarks.

Remark 5.1 (We can assume $p/q > 0$)**.** We can assume $p/q > 0$ without loss of generality. To prove this, we just have to notice that $m(T_{p/q}) \simeq T_{-p/q}$. Then, for Proposition 3.60, we have that we can obtain $\mathrm{HFT}(T_{-p/q})$ from $\mathrm{HFT}(T_{p/q})$.

Remark 5.2 (We can assume $|p| < q$)**.** We can assume $|p| < q$ without loss of generality. To prove this, we show that $T_{p/q} \simeq T_{(p/q)+n}$ for any $n \in \mathbb{Z}$.

In fact, we can easily see this in terms of continued fractions. Let $[a_1, \dots, a_m]$ be a continued fractions corresponding to p/q. Then, adding $n \in \mathbb{Z}$ means to consider the continued fraction $[a_1 + n, a_2, \dots, a_m]$, i.e. we are adding half-twists on the right of the tangle. Hence we found that

$$T_{(p/q)+n} = Q_{p/q} + Q_n + m(Q_{p/q} + Q_n) = Q_{p/q} + Q_n + Q_{-p/q} + Q_{-n}.$$

Using Corollary 1.53 and the second Reidemeister move, we then obtain that

$$\begin{aligned} T_{(p/q)+n} &= Q_{p/q} + Q_n + m(Q_{p/q} + Q_n) \\ &= Q_{p/q} + Q_n + Q_{-p/q} + Q_{-n} \\ \text{(Corollary 1.53)} \quad &\simeq Q_{p/q} + Q_n + Q_{-n} + Q_{-p/q} \\ \text{(II Reidemeister move)} \quad &\simeq Q_{p/q} + Q_{-p/q} \\ &= T_{p/q}. \end{aligned}$$

Remark 5.3 (We can assume $0 < 2p < q$)**.** We can now see that, without loss of generality, we can indeed consider only the tangles in the family $\mathcal{F}$. By Remarks 5.1 and 5.2 we can assume $0 < p < q$. Let p, q be such that $0 < q < 2p$ (i.e. $0 < 1/2 < p/q$); then, for same argument exploited in Remark 5.2, holds

$$T_{p/q} \simeq T_{(p/q)-1} = T_{(p-q)/q}.$$

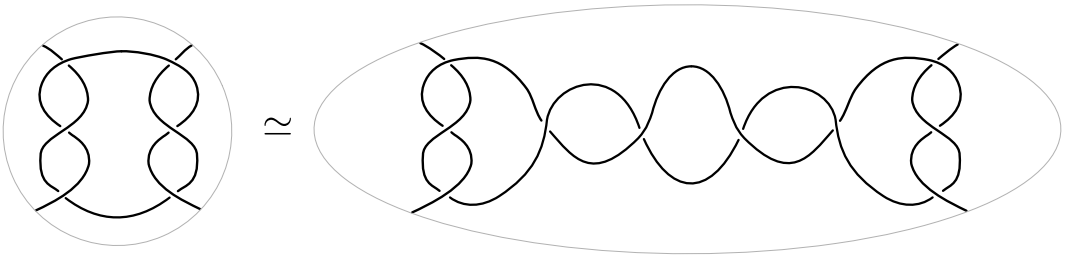

Figure 5.2: Adding n to p/q, we have $2n$ half-twists in the middle of $T_{(p/q)+n}$ that cancel out: example with $T_{1/3}$ and $T_{7/3}$.

Now, as we saw in Remark 5.1, we have

$$T_{(p-q)/q} \simeq \mathrm{m}\left(T_{(q-p)/q}\right)$$

and since

$$0 < \frac{q-p}{q} < \frac{1}{2},$$

we can obtain $\mathrm{HFT}(T_{p/q})$ from $T_{(q-p)/q} \in \mathcal{F}$.

Therefore, by studying the results obtained applying HFT to tangles in the family $\mathcal{F}$, we are studying all the tangles of the form $T_{p/q} = Q_{p/q} + Q_{-p/q}$.

We obtained the computations showed in Table 5.1 for the tangle in $\mathcal{F}$. There are three patterns that seem to be followed, which can be summed up in the following three conjectures.

Conjecture 5.4. *Let $T_{1/q} = Q_{1/q} + Q_{-1/q}$ for q odd. Then,*

$$\mathrm{HFT}\left(T_{1/q}\right) = \mathfrak{r}(0) + 2 \cdot \left(\sum_{i=1}^{(q-1)/2} \mathfrak{s}_{2i}(0) \right).$$

The idea for this conjecture comes by a direct observation of the first column of Table 5.1.

Conjecture 5.5. *Let $T_{p/q} = Q_{p/q} + Q_{-p/q}$ for $p/q \in \mathbb{Q}\,\mathrm{P}^1$, $0 < p$ and $q = 2p + 1$. Then,*

$$\mathrm{HFT}\left(T_{1/q}\right) = \mathfrak{r}(0) + (p^2 + p) \cdot \mathfrak{s}_4(0).$$

We can explain this conjecture by looking at the diagonal $q = 2p+1$ in Table 5.1. We can see that every time that we move to the next value of p, we are increasing the number of special components of length 4 and slope 0 by $2p$. Hence, the number of $\mathfrak{s}_4(0)$ for $T_{p/q}$ is $2\left(\sum_{i=1}^{p} i\right) = 2 \cdot (p(p+1))/2 = p^2 + p$.

With a similar observation on the diagonal $q = 2p + 3$, the following pattern seems to occur.

Conjecture 5.6. *Let $T_{p/q} = Q_{p/q} + Q_{-p/q}$ for $p/q \in \mathbb{Q}\,\mathrm{P}^1$, $0 < p$ and $q = 2p + 3$. Then,*

$$\mathrm{HFT}\left(T_{1/q}\right) = \mathfrak{r}(0) + (p^2 + 3p - 4) \cdot \mathfrak{s}_4(0) + 2 \cdot \mathfrak{s}_8(0).$$

$\mathfrak{q}\backslash\mathfrak{p}$	1	2	3	4	5	6
1	$\mathfrak{r}(0)$					
2						
3	$\mathfrak{r}(0)+2\cdot\mathfrak{s}_4(0)$					
4						
5	$\mathfrak{r}(0)+2\cdot\mathfrak{s}_4(0)+2\cdot\mathfrak{s}_8(0)$	$\mathfrak{r}(0)+6\cdot\mathfrak{s}_4(0)$				
6						
7	$\mathfrak{r}(0)+2\cdot\mathfrak{s}_4(0)+2\cdot\mathfrak{s}_8(0)+2\cdot\mathfrak{s}_{12}(0)$	$\mathfrak{r}(0)+8\cdot\mathfrak{s}_4(0)+2\cdot\mathfrak{s}_8(0)$	$\mathfrak{r}(0)+12\cdot\mathfrak{s}_4(0)$			
8						
9	$\mathfrak{r}(0)+2\cdot\mathfrak{s}_4(0)+2\cdot\mathfrak{s}_8(0)+2\cdot\mathfrak{s}_{12}(0)+2\cdot\mathfrak{s}_{16}(0)$	$\mathfrak{r}(0)+8\cdot\mathfrak{s}_4(0)+6\cdot\mathfrak{s}_8(0)$		$\mathfrak{r}(0)+20\cdot\mathfrak{s}_4(0)$		
10						
11			$\mathfrak{r}(0)+18\cdot\mathfrak{s}_4(0)+6\cdot\mathfrak{s}_8(0)$	$\mathfrak{r}(0)+26\cdot\mathfrak{s}_4(0)+2\cdot\mathfrak{s}_8(0)$	$\mathfrak{r}(0)+30\cdot\mathfrak{s}_4(0)$	
12						
13				$\mathfrak{r}(0)+32\cdot\mathfrak{s}_4(0)+2\cdot\mathfrak{s}_8(0)+2\cdot\mathfrak{s}_{12}(0)$	$\mathfrak{r}(0)+38\cdot\mathfrak{s}_4(0)+2\cdot\mathfrak{s}_8(0)$	$\mathfrak{r}(0)+42\cdot\mathfrak{s}_4(0)$
14						
15				$\mathfrak{r}(0)+32\cdot\mathfrak{s}_4(0)+12\cdot\mathfrak{s}_8(0)$		
16						
17				$\mathfrak{r}(0)+32\cdot\mathfrak{s}_4(0)+20\cdot\mathfrak{s}_8(0)$		$\mathfrak{r}(0)+62\cdot\mathfrak{s}_4(0)+2\cdot\mathfrak{s}_8(0)+2\cdot\mathfrak{s}_{12}(0)$

Table 5.1: HFT for tangles of the form $T_{p/q}$ with $p/q \in \mathbb{Q}\mathrm{P}^1$, q odd and $0 < 2p < q$.

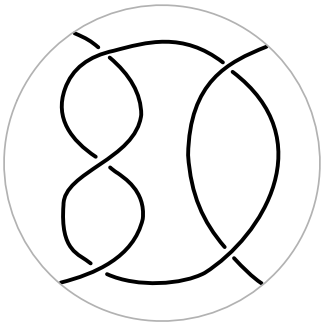

Figure 5.3: The tangle $S_{1/3}(2)$.

To motivate this conjecture, we look at the diagonal $q = 2p+3$ in Table 5.1. We can see that, taking $p = 1$ as starting point, every time that we move to the next value of p, we are increasing the number of special components of length 4 and slope 0 by $2(p+1)$. This means that the number of $\mathfrak{s}_4(0)$ for $T_{p/q}$ is $2 + 2\left(\sum_{i=3}^{p+1} i\right) = 2 + 2 \cdot {}^{((p+1)(p+2))}/_2 - 6 = p^2 + 3p - 4$.

The author was not able to see any other promising pattern in Table 5.1.

5.2 HFT of $Q_{p/q} + Q_{1/(2n)}$

We compute now HFT on tangles of the form

$$S_{p/q}(2n) \coloneqq Q_{p/q} + Q_{1/(2n)}$$

for ${}^p/_q \in \mathbb{Q}\,\mathrm{P}^1$, q odd and $n \in \mathbb{Z}_{>0}$, i.e. rational tangles that we sum to a number of full vertical twists. See Figure 5.3 for the example $S_{1/3}(2)$.

As p, q and n grow, the computations require more time, therefore most of them were done for $n = 1, 2$.

Similar to Section 5.1, we can find some symmetries among this class of tangles. This allows us to restrict ourselves to the investigation of a subset of $\{S_{p/q}(2n) \mid {}^p/_q \in \mathbb{Q}\,\mathrm{P}^1, q \text{ odd and } n \in \mathbb{Z}_{>0}\}$: namely, we just need to compute HFT on the family $\mathcal{G}(2n) = \{S_{p/q}(2n) \mid 0 < p < q\}$. We prove this in the following two remarks.

Remark 5.7 (We can assume ${}^p/_q > 0$)**.** Consider $S_{p/q}(2n)$, where ${}^p/_q < 0$ and let $h \in \mathbb{Z}_{>0}$ be such that ${}^p/_q + h > 0$. Then, it holds

$$\begin{aligned}
S_{p/q}(2n) &= Q_{p/q} + Q_{1/(2n)} \\
\text{(II Reidemeister move)} \quad &\simeq Q_{p/q} + Q_{1/(2n)} + Q_h + Q_{-h} \\
\text{(Corollary 1.53)} \quad &\simeq Q_{p/q} + Q_h + Q_{1/(2n)} + Q_{-h} \\
&= Q_{(p/q)+h} + Q_{1/(2n)} + Q_{-h} \\
&= S_{(p/q)+h}(2n) + Q_{-h}.
\end{aligned}$$

By Theorem 3.63, we can deduce $\mathrm{HFT}(S_{p/q}(2n))$ for ${}^p/_q < 0$ from $\mathrm{HFT}(S_{(p/q)+h}(2n))$, where $0 < {}^p/_q + h$.

Remark 5.8 (We can assume $0 < p < q$)**.** This follows again from Corollary 1.53: if we consider the tangle $S_{(p/q)+m}(2n)$ for $m \in \mathbb{Z}$, then it holds

$$\begin{aligned} S_{(p/q)+m}(2n) &= Q_{p/q} + Q_m + Q_{1/(2n)} \\ &= Q_{p/q} + Q_{1/(2n)} + Q_m \\ &= S_{p/q}(2n) + Q_m, \end{aligned}$$

and since we know by Theorem 3.63 how the addition of some horizontal twists affects HFT of a given tangle, we can recover $\mathrm{HFT}(S_{(p/q)+m}(2n))$ from $\mathrm{HFT}(S_{p/q}(2n))$. Therefore, without loss of generality, we can assume that $0 < p < q$.

5.2.1 Computations for $S_{p/q}(2)$

We begin by looking at the tangles obtained by adding a single full twist. Here, we can actually restrict ourselves to a smaller pool of tangles: we only need to compute the invariants of the family $\mathcal{G}'(2) = \{S_{p/q}(2) \mid 0 < 2p < q\} \subset \mathcal{G}(2)$. Once again, the key to prove this is to use Corollary 1.53. Let $0 < p < q$ and consider a tangle $S_{p/q}(2)$ where $0 < 1/2 < p/q$; then the following holds:

$$\begin{aligned} S_{p/q}(2) &= Q_{p/q} + Q_{1/2} \\ &\simeq m\left(Q_{-p/q} + Q_{-1/2}\right) \\ &\simeq m\left(Q_{-p/q} + Q_{-1} + Q_{1/2}\right) \\ &\simeq m\left(Q_{(-p/q)-1} + Q_{1/2}\right) \\ \text{(II Reidemeister move)} \quad &\simeq m\left(Q_{(-p/q)+1} + Q_{-2} + Q_{1/2}\right) \\ \text{(Corollary 1.53)} \quad &\simeq m\left(Q_{(-p/q)+1} + Q_{1/2} + Q_{-2}\right) \\ &= m\left(S_{(-p/q)+1}(2) + Q_{-2}\right) \\ &= m\left(S_{(-p/q)+1}(2)\right) + m\left(Q_{-2}\right) \\ &= m\left(S_{(-p/q)+1}(2)\right) + Q_2. \end{aligned}$$

The combination of Proposition 3.60 and Theorem 3.63 allows us to show that $\mathrm{HFT}(S_{p/q}(2))$ can be obtained from $\mathrm{HFT}(S_{(-p/q)+1}(2))$, where

$$0 < -\frac{p}{q} + 1 < \frac{1}{2}.$$

The computations obtained for $S_{p/q}(2)$ with $0 < 2p < q$ are collected in Table 5.2.

There seems to be a very regular pattern in the computations, which is presented in the following conjecture.

$\mathbf{q}\backslash\mathbf{P}$	1	2	3	4	5	6	7	8
1								
2								
3	$1\cdot\mathfrak{r}\left(1/2\right)+$ $1\cdot\mathfrak{s}_4\left(1\right)$							
4								
5	$3\cdot\mathfrak{r}\left(1/2\right)+$ $1\cdot\mathfrak{s}_4\left(1\right)$	$1\cdot\mathfrak{r}\left(1/2\right)+$ $2\cdot\mathfrak{s}_4\left(1\right)$						
6								
7	$5\cdot\mathfrak{r}\left(1/2\right)+$ $1\cdot\mathfrak{s}_4\left(1\right)$	$3\cdot\mathfrak{r}\left(1/2\right)+$ $2\cdot\mathfrak{s}_4\left(1\right)$	$1\cdot\mathfrak{r}\left(1/2\right)+$ $3\cdot\mathfrak{s}_4\left(1\right)$					
8								
9	$7\cdot\mathfrak{r}\left(1/2\right)+$ $1\cdot\mathfrak{s}_4\left(1\right)$	$5\cdot\mathfrak{r}\left(1/2\right)+$ $2\cdot\mathfrak{s}_4\left(1\right)$		$1\cdot\mathfrak{r}\left(1/2\right)+$ $4\cdot\mathfrak{s}_4\left(1\right)$				
10								
11	$9\cdot\mathfrak{r}\left(1/2\right)+$ $1\cdot\mathfrak{s}_4\left(1\right)$	$7\cdot\mathfrak{r}\left(1/2\right)+$ $2\cdot\mathfrak{s}_4\left(1\right)$	$5\cdot\mathfrak{r}\left(1/2\right)+$ $3\cdot\mathfrak{s}_4\left(1\right)$	$3\cdot\mathfrak{r}\left(1/2\right)+$ $4\cdot\mathfrak{s}_4\left(1\right)$	$1\cdot\mathfrak{r}\left(1/2\right)+$ $5\cdot\mathfrak{s}_4\left(1\right)$			
12								
13	$11\cdot\mathfrak{r}\left(1/2\right)+$ $1\cdot\mathfrak{s}_4\left(1\right)$	$9\cdot\mathfrak{r}\left(1/2\right)+$ $2\cdot\mathfrak{s}_4\left(1\right)$	$7\cdot\mathfrak{r}\left(1/2\right)+$ $3\cdot\mathfrak{s}_4\left(1\right)$	$5\cdot\mathfrak{r}\left(1/2\right)+$ $4\cdot\mathfrak{s}_4\left(1\right)$	$3\cdot\mathfrak{r}\left(1/2\right)+$ $5\cdot\mathfrak{s}_4\left(1\right)$			
14								
15								
16								
17						$5\cdot\mathfrak{r}\left(1/2\right)+$ $6\cdot\mathfrak{s}_4\left(1\right)$		
18								
19		$15\cdot\mathfrak{r}\left(1/2\right)+$ $2\cdot\mathfrak{s}_4\left(1\right)$					$5\cdot\mathfrak{r}\left(1/2\right)+$ $7\cdot\mathfrak{s}_4\left(1\right)$	
20								
21								$5\cdot\mathfrak{r}\left(1/2\right)+$ $8\cdot\mathfrak{s}_4\left(1\right)$

Table 5.2: HFT for tangles of the form $S_{p/q}(2)$ with $p/q \in \mathbb{Q}\mathrm{P}^1$, q odd and $0 < 2p < q$.

Conjecture 5.9. *Let* $S_{p/q}(2) = Q_{p/q} + Q_{1/2}$ *with* $p/q \in \mathbb{Q}\,\mathrm{P}^1$, q *odd and* $0 < 2p < q$. *Then,*

$$\mathrm{HFT}\left(S_{p/q}(2)\right) = (q-2p)\cdot\mathfrak{r}(1/2) + p\cdot\mathfrak{s}_4(1).$$

5.2.2 Computations for $S_{p/q}(4)$

Next, we focus on tangles obtained by adding two complete vertical twists to a rational tangles, i.e., tangles of the form $S_{p/q}(4)$. Unfortunately, we could not find any symmetries that would allow us to reduce the set of tangles we need to compute HFT on. Therefore, we performed the computations for tangles of the form $S_{p/q}(4)$, where $p/q \in \mathbb{Q}\,\mathrm{P}^1$, $0 < p < q$, and q is odd.

The computations obtained for these tangles are collected in in Table 5.3.

By looking at these new computations, the pattern presented in Conjecture 5.9 seems to generalise to the following conjecture.

Conjecture 5.10. *Let* $S_{p/q}(4) = Q_{p/q} + Q_{1/4}$ *with* $p/q \in \mathbb{Q}\,\mathrm{P}^1$, q *odd and* $0 < 4p < q$. *Then,*

$$\mathrm{HFT}\left(S_{p/q}(4)\right) = (q-4p)\cdot\mathfrak{r}(1/4) + p\cdot\left(\mathfrak{s}_4(1) + \mathfrak{s}_4(1/3)\right).$$

The author did not identify any particular pattern in the computations with $p < q < 4p$. However, a behavior like this seems reasonable: also in other cases (e.g. Pretzel tangles) the tangles split into two sub-families within which there are substantially different patterns followed.

5.2.3 Conjecture for $\mathrm{HFT}(S_{p/q}(2n))$

With the hints given by $S_{p/q}(2)$ and $S_{p/q}(4)$, also computations for some basic cases of $S_{p/q}(6)$ and $S_{p/q}(8)$ where $p/q \in \mathbb{Q}\,\mathrm{P}^1$, q odd and $0 < 2n\cdot p < q$ were done, with $n = 3, 4$ respectively. These are collected in Tables 5.4 and 5.5.

q**p**	1	2
7	$1\cdot\mathfrak{r}(1/6) + 1\cdot\mathfrak{s}_4(1) + 1\cdot\mathfrak{s}_4(1/3) + 1\cdot\mathfrak{s}_4(1/5)$	
8		
9	$3\cdot\mathfrak{r}(1/6) + 1\cdot\mathfrak{s}_4(1) + 1\cdot\mathfrak{s}_4(1/3) + 1\cdot\mathfrak{s}_4(1/5)$	
10		
11		
12		
13		$1\cdot\mathfrak{r}(1/6) + 2\cdot\mathfrak{s}_4(1) + 2\cdot\mathfrak{s}_4(1/3) + 2\cdot\mathfrak{s}_4(1/5)$

Table 5.4: HFT for tangles of the form $S_{p/q}(6)$ with $p/q \in \mathbb{Q}\mathrm{P}^1$, q odd and $0 < 6p < q$.

$\mathbf{q}\backslash\mathbf{p}$	1	2	3	4	5	6
1						
2						
3	$1\cdot\mathfrak{r}\left(3/8\right)+1\cdot\mathfrak{s}_4\left(1\right)$	$1\cdot\mathfrak{r}\left(3/4\right)+2\cdot\mathfrak{s}_4\left(1\right)$				
4						
5	$1\cdot\mathfrak{r}\left(1/4\right)+1\cdot\mathfrak{s}_4\left(1\right)+1\cdot\mathfrak{s}_4\left(1/3\right)$	$1\cdot\mathfrak{r}\left(5/12\right)+2\cdot\mathfrak{s}_4\left(1\right)$	$1\cdot\mathfrak{r}\left(5/8\right)+3\cdot\mathfrak{s}_4\left(1\right)$	$1\cdot\mathfrak{r}\left(5/4\right)+2\cdot\mathfrak{s}_4\left(1\right)+1\cdot\mathfrak{s}_8\left(1\right)$		
6						
7	$3\cdot\mathfrak{r}\left(1/4\right)+1\cdot\mathfrak{s}_4\left(1\right)+1\cdot\mathfrak{s}_4\left(1/3\right)$	$1\cdot\mathfrak{r}\left(3/8\right)+2\cdot\mathfrak{s}_4\left(1\right)+1\cdot\mathfrak{s}_4\left(1/3\right)$	$1\cdot\mathfrak{r}\left(7/16\right)+3\cdot\mathfrak{s}_4\left(1\right)$	$1\cdot\mathfrak{r}\left(7/12\right)+4\cdot\mathfrak{s}_4\left(1\right)$	$1\cdot\mathfrak{r}\left(3/4\right)+4\cdot\mathfrak{s}_4\left(1\right)+1\cdot\mathfrak{s}_8\left(1\right)$	$3\cdot\mathfrak{r}\left(5/4\right)+2\cdot\mathfrak{s}_4\left(1\right)+1\cdot\mathfrak{s}_8\left(1\right)$
8						
9	$5\cdot\mathfrak{r}\left(1/4\right)+1\cdot\mathfrak{s}_4\left(1\right)+1\cdot\mathfrak{s}_4\left(1/3\right)$	$1\cdot\mathfrak{r}\left(1/4\right)+2\cdot\mathfrak{s}_4\left(1\right)+2\cdot\mathfrak{s}_4\left(1/3\right)$		$1\cdot\mathfrak{r}\left(9/20\right)+4\cdot\mathfrak{s}_4\left(1\right)$	$1\cdot\mathfrak{r}\left(9/16\right)+5\cdot\mathfrak{s}_4\left(1\right)$	
10						
11	$7\cdot\mathfrak{r}\left(1/4\right)+1\cdot\mathfrak{s}_4\left(1\right)+1\cdot\mathfrak{s}_4\left(1/3\right)$	$3\cdot\mathfrak{r}\left(1/4\right)+2\cdot\mathfrak{s}_4\left(1\right)+2\cdot\mathfrak{s}_4\left(1/3\right)$	$1\cdot\mathfrak{r}\left(3/8\right)+3\cdot\mathfrak{s}_4\left(1\right)+2\cdot\mathfrak{s}_4\left(1/3\right)$	$1\cdot\mathfrak{r}\left(3/8\right)+4\cdot\mathfrak{s}_4\left(1\right)+1\cdot\mathfrak{s}_4\left(2/5\right)$	$1\cdot\mathfrak{r}\left(11/24\right)+5\cdot\mathfrak{s}_4\left(1\right)$	$1\cdot\mathfrak{r}\left(11/20\right)+6\cdot\mathfrak{s}_4\left(1\right)$
12						
13	$9\cdot\mathfrak{r}\left(1/4\right)+1\cdot\mathfrak{s}_4\left(1\right)+1\cdot\mathfrak{s}_4\left(1/3\right)$		$1\cdot\mathfrak{r}\left(3/8\right)+3\cdot\mathfrak{s}_4\left(1\right)+3\cdot\mathfrak{s}_4\left(1/3\right)$	$3\cdot\mathfrak{r}\left(3/8\right)+4\cdot\mathfrak{s}_4\left(1\right)+1\cdot\mathfrak{s}_4\left(1/3\right)$	$1\cdot\mathfrak{r}\left(5/12\right)+5\cdot\mathfrak{s}_4\left(1\right)+1\cdot\mathfrak{s}_4\left(2/5\right)$	$1\cdot\mathfrak{r}\left(13/28\right)+6\cdot\mathfrak{s}_4\left(1\right)$
14						
15				$1\cdot\mathfrak{r}\left(3/8\right)+4\cdot\mathfrak{s}_4\left(1\right)+3\cdot\mathfrak{s}_4\left(1/3\right)$		
16						
17						$1\cdot\mathfrak{r}\left(3/8\right)+6\cdot\mathfrak{s}_4\left(1\right)+1\cdot\mathfrak{s}_4\left(2/5\right)$

Table 5.3: HFT for tangles of the form $S_{p/q}(4)$ with $p/q \in \mathbb{Q}\mathrm{P}^1$, q odd and $0 < p < q$.

$\mathbf{q}\backslash\mathbf{p}$	1
9	$1\cdot\mathfrak{r}(1/8)+1\cdot\mathfrak{s}_4(1)+1\cdot\mathfrak{s}_4(1/3)+$ $1\cdot\mathfrak{s}_4(1/5)+1\cdot\mathfrak{s}_4(1/7)$
10	
11	$3\cdot\mathfrak{r}(1/8)+1\cdot\mathfrak{s}_4(1)+1\cdot\mathfrak{s}_4(1/3)+$ $1\cdot\mathfrak{s}_4(1/5)+1\cdot\mathfrak{s}_4(1/7)$

Table 5.5: HFT for tangles of the form $S_{p/q}(8)$ with $p/q \in \mathbb{Q}\mathrm{P}^1$, q odd and $0 < 8p < q$.

All these computations, seem to point to a more general pattern followed by HFT for tangles of the form $S_{p/q}(2n)$ with $p/q \in \mathbb{Q}\,\mathrm{P}^1$, q odd and $0 < 2n \cdot p < q$, which is presented in the next conjecture.

Conjecture 5.11. *Let $S_{p/q}(2n)$ be the tangle $S_{p/q}(2n) = Q_{p/q} + Q_{1/2n}$ with $p/q \in \mathbb{Q}\,\mathrm{P}^1$, q odd and $0 < 2n \cdot p < q$. Then,*

$$\mathrm{HFT}\left(S_{p/q}(2n)\right) = (q - 2n\cdot p)\cdot\mathfrak{r}\left(1/(2n)\right) + p\cdot\left(\sum_{i=0}^{n-1}\mathfrak{s}_4\left(1/(2i+1)\right)\right).$$

Remark 5.12 (A confirmation from the Pretzel tangles)**.** As anticipated in the Introduction, Conjecture 5.11 seems to be in part confirmed by the know multicurves of the Pretzel tangles.

In fact, the $(2r, -2s-1)$-Pretzel tangle is defined as $Q_{1/(2r)} + Q_{-1/(2s+1)}$, which is clearly a subfamily of the tangles of the form $S_{p/q}(2n)$. For these tangles, the Tangle Floer Homology is known (see Theorem 6.9 of [Zib20]) and it agrees with what is stated in Conjecture 5.11.

Appendix A

Manual for `nicepy`, version 1.0

This appendix is a manual for version 1.0 of the [`nicepy`] Python Package, an implementation of the Nicefication Algorithm for Python 3.10.2.

A.1 Input preparation

The input is a text file, call it `input.txt`, with a certain number of lines. The first line, saved under `type_of_diagram`, states the type of input; it can be one of the following:

a. "normal", which means that we are giving a (bordered sutured) Heegaard diagram as input;

b. "tangle", which means that we are giving a 4-ended tangle diagram as input;

c. "rational", which means that we are giving a (list of) rational tangle(s) of the form $Q_{p/q}$.

Depending on the type of `input.txt`, the successive lines change.

Input of type "normal"

Let $\mathcal{H} = (\Sigma, \boldsymbol{\alpha} = \boldsymbol{\alpha}^c \cup \boldsymbol{\alpha}^a, \boldsymbol{\beta})$ be the Heegaard diagram that we want to give as input. This diagram can be of the following types: a closed Heegaard diagram (in which $\boldsymbol{\alpha}^a = \emptyset$ and we have a basepoint z), a bordered Heegaard diagram (in which we have one basepoint z in one of the regions on the border), or, more generally, a bordered sutured Heegaard diagram with $\boldsymbol{\alpha}$-arcs ($\boldsymbol{\beta}$-arcs are not allowed in this version of the [`nicepy`]) with some basepoints on it such that every connected component of $\Sigma \setminus \boldsymbol{\alpha}$ contains at least one multiplicity zero regions.

We require the following three properties on $\mathcal{H}$:

- every $\boldsymbol{\alpha}$-curve intersects at least one $\boldsymbol{\beta}$-circle and that every $\boldsymbol{\beta}$-circle intersects at least one $\boldsymbol{\alpha}$-curves,

- every region of $\mathcal{H}$ is a disc,
- every $\boldsymbol{\alpha}$- and $\boldsymbol{\beta}$-circle has at least three intersection points on it.

The first two properties can be obtained by applying Step 1 of the Nicefication Algorithm, as explained in Subsection 4.2.1. The third property is crucial for the program. This is because edges obtained from a circle with only one or two intersection points are not uniquely identified by their endpoints. To ensure uniqueness, it is necessary to perform one or more finger moves to achieve this property.

The procedure to write the input starts by drawing the diagram of interest and labeling the regions from 1 to m. These regions are referred to as $e_1, \dots, e_m$. The next step involves labeling the intersection points obtained by $\boldsymbol{\alpha} \cap \boldsymbol{\beta}$ and $\boldsymbol{\alpha}^a \cap \partial\Sigma$, starting from the ones on the border, if there are any. The labels are denoted by $1, \dots, k, \dots n$, where points $1, \dots, k$ represent the points in $\boldsymbol{\alpha}^a \cap \partial\Sigma$. Furthermore, the labels for the border points must be placed in an increasing order going counter-clockwise. For example, if there are h_1 points on the first border component, their labels should be $1, \dots, h_1$ in an increasing order going counter-clockwise. Similarly, if there are h_2 points on the second border component, their labels should be $h_1 + 1, \dots, h_1 + h_2$ in an increasing order going counter-clockwise, and so on.

We need the following lines in `input.txt` in the presented order.

1. `number_border_points`. This is the number of border points, i.e. the number of intersection points $\boldsymbol{\alpha}^a \cap \partial\Sigma$ (it can be 0). In the notation adopted above, this is k.

2. `number_intersection_points`. This is the total number of intersection points of the diagram (including the border points), i.e. all the points $\boldsymbol{\alpha} \cap \boldsymbol{\beta}$ and $\boldsymbol{\alpha}^a \cap \partial\Sigma$. In the notation above, it is n.

3. `regions_input`. This is the essential data of the diagram, constructed as a list `L`. Given any region e_i, we construct a list `L_i` with the labels of the corners of e_i, such that

   - the labels are given reading them from the region going counter-clockwise,
   - the first two labels are the endpoints of an $\boldsymbol{\alpha}$-edge of e_i.

   Then `L` is the list containing the lists `L_i` in order. Notice in particular that, if a region has a corner whose label is less or equal to k, then it is a boundary region of the diagram.

4. `multiplicity_zero_regions`. This is the list of the labels of multiplicity zero regions, i.e. regions that have a basepoint. This is a list of labels, i.e. only numbers.

Input of type "tangle"

Let T be a 4-ended tangle without closed components. Let $\mathcal{H} = (\Sigma, \boldsymbol{\alpha} = \boldsymbol{\alpha}^c \cup \boldsymbol{\alpha}^a, \boldsymbol{\beta})$ be the tangle Heegaard diagram that we want to give as input (not peculiar).

We require the following three properties on $\mathcal{H}$:

- every $\boldsymbol{\alpha}$-curve intersects at least one $\boldsymbol{\beta}$-circle and that every $\boldsymbol{\beta}$-circle intersects at least one $\boldsymbol{\alpha}$-curves,
- every region of $\mathcal{H}$ is a disc,
- every $\boldsymbol{\alpha}$- and $\boldsymbol{\beta}$-circle has at least three intersection points on it.

The first two properties can be obtained by applying Step 1 of the Nicefication Algorithm, as explained in Subsection 4.2.1. The third property is crucial for the program. This is because edges obtained from a circle with only one or two intersection points are not uniquely identified by their endpoints. To ensure uniqueness, it is necessary to perform one or more finger moves to achieve this property.

The procedure to write the input starts by drawing the diagram of interest and labeling the regions from 1 to m. These regions are referred to as $e_1, \dots, e_m$. The next step involves labeling the intersection points obtained by $\boldsymbol{\alpha} \cap \boldsymbol{\beta}$ and $\boldsymbol{\alpha}^a \cap \partial\Sigma$, starting from the ones on the punctures, and we denote them by $1, \dots n$, where the points $1, \dots, 8$ are the endpoints of the $\boldsymbol{\alpha}$-arcs.

We need the following lines in `input.txt` in the presented order.

1. `number_border_points`. This is the number of border points, i.e. it is 8.
2. `number_intersection_points`. This is the total number of intersection points of the diagram (including the border points), i.e. all the points $\boldsymbol{\alpha} \cap \boldsymbol{\beta}$ and $\boldsymbol{\alpha}^a \cap \partial\Sigma$. In the notation above, it is n.
3. `regions_input`. This is the essential data of the diagram, constructed as a list `L`. Given any region e_i, we construct a list `L_i` with the labels of the corners of e_i, such that
   - the labels are given reading them from the region going counter-clockwise,
   - the first two labels are the endpoints of an $\boldsymbol{\alpha}$-edge of e_i.

   Then `L` is the list containing the lists `L_i` in order. Notice in particular that if a region has a corner whose label is less or equal to k, then it is a boundary region of the diagram.
4. `multiplicity_zero_regions`. Recall that, once we convert the tangle Heegaard diagram to a peculiar Heegaard diagram, we have to choose two special basepoints: one among the p_i's and one among the q_j's. Therefore, we give here a list of the form `[[i, 0], [j, 1]]` as input, where e_i is the multiplicity zero region on the front and e_j is a region on the back. The program is able to

try to nicefy all the 16 possible combinations of multiplicity zero regions (see Section A.3), however it needs an initial input to understand which regions stay on the back of $\mathcal{S}^2_4$ and which stay on the front. Thus this line is required in any case.

5. `alpha_arcs_sites`. This list is needed in order to understand which $\boldsymbol{\alpha}$-arc corresponds to which site. We give a list of four labels, each one corresponding to a border point of the diagram, ordered with respect to the $\boldsymbol{\alpha}$-arc sites. For instance, consider the list `[i,j,k,l]`. This list encodes the information that the border point labeled i is one endpoint of the $\boldsymbol{\alpha}$-arc associated with site a, the border point labeled j is one endpoint of the $\boldsymbol{\alpha}$-arc associated with site b, the border point labeled k is one endpoint of the $\boldsymbol{\alpha}$-arc associated with site c, and the border point labeled l is one endpoint of the $\boldsymbol{\alpha}$-arc associated with site d.

6. `alexander_grading`. This list encodes the data of the Alexander grading of the border regions. It is a list of 4 elements, where each element is an endpoint of a vertical $\boldsymbol{\alpha}$-arc and such points are in the following order with respect to Alexander grading: `[(1,0), (-1,0), (0,1), (0,-1)]`.

Input of type "rational"

Let T be a 4-ended tangle without closed components. We can cut T so that it can be reconstructed by gluing together some rational tangles $R_1, \dots, R_h$, each of which is also a 4-ended tangle. However, it is not allowed to decompose T in such a way that we have retrieve it by adding or multiplying some $Q_{\pm 1}$'s. While there may be multiple $Q_{\pm 1}$ tangles present among the R_i's, it is not allowed to glue them together via the sum or multiplication of 4-ended tangles (for the definition of these operations, refer to Section 1.6).

Given any R_i, we label the endpoints of its strings as follows: 1 corresponds to the end in the north-west puncture, 2 to the end in the south-west puncture, 3 to the end in the south-east puncture and 4 to the end in the north-east puncture; we label the endpoints of the strings of T in the same way. Moreover, we also label the $2h-2$ gluing points and we refer to them as $g_1, \dots, g_{2h-2}$.

We need the following lines in `input.txt` in the presented order.

1. `number_of_tangles`. This is the number of tangles; in the setting above it is h.

2. `tangles_input`. This is a list `L` with the data of the single rational tangles. For any $R_i = Q_{p_i/q_i}$, we construct a list `L_i`, where the first element is `0` if $p_i/q_i < 0$ and `1` if $p_i/q_i > 0$, the second is `p_i` and the third is `q_i`. Then, `L` is the list where the i-th element is `L_i`.

3. `gluing_instructions`. This is a list `G` with the instruction for the gluing of the tangles R_i. Let g_j the gluing point between the tangles R_{i_1} and R_{i_2},

along end_1 (one string's end for R_{i_1}) and end_2 (one string's end for R_{i_2}). We construct the list `G_j` corresponding to g_j as `[i_1, end_1, i_2, end_2]`.

Then `G` is the list where the j-th element is `G_j`. If there is only one tangle in `tangles_input`, `G` is an empty list.

4. `alexander_grading_tangle`. This list encode the data of the Alexander gradings of the border regions. It is a list of the numbers from 1 to 4, indicating the endpoint of the string of T, where the order of them is given with respect to Alexander grading: `[(1,0), (-1,0), (0,1), (0,-1)]`.

In this case, we do not need the information about the $\boldsymbol{\alpha}$-arc sites for the diagram of T, as it is automatically interpreted as follows:

- the site a is from the string's endpoint 1 to the string's endpoint 2,
- the site b is from the string's endpoint 2 to the string's endpoint 3,
- the site c is from the string's endpoint 3 to the string's endpoint 4,
- the site d is from the string's endpoint 4 to the string's endpoint 1.

Placing the input

Once the input file is ready, it needs to be provided as input to the program.

We save the path to `input.txt` in the variable `input_path` which can be found in the top part of `main_run.py`. `input_path` is a tuple, where the first entry is a string containing the (possibly relative to the path of `main_run.py`) path to the folder in which `input.txt` is and the second entry is a string containing the name of the input file itself.

```
1 input_path = ("C:/Users/user1/Documents/", "input.txt")
```

Listing A.1: Example of `input_path` if the path to the input file is C:/Users/user1/Documents/input.txt.

```
1 input_path = ("./inputs/", "input.txt")
```

Listing A.2: Example of `input_path` if the input file is in a subfolder called **inputs** of the folder in which `main_run.py` is.

A.2 Examples of input

We see some examples of Heegaard diagrams and their inputs.

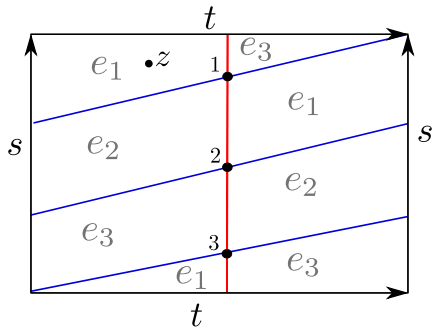

Figure A.1: Closed Heegaard diagram for $L(3,1)$.

Closed Heegaard diagram

This is an example of an input where the first line is "normal".

Suppose to have the closed Heegaard diagram for the lens space $L(1,3)$ as represented in Figure A.1. Then, `input.txt` is the following.

```
normal
0
3
[[1,2,1,3],[2,3,2,1],[3,1,3,2]]
[1]
```

Bordered sutured Heegaard diagram with α-arcs

This is an example of an input where the first line is "normal".

Suppose to have the bordered sutured Heegaard diagram in Figure A.2. Then, `input.txt` is the following.

```
normal
10
25
[[15,16,17,20,23,14],[20,21,22,23],[23,22],[21,20],[18,21,20,17],
    [14,23,22,13],[2,12,15,3],[12,2,5,13],[13,5,4,14],[3,15,14,4],
    [19,7,6,16],[16,6,9,17],[8,18,17,9],[18,8,7,19],[1,11,24,25,11,1],
     [16,15,12,25,24,11,25,12,13,22,21,18,19,10,10,19],[25,24],
    [11,24]]
[15,9,13,4,3,16]
```

Tangle Heegaard diagram

This is an example of an input where the first line is "tangle".

Consider the $(2,-3)$-Pretzel tangle with the orientation on the stings as in Figure A.3 and its tangle Heegaard diagram represented in Figure A.4. Then, `input.txt` is the following.

```
tangle
```

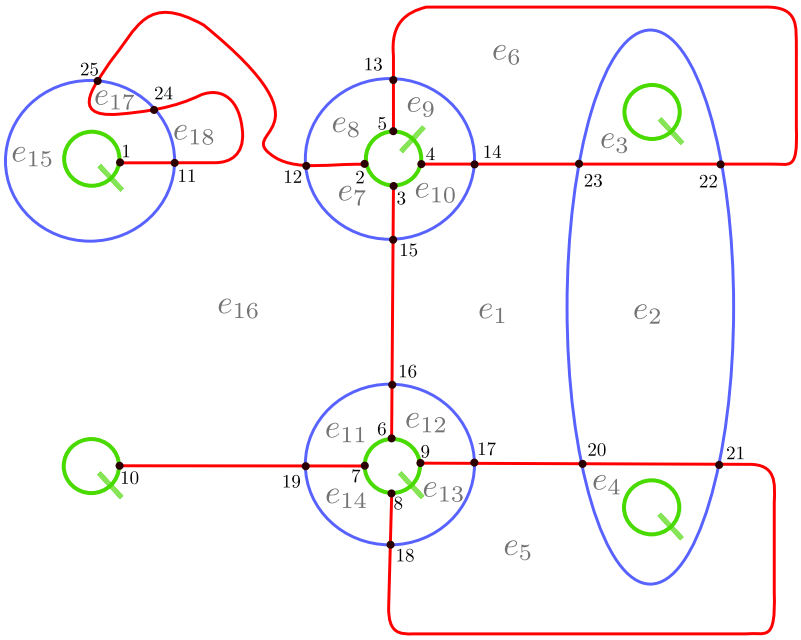

Figure A.2: A bordered sutured Heegaard diagram.

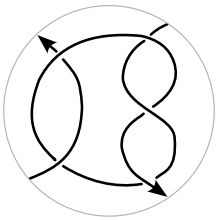

Figure A.3: $(2,-3)$-Pretzel tangle with oriented strings.

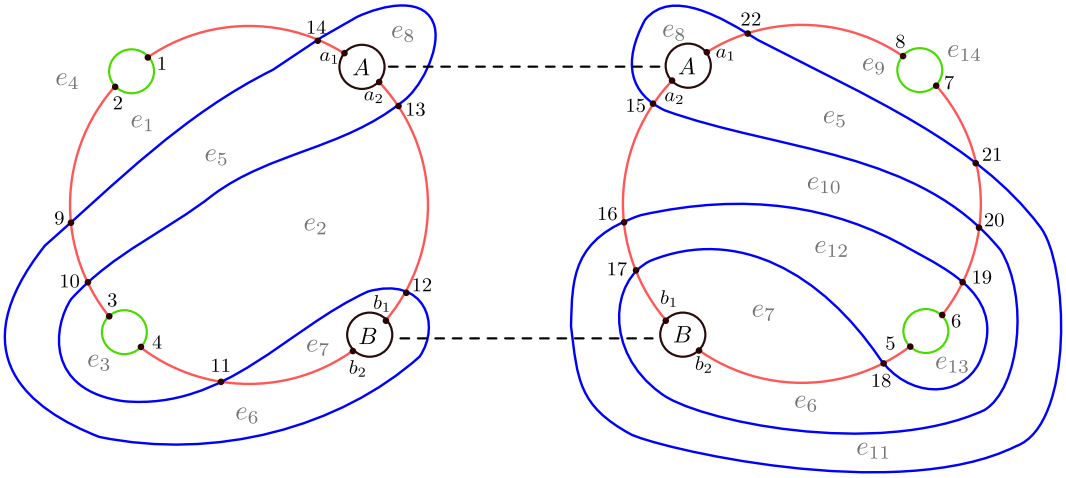

Figure A.4: Tangle Heegaard diagram for the $(2,-3)$-Pretzel tangle.

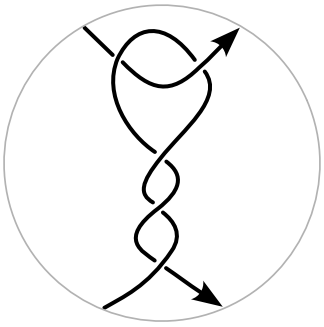

Figure A.5: Oriented tangle diagram for $Q_{3/7}$.

```
8
22
[[1,11,9,2],[4,13,14,10,12,3],[3,12,13,4],[11,1,2,9,10,14],
    [11,12,10,16,18,17,15,9],[12,11,14,19,18,21,22,13],[13,22,19,14],
    [9,15,16,10],[5,15,17,6],[16,20,21,18],[17,18,19,20],
    [20,19,22,8,7,21],[8,22,21,7],[20,16,15,5,6,17]]
[[1, 0],[3, 1]]
[2,4,6,8]
[2,3,6,7]
```

Single rational tangle

This is an example of an input where the first line is "rational".

Consider the rational tangle $Q_{3/7}$, represented in Figure A.5. Then, `input.txt` is the following.

```
rational
1
[[1, 3, 7]]
[]
[4,1,3,2]
```

Non-rational tangle

This is an example of an input where the first line is "rational".

Consider the tangle T, represented in Figure A.6, where we label the rational pieces and the gluing points according to the image. Then, `input.txt` is the following.

```
rational
3
[[1,1,2],[0,1,3],[1,1,1]]
[[1,4,2,1],[1,3,2,2],[1,2,3,1],[2,3,3,4]]
[3,1,4,2]
```

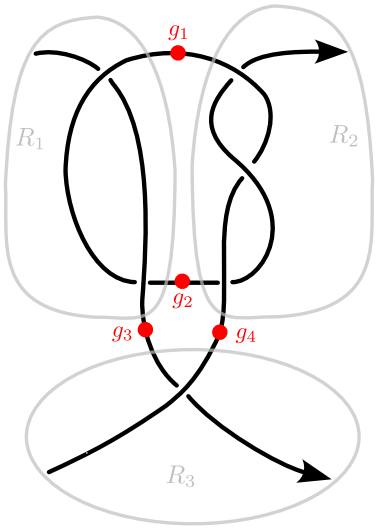

Figure A.6: Oriented tangle diagram for T, divided in rational components.

A.3 Additional settings

There are some additional parameters that can be set manually inside `main.py`. They are the following.

- `user_experience`. This flag, if set to `True`, stops the run in different points and asks for an manual confirmation in order to proceed. If set to `False`, the run does not stop until the end or until it finds an error in the input data.
- `input_check`. "If this flag is set to `True`, the program stops after pre-processing the input, giving the user the opportunity to check if the input given is correct. A message is printed on the screen, and the program asks for manual confirmation before proceeding. If this flag is set to `False`, the program does not print the initial diagram and skips this step.
- `try_multiplicity_zero_regions_choices`. This flag, if set to `True`, allows the program to generate others diagrams where the only difference from the one given in the input is the choice of the multiplicity zero regions (this is only implemented for the cases "tangle" and "rational"). If set to `False`, only the given input will be nicefied. In the case of an input of type "rational", this flag is automatically set to `True`.
- `print_distance_complexities`. This flag, if set to `True`, prints after every iteration of the algorithm the distance complexities, the total complexity and the number of generators of the diagram obtained with the last cycle. If set to `False`, the above data is not printed between the cycles.
- `print_intermediate_steps`. This flag, if set to `True`, prints after every iteration of the algorithm the new diagram obtained with the last modification.

One of the data displayed, is the last move done on the previous diagram; it is presented as showed below.

```
Regions of the last diagram that we modified:
        Type of move: Handleslide
        Starting region: Region 4
        Edge modified: [12, 9]
        Ending region: Region 4
        Neighbour region: Region 6
        Middle regions:
                Region 27
                Region 28
        Edges crossed:
                [5, 12]
                [2, 33]
                [4, 7]
```

If set to `False`, the diagrams generated are not printed between the cycles.

- `print_final_diagram`. This flag, if set to `True`, prints the final diagram obtained at the end of the run. If set to `False`, the final diagram is not printed at the end of the execution of the program.

- `print_details_nicefied_diagram`. This flag, if set to `True`, print the following details of the run: number of generators of the final diagram, number of regions of the final diagram, number of cycles of the algorithm needed to obtain the final diagram. If set to `False`, none of this information is saved.

- `print_output_for_PQM`. This flag is effective only for diagrams of type "tangle" or "rational". If set to `True`, at the end of the run it formats in a string the final diagram as it is needed for the input of [`PQM.m`] and it prints this string on screen. If set to `False`, this string is not printed.

- `save_on_file`. If the flag is set to `True`, the program is enabled to save various data relative to the run on a file, as specified by the parameters listed below. To save such data, there needs to be a folder named **`nicefied_diagrams`** in the same folder where the `input.txt` file is located. After the run, the file is saved in that folder with the name `input_nicefied_diagram.txt`. However, if the flag is set to `False`, the program will not save anything, so even if the next flags are set to `True`, they will not have any effect.

- `save_intermediate_steps`. This flag, if set to `True`, saves all the intermediate diagrams obtained in `input_nicefied_diagram.txt` (if we previously set `try_multiplicity_zero_regions_choices = True`, it saves the intermediate diagrams only for the final diagram). If set to `False`, the intermediate diagrams are not saved.

- `save_final_diagram`. This flag, if set to `True`, saves the final diagram obtained at the end of the run in `input_nicefied_diagram.txt`. If set to `False`, the final diagram is not saved.
- `save_details_nicefied_diagram`. This flag, if set to `True`, saves some details of the run in `input_nicefied_diagram.txt`. These details are: number of generators of the final diagram, number of regions of the final diagram, number of cycles of the algorithm needed to obtain the final diagram. If set to `False`, none of this information is saved.
- `save_output_for_PQM`. This flag is effective only for diagrams of type "tangle" or "rational". When set to `True`, the program formats the final diagram into a string that can be used as input for [`PQM.m`] and saves it in the file `input_nicefied_diagram.txt`. If set to `False`, the program does not save this string.

A.4 Pre-processing of the input

After the input is prepared and the additional settings are assigned, it is possible to run the program. This is done by executing the python script `main_run.py`.

The pre-processing stage refers to the initial processing that is performed on the input before the algorithm is applied. It includes reading the input and conducting a series of sanity checks to ensure that the input is valid and can be properly processed by the program.

Pre-processing of type "normal"

In the case the diagram is of type "normal", the program initially calculates the curves and verifies that each circle, except for arcs, has at least three intersection points. If the verification fails, the program prompts the user to manipulate the diagram to increase the intersection points on the deficient circles.

After passing this check, the program performs another sanity check by examining the edges of the diagram, identified by their endpoints, to locate all the edges twice with opposite orientations. If this check also passes, the Heegaard diagram is created.

The next step involves checking if the input diagram is bordered. If it is, the program then proceeds to check each of the border regions to see if they are already square regions, or if an initial finger move is required to transform them to squares. In the latter case, the `finger_move_beginning_bordered()` method is called to perform the necessary move.

Pre-processing of type "tangle"

If the input diagram is of type "tangle", the program begins by computing the curves of the diagram and verifying that each circle (excluding arcs) has at least three

intersection points on it. If this check fails, the program terminates and prompts the user to perform finger moves to increase the number of intersection points on the deficient circles.

Once this check is passed, the program proceeds to a second sanity check by scanning the edges of the diagram, identified by their endpoints, in an attempt to find all edges twice in opposite orientation. If this check also passes, the program generates the Heegaard diagram.

After the sanity checks, the program converts it into a peculiar Heegaard diagram by removing the sutures around the tangle's endpoints, concatenating the $\boldsymbol{\alpha}$-arcs, and placing the basepoints p_i's and q_j's along with the two special ones in the designated regions. If the flag `try_multiplicity_zero_regions_choices` is enabled, the program generates all sixteen possible Heegaard diagrams with different combinations for the choice of special basepoints p_i and q_j.

Pre-processing of type "rational"

If the input diagram is of type "rational", the program performs several steps to construct the tangle Heegaard diagram for T.

Firstly, it builds the tangle Heegaard diagrams of $R_1, \dots, R_h$ with the procedure described in Section 2.6.1 and glues them together according to the instructions given in `gluing_instructions`.

During this process, the program conducts two sanity checks. Firstly, for any rational tangle $Q_{p/q}$, it verifies that p and q are coprime; if they are not, the program terminates. Secondly, when gluing two tangles Q_{p_i/q_i} and Q_{p_j/q_j}, the program checks that neither both p_i and p_j are odd nor both q_i and q_j are even. The purpose of the second check is to avoid the creation of a closed component in T. If the condition mentioned above is satisfied, it ensures that no closed components are formed. In case this situation arises, the program alerts the user, but it does not terminate the program unless the user decides to override the warning. This serves as a precautionary measure to prompt the user to carefully examine the tangle for any closed components.

After constructing the tangle Heegaard diagram, the program transforms it into a peculiar Heegaard diagram by removing the sutures around the tangle's endpoints, concatenating the $\boldsymbol{\alpha}$-arcs, placing the basepoints p_i's and q_j's, and generating all the sixteen Heegaard diagrams carrying different combinations for the choice of the special basepoints p_i and q_j.

A.5 Application of the Nicefication Algorithm

After the pre-processing stage, the input Heegaard diagram undergoes the Nicefication Algorithm. The algorithm is implemented as described in Section 4.2, but with the modifications outlined in Section 4.5.

If the flag `try_multiplicity_zero_regions_choices` is activated, the program runs the algorithm on all the possible sixteen diagrams. It starts with the diagrams

that appear to be the most promising, i.e., those with a smaller total complexity, and then moves on to the others. The first diagram is fully nicefied, and let $\#gen$ be the number of generators of the resulting diagram. The program then nicefies the other diagrams until the number of generators exceeds $\#gen$. If this happens, the algorithm stops, and the program moves on to the next diagram on the list. If a diagram is nicefied and the final number of generators is $\#gen' < \#gen$, then this is stored as temporary final diagram and the number of generators of the successive diagrams are compared with $\#gen'$.

A.6 Examples of output

The output of the program is built with respect to the additional parameters presented in Section A.3. We see some examples of output obtained when these parameters are activated.

If `print_final_diagram` or `save_final_diagram`

If one of the above flags is activated, the respective string generated is of the following form.

```
The algorithm worked!

We were able to nicefy the input given in ./inputs/ for the diagram
    input.txt

Details of the Heegaard diagram:

        Is it nice: True

        Number of regions: 22
        Number of intersection points: 29
        Number of border points: 10

        Regions of the diagram:
                Region 1:
                        Input: [27, 16, 17, 20]
                        Badness: 0
                        Distance: 2
                        Is a border region: False

                Region 2:
                        Input: [29, 27, 20, 21]
                        Badness: 0
                        Distance: 1
                        Is a border region: False

                ...


                Region 22:
                        Input: [29, 28]
```

```
                          Badness: 0
                          Distance: 2
                          Is a border region: False
```

If `print_details_nicefied_diagram` or `save_details_nicefied_diagram`

If one of the above flags is activated, the respective string generated is of the following form.

```
Number of generators of the diagram: 45
Number of cycles of the algorithm: 2
Number of regions of the diagram: 22
```

If `print_output_for_PQM` or `save_output_for_PQM`

If one of the above flags is activated, the respective string generated is of the following form.

```
regionsInput = ( {{1,9,36,35,38},{2,12,13,14,29},{3,13,12,11,21},...
    ...,{39,42,41,39,40},{40,41,42,\[Placeholder],\[Placeholder]}} );

alphasInput = ( {{1,{1,24,19,20,25,8,29,14,13,12,11,21,4,33,42,41,...
    ...28,10,9,36,7,26,18,17,23,6,31,39,40,34}}} );

betasInput = ( {{1,{1,8,7,2,5,4,3,6}},{2,{9,38,40,42,41,39,37,14,...
    ...15,11,12,29,30,31,32,33,34,35,36}}} );

cancellationSortListInput = ( { } );

alphaArcs = ( {{"a
    ",{42,41,32,3,22,15,16,27,2,35,38,37,30,1,24,19,20}}, {"b",{11,21,
     4,33}},{"c",{13,12}},{"d",{25,8,29,14}}} );

basepointRegions = ( {{7,p,{1,0},-2},{8,q,{1,0},-2},{9,p,{-1,0},-2},
    {10,q,{-1,0},-2},{11,p,{0,-1},-2},{12,q,{0,1},-2}} );

multiplicity0Regions = ( {{41,{{4,5},{28,10},{9,38},{37,14},{13,21}},
    {0,1},-4},{42,{{8,7},{36,9},{10,16},{15,11},{12,29}},{0,-1},-4}});
```

This string is already formatted to be used as input of [PQM.m]. For details on this Software, we refer to the documentation of [PQM.m].

Bibliography

[nicepy] Ludovico Morellato. *nicepy*. Python package, 2022. URL: https://github.com/ludomorellato/nicepy.

[PQM.m] Claudius B. Zibrowius. *PQM.m*. Mathematica package, ancillary file to (arXiv:1712.05050v2), 2020. URL: https://cbz20.raspberryip.com/#code.

[Abo+13] Mohammed Abouzaid et al. "Homological mirror symmetry for punctured spheres". In: *Journal of the American Mathematical Society* 26.4 (2013), pp. 1051–1083.

[Abo08] Mohammed Abouzaid. "On the Fukaya categories of higher genus surfaces". In: *Advances in Mathematics* 217.3 (2008), pp. 1192–1235.

[Ada94] Colin C. Adams. *The Knot Book: An Elementary Introduction to the Mathematical Theory of Knots*. American Mathematical Soc., 1994.

[Alt13] Irida Altman. *Introduction to sutured Floer homology*. arXiv, 2013. URL: https://arxiv.org/abs/1304.2606.

[Aub22] Benedikt Aubeck. *Determining the Seifert genus via the Heegaard Floer tangle invariant HFT*. Master thesis, Universität Regensburg, 2022. URL: https://cbz20.raspberryip.com/documents/2021-Aubeck-Thesis-MSc.pdf.

[Bar22] Davide Barilari. *Lecture notes on Differential Geometry*. Notes from the course of differential geometry at the University of Padova, 2022. URL: https://www.math.unipd.it/~barilari/teaching.php.

[Con70] John H. Conway. "An enumeration of knots and links, and some of their algebraic properties". In: *Computational Problems in Abstract Algebra* (1970), pp. 329–358.

[Fuk93] Kenji Fukaya. "Morse homotopy, A^∞-category, and Floer homologies". In: *Proceedings of GARC Workshop on Geometry and Topology '93 (Seoul, 1993)* (1993), pp. 1–102. URL: https://www.math.kyoto-u.ac.jp/~fukaya/mfikki.pdf.

[GS99] Robert E. Gompf and András I. Stipsicz. *4-Manifolds and Kirby Calculus*. Graduate studies in mathematics. American Mathematical Society, 1999.

[Hom19] Jennifer Hom. "Lecture notes on Heegaard Floer homology". In: *Lecture notes for a course on Heegaard Floer homology held at PCMI in Summer 2019* (2019). URL: https://arxiv.org/abs/2008.01836.

[Juh06] András Juhász. "Holomorphic discs and sutured manifolds". In: *Algebraic & Geometric Topology* 6.3 (2006), pp. 1429–1457.

[Juh13] Andras Juhász. *A survey of Heegaard Floer homology*. arXiv, 2013. URL: https://arxiv.org/abs/1310.3418.

[KL04] Louis H Kauffman and Sofia Lambropoulou. "On the classification of rational tangles". In: *Advances in Applied Mathematics* 33.2 (2004), pp. 199–237.

[KT13] Sadok Kallel and Walid Taamallah. "The geometry and fundamental group of permutation products and fat diagonals". In: *Canadian Journal of Mathematics* 65.3 (2013), pp. 575–599.

[Lip06] Robert Lipshitz. "A cylindrical reformulation of Heegaard Floer homology". In: *Geometry & Topology* 10.2 (2006), pp. 955–1096.

[LMW08] Robert Lipshitz, Ciprian Manolescu, and Jiajun Wang. "Combinatorial cobordism maps in hat Heegaard Floer theory". In: *Duke Mathematical Journal* 145.2 (2008).

[LMZ20] Tye Lidman, Allison H. Moore, and Claudius B. Zibrowius. *L-space knots have no essential Conway spheres*. arXiv, 2020. URL: https://arxiv.org/abs/2006.03521.

[Löh21] Clara Löh. *Differential Geometry I*. Notes from the course Differential Geometry I at the University of Regensburg, 2021. URL: https://loeh.app.uni-regensburg.de/teaching/diffgeo_ws2021/lecture_notes.pdf.

[LOT18] Robert Lipshitz, Peter Ozsváth, and Dylan Thurston. *Bordered Heegaard Floer homology*. Vol. 254. 1216. American Mathematical Society, 2018.

[Mac62] Ian G Macdonald. *Symmetric products of an algebraic curve*. Vol. 1. 4. Pergamon, 1962, pp. 319–343.

[Mil63] John Milnor. *Morse theory*. Vol. 51. Based on lecture notes by M. Spivak and R. Wells. Princeton University Press, 1963.

[OS04a] Peter Ozsváth and Zoltán Szabó. "Holomorphic disks and knot invariants". In: *Advances in Mathematics* 186.1 (2004), pp. 58–116.

[OS04b] Peter Ozsváth and Zoltán Szabó. "Holomorphic disks and topological invariants for closed three-manifolds". In: *Annals of Mathematics* (2004), pp. 1027–1158.

[OS06a] Peter Ozsváth and Zoltán Szabó. "An introduction to Heegaard Floer homology". In: *Floer homology, gauge theory, and low-dimensional topology* 5 (2006), pp. 3–27.

[OS06b] Peter Ozsváth and Zoltán Szabó. "Holomorphic triangles and invariants for smooth four-manifolds". In: *Advances in Mathematics* 202.2 (2006), pp. 326–400.

[Ras03] Jacob Rasmussen. "Floer homology and knot complements". In: (2003). URL: https://arxiv.org/abs/math/0306378.

[Rei33] Kurt Reidemeister. "Zur dreidimensionalen topologie". In: 9 (1933), pp. 189–194.

[Sar11] Sucharit Sarkar. "Maslov index formulas for Whitney n-gons". In: *Journal of Symplectic Geometry* 9.2 (2011), pp. 251–270.

[Sin33] James Singer. "Three-dimensional manifolds and their Heegaard diagrams". In: *Transactions of the American Mathematical Society* 35.1 (1933), pp. 88–111.

[SW10] Sucharit Sarkar and Jiajun Wang. "An algorithm for computing some Heegaard Floer homologies". In: *Annals of mathematics* (2010), pp. 1213–1236.

[Zar09] Rumen Zarev. *Bordered Floer homology for sutured manifolds.* arXiv, 2009. URL: https://arxiv.org/abs/0908.1106.

[Zar11] Rumen Zarev. *Bordered sutured Floer homology.* Thesis (Ph.D.) - Columbia University, 2011. DOI: 10.7916/D83R10V410.7916/D83R10V4.

[Zib17] Claudius B. Zibrowius. *On a Heegaard Floer theory for tangles.* Apollo - University of Cambridge Repository, 2017. URL: https://www.repository.cam.ac.uk/handle/1810/263367.

[Zib19] Claudius B. Zibrowius. "On symmetries of peculiar modules; or, δ-graded link Floer homology is mutation invariant". In: (2019). URL: https://arxiv.org/abs/1909.04267.

[Zib20] Claudius B. Zibrowius. "Peculiar modules for 4-ended tangles". In: *Journal of Topology* 13.1 (2020), pp. 77–158.